NAVAL FACILITIES ENGINEERING SERVICE CENTER
Port Hueneme, California 93043-4370

Contract Report
CR 96.010

IMPLEMENTATION OF A BOND MODEL, INCLUDING DILATION, FOR REINFORCED MATERIALS IN A FINITE ELEMENT ANALYSIS

by

Joseph D. Mello and
Leonard R. Herrmann

August 1996

ABSTRACT The objective of this research was to develop a composite finite element analysis that is capable of including the nonlinear, elastic-plastic response of the bond between reinforcing fibers or bars and matrix material. This bond is very important in determining the behavior of reinforced weak or brittle matrix materials, such as reinforced-concrete or ceramic-matrix composites. A composite element captures the response of a reinforced material without the expense of a discrete model which treats each constituent with different element or material types. This report documents the development, implementation, and verification of the composite element with bond modeling capabilities.

The composite continuum element employs a bond model based on classical non-associative, elasticity-plasticity theory. The element is two-dimensional, plane strain, with reinforcement in one coordinate direction. The element has two added degrees of freedom per node: bond slip and dilation. These local deformations are approximated as continuous field variables in the finite element scheme.

The finite element scheme requires special composite material constitutive relations which include bond slip and dilation effects. A unit cell micromechanics analysis based on virtual work concepts was used to derive the required relations.

The inelastic bond constitutive relations were evaluated using a Reduced-Newton algorithm developed especially for this bond model. The global finite element solution uses an incremental Newton-Raphson process to solve the resulting nonlinear system of equations.

The element was tested at various stages of its development. Specializing the bond model for the case of perfect bond conditions allowed for simple verification of the underlying micro-mechanics representation of the composite system. The numerical implementation of the plasticity-based bond model during testing reproduced the salient features of the theoretical bond model as a stand-alone unit prior to its implementation in the finite element setting. After the composite finite element was incorporated in a finite element code, analyses of published beam and bond tension tests were conducted. The predicted results compared favorably with the published data, considering the limitations of modeling the behavior of the matrix and the reinforcement as linear elastic. The beam analyses illustrated the ease with which the composite analysis can be applied to practical problems. The bond tension tests clearly demonstrated the element's capacity to model bond behavior.

DISCLAIMER NOTICE

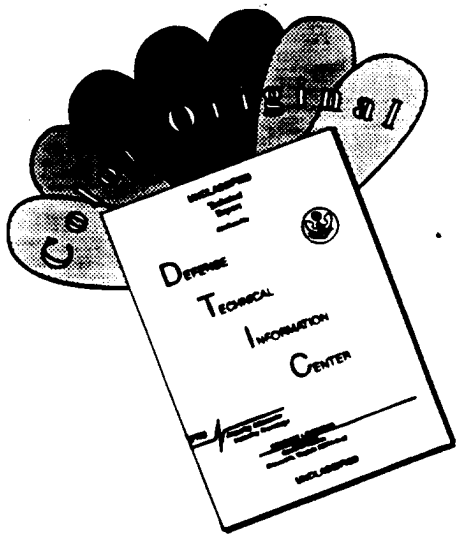

THIS DOCUMENT IS BEST QUALITY AVAILABLE. THE COPY FURNISHED TO DTIC CONTAINED A SIGNIFICANT NUMBER OF COLOR PAGES WHICH DO NOT REPRODUCE LEGIBLY ON BLACK AND WHITE MICROFICHE.

REPORT DOCUMENTATION PAGE

Form Approved
OMB No. 0704-018

1. AGENCY USE ONLY *(Leave blank)*	2. REPORT DATE	3. REPORT TYPE AND DATES COVERED
	August 1996	Final; Mar 1993 through Dec 1995

4. TITLE AND SUBTITLE
IMPLEMENTATION OF A BOND MODEL, INCLUDING DILATION, FOR REINFORCED MATERIALS IN A FINITE ELEMENT ANALYSIS

5. FUNDING NUMBERS
PE - 61153N
Contract No. N47408-93-C-7307

6. AUTHOR(S)
Joseph D. Mello and Leonard R. Herrmann

7. PERFORMING ORGANIZATION NAME(S) AND ADDRESSE(S)
Department of Civil Engineering
University of California
Davis, CA 95616

8. PERFORMING ORGANIZATION REPORT NUMBER
CR 96.010

9. SPONSORING/MONITORING AGENCY NAME(S) AND ADDRESSES
Office of Naval Research
Arlington, VA 22217-5660

10. SPONSORING/MONITORING AGENCY REPORT NUMBER

11. SUPPLEMENTARY NOTES

12a. DISTRIBUTION/AVAILABILITY STATEMENT
Approved for public release; distribution unlimited.

12b. DISTRIBUTION CODE

13. ABSTRACT *(Maximum 200 words)*

The objective of this research was to develop a composite finite element analysis that is capable of including the nonlinear, elastic-plastic response of the bond between reinforcing fibers or bars and matrix material. This bond is very important in determining the behavior of reinforced weak or brittle matrix materials, such as reinforced-concrete or ceramic-matrix composites. A composite element captures the response of a reinforced material without the expense of a discrete model which treats each constituent with different element or material types. This report documents the development, implementation, and verification of the composite element with bond modeling capabilities. The numerical implementation of the plasticity-based bond model during testing reproduced the salient features of the theoretical bond model as a stand-alone unit prior to its implementation in the finite element setting. After the composite finite element was incorporated in a finite element code, analyses of published beam and bond tension tests were conducted. The predicted results compared favorably with the published data, considering the limitations of modeling the behavior of the matrix and the reinforcement as linear elastic. The beam analyses illustrated the ease with which the composite analysis can be applied to practical problems. The bond tension tests clearly demonstrated the element's capacity to model bond behavior.

14. SUBJECT TERMS	15. NUMBER OF PAGES
Finite element modeling, reinforced concrete, composite finite element, bond-slip, elasto-plastic bond model, Reduced-Newton algorithm, beams	122
	16. PRICE CODE

17. SECURITY CLASSIFICATION OF REPORT	18. SECURITY CLASSIFICATION OF THIS PAGE	19. SECURITY CLASSIFICATION OF ABSTRACT	
Unclassified	Unclassified	Unclassified	UL

CONTENTS

1. INTRODUCTION

This project as originally conceived was to span 5 years; however, early in the project, changes in funding priorities required a substantial shortening of the proposed research. The chief goal of the original project was the numerical implementation, in a composite finite element analyses, of a plasticity bond model for reinforced materials. The model was to include both bond slippage and dilation and was to be of the general form of the model developed by Herrmann and Cox (1992) for reinforced concrete. The applications of the analysis were to include both reinforced concrete and fiber-reinforced composites. When the overall duration and magnitude of the project were reduced, it was necessary to substantially reduce the goals of the project. As a result of this redefinition, the study was restricted to circumstances where the cyclic plasticity features of the model could be ignored. In addition, the matrix and reinforcing materials were assumed to be linear elastic, and the analysis was restricted to plane strain conditions. Finally, examples were limited to simple reinforced-concrete tests and structures.

While the above reduction in the overall goals of the project limits its immediate applicability, it does not really affect the primary objective of demonstrating the feasibility of incorporating a plasticity-based bond law that includes bond dilation into a composite finite element analysis for reinforced structures. The possible future extension of the analysis to three-dimensional problems and its incorporation into the analysis of inelasticity material models for matrix and reinforcing materials are all steps that are well understood (albeit rather long and tedious). Finally, the application to fiber-reinforced composites only depends upon the calibration of the bond model for such materials.

The research was carried out as a collaborative effort by the two authors and constituted the doctoral research of the first author. The resulting thesis contains additional material not covered in this report, such as a description of the finite element code used to evaluate the numerical implementation of the bond model. The reader is referred to Mello (1996) for this additional information.

The research had four main components. The first was the development of a three-dimensional composite material representation of a reinforced solid, including a bond model that accounted for both slippage between the reinforcement and the matrix and dilation of the bond zone. In the initial development the bond model was taken to be linear elastic. The composite material representation was developed by using a micro-mechanics model consisting of an

approximate "representative volume" for an assumed hexagonal packing of a fiber- or bar-reinforced solid.

In the second phase the resulting composite model was incorporated into a plane strain finite element code with four degrees of freedom at each node (average displacements, bond slippage, and bond dilation).

The third phase consisted of developing and calibrating a somewhat simplified version of the plasticity bond model for reinforced concrete that was originally developed by Herrmann and Cox (1992). A robust numerical implementation scheme for evaluating the model was developed and tested for a range of bond strain and stress states. The bond plasticity model was then incorporated into the composite analysis and accompanying two-dimensional finite element code.

The final phase consisted of applying the analysis to a number of tests reported in the literature for reinforced concrete. The results of this final phase clearly demonstrated the feasibility of incorporating a bond model that includes both bond slippage and dilation into a composite representation and accompanying finite element analysis for unidirectional reinforced materials.

Structures fabricated of reinforced composite materials are commonplace. Reinforced-concrete highway bridges, fiber-reinforced polymer-matrix aircraft skins/spars, and high temperature fiber-reinforced ceramic-matrix engine components serve as a few examples. For modeling purposes, these materials can be viewed as consisting of three general constituents: fiber, matrix, and bond. Bond refers to the interaction between reinforcing fibers, or bars, and the matrix material. For many reinforced systems, the bond behavior is very important to the overall response of the structure.

Because these composite materials are used in many important structures, the need to perform detailed structural analyses is obvious. Current analysis techniques generally fall into two categories: composite and discrete. In a composite analysis, the reinforced material is approximated as a continuum with properties determined from micro-mechanics analyses and/or empirical test data. Mechanics of materials, elasticity, and finite element analysis techniques for continuum materials may then be applied. These analyses generally assume perfect bonding and linear response of fiber/matrix, which severely limits their applicability. They may be valid for the analysis of fiber-reinforced plastics for instance, but inadequate for reinforced concrete or high temperature ceramic-matrix composites. Discrete analyses employ finite element techniques to model matrix, fiber, and bond separately. Interface elements are used to model the bond between two-dimensional or three-dimensional continuum elements which separately represent the matrix and the reinforcement. If nonlinear material models exist for the constituents, then the results of these models can be very accurate. The problem with this approach is cost; it is costly to formulate and develop the input for the analyses, and computationally expensive to run the very large problems that result.

This report documents the development of a composite finite element that includes nonlinear response due to the interface bond. This approach results in finite element models that are relatively easy to formulate, inexpensive to run, and yet capture most of the discrete response behavior of the constituents. The development, which includes a specialized finite element scheme and an integrated composite micro-mechanics analysis, implements an elastic-plastic bond model that was developed for reinforced concrete. However, the resulting analysis technique is general and may be applied to a variety of reinforced materials, assuming the bond model used in the analysis can be successfully calibrated for the system at hand.

2. REINFORCED MATERIALS AND ANALYSIS

2.1 Reinforced Materials

The most common reinforced material is a unidirectional composite. This composite configuration, shown in Figure 1, is found, for example, in reinforced-concrete bridge structures and aircraft wing spars. A reinforced system arranged in this manner forms an orthotropic composite.

Microscopically, this material is heterogeneous by definition. The reinforcing fibers are typically stronger and stiffer than the matrix material, and thus the resulting longitudinal stiffness and strength of the composite is usually much greater than in the transverse directions. The mechanical properties of each constituent is usually well characterized and documented.

In most reinforced-material structures, the load is applied to the matrix material and not directly to the reinforcing fibers. The load, for the most part, is transferred to the fibers through a small region near the fiber ends, thus creating end effects. When the fiber is much longer than the length over which the load transfer takes place, these end effects are usually neglected. In the case of brittle or weak matrix materials, such as ceramic-matrix composites or reinforced concrete, matrix cracks can form, and these end effects may then be present in the middle of the structure.

The interfacial bond between the reinforcing fiber and matrix is very important as it influences the mechanical properties and overall performance of the reinforced material. Because this interface is responsible for transmitting the load to the fibers, the

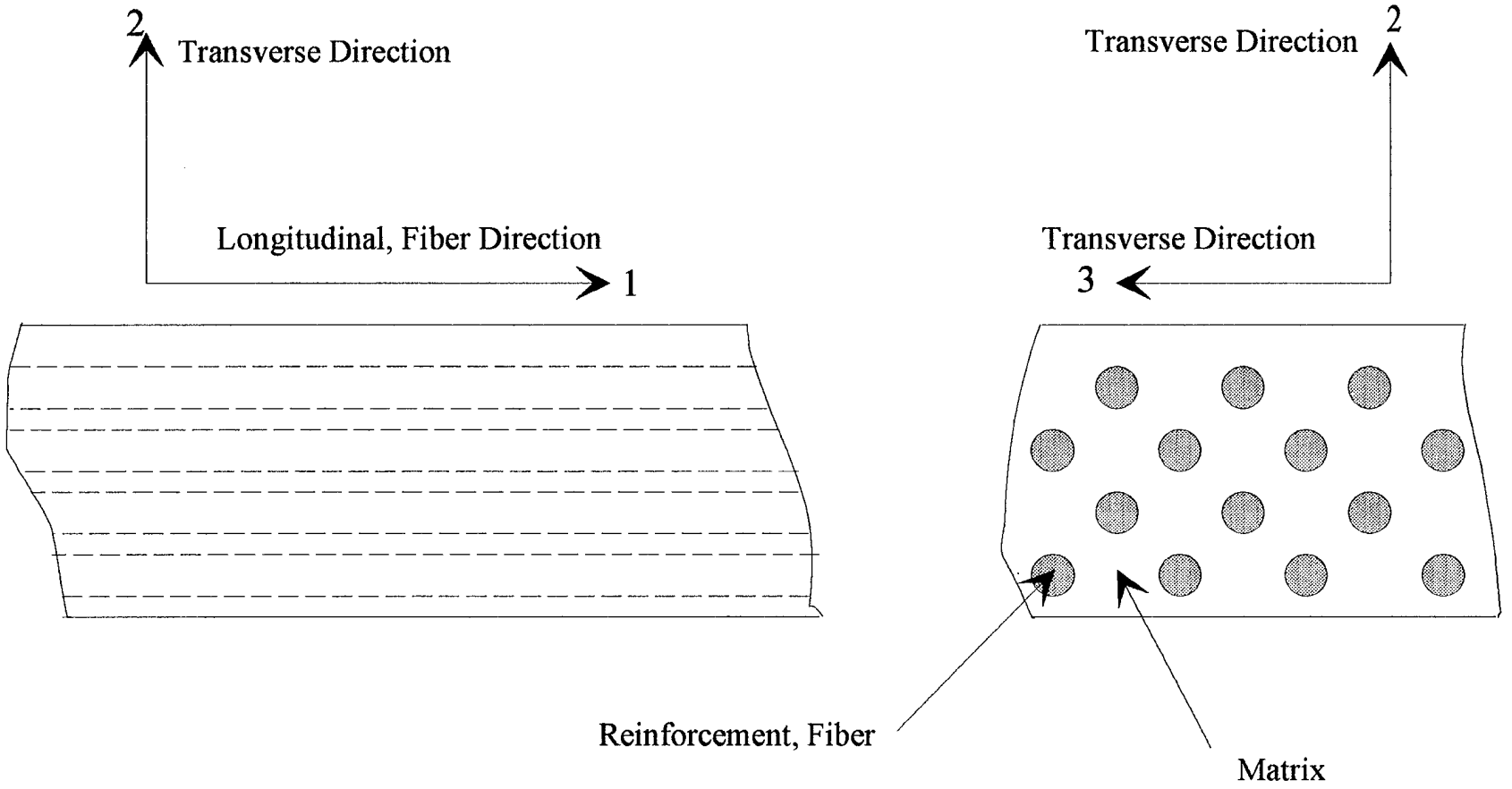

Figure 1. - Unidirectional Reinforced Material

importance of the interface has been recognized and much research has been undertaken to understand its influence. Most researchers consider this interface to be really a third material; Theocaris (1987), for example, calls it a "mesophase" and has devoted an entire book to its study.

Because of the complexity of incorporating the interface behavior into the analysis of composite materials, the bond is assumed to be perfect in a majority of cases, and designers must often rely on empirical data to ensure integrity.

2.2 Reinforced Materials Analysis

2.2.1 Perfect Composite. A common method used to analyze composite materials is to assume the bond between the fiber and matrix is perfect and that no local movement or deformations exist. If one further assumes that the reinforcement is arranged uniformly, and that each constituent is linear elastic, then macroscopic properties can be obtained by analyzing a unit cell or representative volume element (RVE) of material. This process of generating composite continuum properties is called a micro-mechanics analysis. Much research has been done in this area (see Hashin-Rosen, 1964 or Jones, 1975, for example). Most micro-mechanics analyses use mechanics of materials, elasticity, or energy methods to compute composite elastic constants and strengths in terms of volume fractions of constituents. Aboudi (1991) in his text on micro-mechanics uses a direct approach in what he calls the "method of cells" to obtain elastic constants. He has also examined constituent material nonlinearity using micro-mechanics. This work will be discussed in the next section. Because of the approximations in micro-mechanics analyses, empirical test data are sometimes used to supplement the theoretical calculation of elastic constants and strength data (Tsai, 1992).

Given an approximate material model, derived by micro-mechanics methods, the analyst may use well-established mechanics of materials, elasticity, or finite element techniques to analyze a composite structure constructed of the idealized material. This method works well for polymer-matrix composites, such as graphite fiber-reinforced epoxy, which is usually limited to linear-elastic deformations. Care still must be taken near "close outs" or "holes" where edge effects may be present, or in the case of highly loaded structures where material nonlinearities are indeed present.

2.2.2 Composite Nonlinear or Imperfect Interface Micro-Mechanics. Aboudi (1991) has developed a micro-mechanics approach to model composite materials with inelastic matrix materials and imperfect bonding. The approach is an extension of his "method of cells" which leads to average composite stress-strain relations. As with most micro-mechanics methods, the reinforcement is assumed to be in a periodic array, allowing the behavior of the

composite to be found from analyzing a unit cell of material. Briefly, his analysis of the unit cell includes imposition of traction and displacement boundary conditions on a square unit cell. The square cell is divided into four square sub-cells - three represent matrix material and one represents the fiber material. The displacements in each sub-cell are expanded in terms of distances from the center of the unit cell. The constituent strains are evaluated using the small strain tensor. Conditions of continuity of displacements and tractions are imposed between sub-cells, and an average stress theorem is used to derive composite stresses. With this method, Aboudi has examined sub-cell interfacial conditions with Mohr-Coulomb frictional behavior. This direct approach has advantages in that it can also be extended to inelastic composites, while a minimum potential energy-based approach cannot.

Aboudi has successfully modeled the inelastic behavior of metal-matrix composites, such as graphite-aluminum or boron-aluminum, for loading conditions given by uniaxial material-characterization tests. He also has used the same basic approach to determine effective properties for a composite whose fiber-matrix interfaces are completely debonded. These general methods are considered to be powerful, yet they are inadequate in modeling an interface with a complicated plasticity bond model that depends on the relative axial displacement of the fiber and matrix and the dilation of the bond zone. To accommodate such complicated interfacing material models and more generalized loading conditions, one must appeal to either a discrete treatment of the constituents or a hybrid approach that treats some behavior as composite while handling the complex material models discretely. A discussion of both follows.

2.2.3 Discrete Analyses. For reinforced-material structures where edge effects or material nonlinearities are important, a discrete model may be used to analyze performance. This method employs finite element techniques to model separately the behavior of fiber, matrix, and the bond interface. Continuum elements are used for fiber and matrix, and an interface element for the bond. See Figure 2 for a sketch of what a finite element mesh might look like in such a model.

There are no restrictions with this type of analysis except those associated with finite element theory itself. The matrix, fiber, and bond may be modeled with material nonlinearities, assuming that adequate material models exist. The problem with this type of analysis is that the cost to formulate and run the model limits the applicability. The simple reinforced prism in Figure 2 would require a large number of elements, the geometry of a real structure would be significantly more complex. This type of analysis is usually reserved for a sub-model of a joint, for example, while the structural designer uses a simpler more approximate analysis for the complete structure.

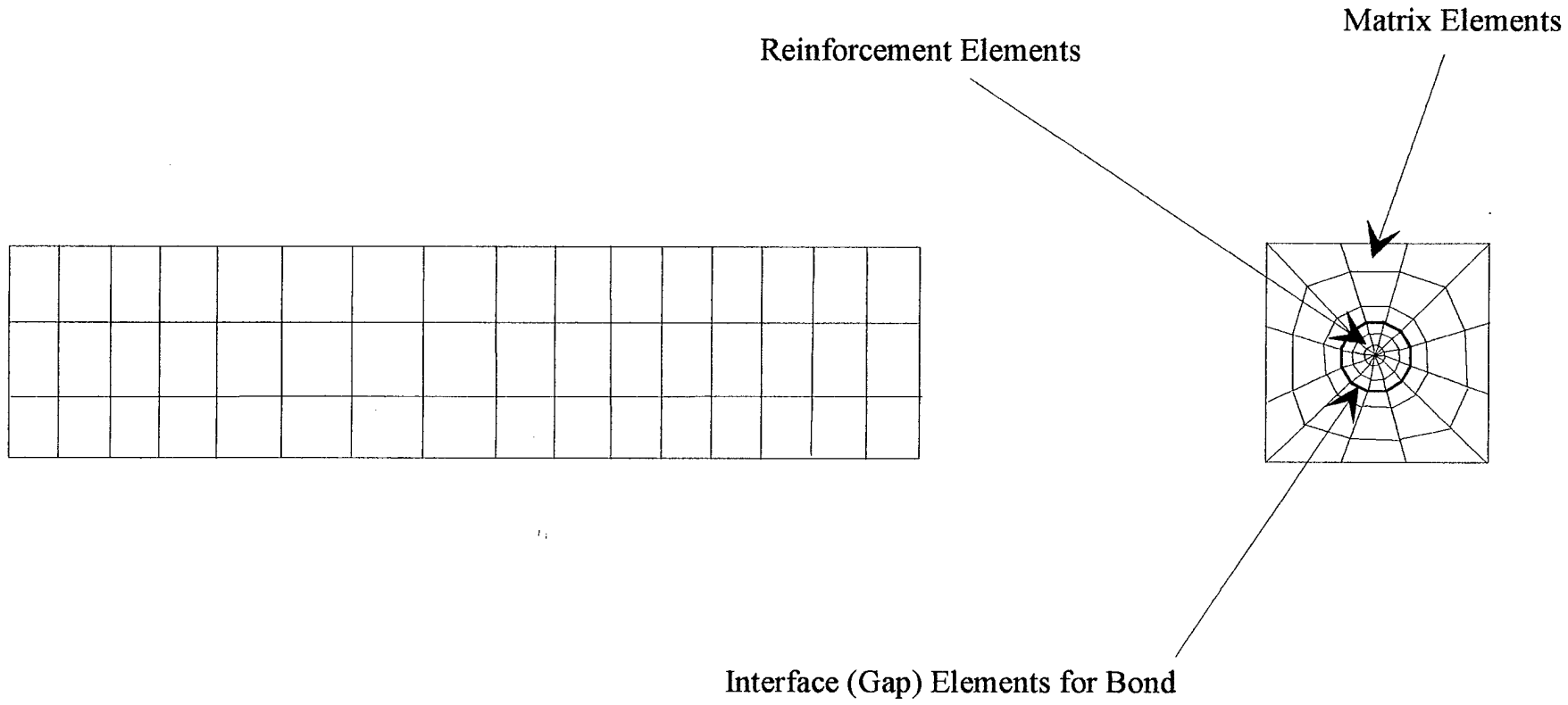

Figure 2. - Reinforced Prism Discrete Model

2.2.4 Composite Discrete Hybrid Analysis. There have been some analysis techniques developed that lie between a fully homogenous and a discrete analysis of reinforced materials. These hybrid analyses offer a compromise between the perfect composite assumption and the fully discrete treatment.

Pecknold and Hajali (1993) have integrated a three-dimensional, nonlinear, micro-mechanics materials model directly into a structural finite element analysis for laminated composites using standard displacement-based isoparametric elements. Their analysis technique has three levels: (1) a nonlinear micro-mechanics material model, (2) a sub-laminate model, and (3) a finite element model. The resulting twenty-node brick element was used to model the effects of nonlinear matrix behavior in the response of thick, axisymmetrically loaded cylinders. The local stress gradients at the fiber-matrix interfaces were not treated explicitly with this procedure, but in other respects the analysis scheme of the micro-mechanics model, integrated with the finite element procedure, is similar to that used in the present study.

Herrmann and Al-Yassin (1978) have developed a composite finite element analysis for reinforced-soil systems whose continuum element material properties reflect the response of the matrix material (soil), the reinforcing sheets, and their interaction. This composite representation explicitly models reinforcement slippage between constituents. This behavior is particularly important for soils where the bond results from friction and is weak. The technique involved introducing an additional nodal degree of freedom in the finite element scheme. For the plane strain case that was studied, the unknowns were composite x and y displacements and slippage (the relative displacement between the reinforcement and soil). This local slippage response was approximated as a continuous field variable. This approach, combined with the technique of integrating a micro-mechanics model with the finite element scheme, is used in the current research involving the development of a composite element that includes interface bond behavior.

3. COMPOSITE FIBER-REINFORCED ELEMENT INCLUDING BOND

3.1 Objectives and Assumptions

The objective of this work was to develop a composite finite element that is capable of including the nonlinear, elastic-plastic response of the bond between the reinforcing fibers and matrix material. Such an element is applicable to reinforced-concrete, ceramic, or carbon-matrix composites, and other weak or brittle matrix materials where the interface with the reinforcement cannot be assumed to be perfectly bonded.

Several important assumptions or restrictions are used in the development:

1. Plane strain - No composite strain in one of the directions transverse to the fiber.

2. Unidirectional reinforcement - Fibers are assumed to be parallel to one of the in-plane directions.

3. Linear elastic fiber-matrix - Fiber and matrix constituents are assumed to be isotropic and linear elastic.

These assumptions allow the development to focus on inclusion of bond without the added difficulties of three-dimensional geometry, angled reinforcement, or nonlinear fiber and matrix behavior. These effects can be addressed in future work once it is shown that the elastic-plastic bond response can be included in a composite representation.

3.2 Bond Model (Linear Elastic)

The bond model that is the key feature of this study is introduced here. It is a simplified version of the model developed by Herrmann and Cox (1992) for reinforced concrete. They studied the results of a large number of experiments designed to determine the bond behavior of reinforced concrete and, from this information, developed a comprehensive bond model. The model was conceived, tested, and shown to model the behavior of a concrete-reinforcement interface. The linear-elastic portion of the bond model is introduced here, as it is essential in understanding the composite material constitutive relations into which the bond model is to be embedded. The details of the simplified nonlinear model are described later. It should be noted that test data similar to that used to develop the concrete bond model exist for ceramic, glass, and metal-matrix composites (Makin, Warren, and Evans, 1992; and Valente, 1994), but as yet no elastic-plastic models have been developed. When suitable models are developed for these materials, and if they use the same basic framework as the Herrmann and Cox model, the composite finite element developed here could then be used to model structures made with them.

The bond model idealizes the bond zone, the interface between the reinforcement and matrix, as a region having zero thickness. Aboudi (1991) made similar assumptions when developing micro-mechanics relations for imperfect interfaces. The bond stresses are limited to a longitudinal shear stress, τ, and a normal stress component, σ; see Figure 3. The conjugate strains are:

$$q_1 = s/r_b \qquad \text{slip strain} \tag{3.1}$$

$$q_2 = \delta/r_b \qquad \text{dilation strain} \tag{3.2}$$

They are obtained by normalizing the axial slip, s, that is, the sliding of the reinforcement relative to the matrix, and the dilation, δ, of the bond layer. The bar radius, r_b, is used to render the bond model independent of reinforcing fiber size.

The linear-elastic portion of the law for bond developed by Herrmann and Cox has the following form:

$$\begin{Bmatrix} \tau \\ \sigma \end{Bmatrix} = \begin{bmatrix} d_{11} & d_{12} \\ d_{21} & d_{22} \end{bmatrix} \begin{Bmatrix} q_1 \\ q_2 \end{Bmatrix} \tag{3.3}$$

This is different from the simpler relation used by Aboudi which ignored dilation of the bond zone. The complete inelastic bond relations derived from Herrmann and Cox's work are presented in a later section.

3.3 Composite Element Including Bond

The composite finite element scheme includes an integrated composite micro-mechanics model. These composite relations are developed using energy methods and are defined in detail in Section 4. The resulting three-dimensional composite linear elastic stress-strain relations are:

$$\begin{Bmatrix} \sigma_x \\ \sigma_y \\ (1-\rho)\sigma_z \\ \tau_{xy} \\ \tau_{yz} \\ \tau_{xz} \\ \rho\sigma_f \\ 2\rho\tau \\ 2\rho\sigma^* \end{Bmatrix} = \begin{bmatrix} \quad \\ \quad \\ \quad \\ \quad \\ \quad \\ \quad \\ \quad \\ \quad \\ \quad \end{bmatrix} \begin{Bmatrix} \varepsilon_x \\ \varepsilon_y \\ \varepsilon_z \\ \gamma_{xy} \\ \gamma_{yz} \\ \gamma_{xz} \\ \varepsilon_f \\ s/r_b \\ \delta/r_b \end{Bmatrix} \tag{3.4}$$

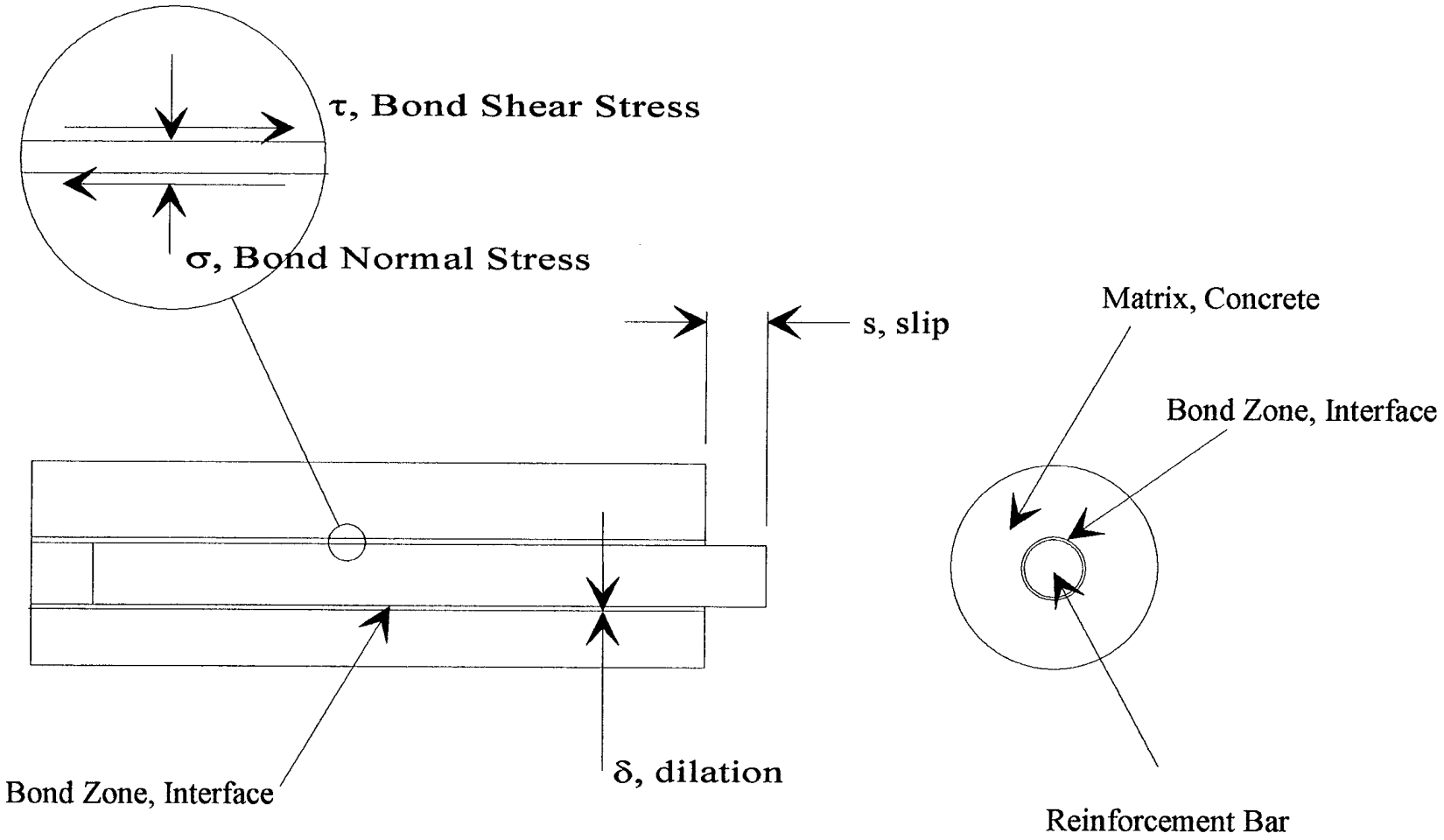

Figure 3. Bond Model Deformation and Stresses

where ρ is the fiber volume fraction and the stress-strain matrix [D] is a function of E_m, ν_m (the matrix elastic constants), E_f, ν_f (the fiber elastic constants), [d] (the bond elastic constants), and ρ. The definitions of the stresses and conjugate strains are developed and presented in Section 4 following the definition of the finite element displacement unknowns.

The stress-strain relations given above are used in a finite element scheme similar to that of Herrmann and Al-Yassin (1978) discussed earlier. The plane strain element that is developed is pictured in Figure 4. The displacement unknowns are defined as:

- u - x displacement of matrix
- u_f - x displacement of fiber
- v - composite y displacement
- δ - bond dilation

Note that the bond slip is given by

$$s = u - u_f$$

which is the relative displacement of the fiber and matrix.

Bilinear shape functions are used to describe both matrix and fiber displacement as nodal unknowns. Fiber displacement (instead of slip) is selected as a global unknown because it offers more flexibility in imposition of boundary conditions.

The slip and dilation, which are local to the interface of fiber and matrix, are modeled as continuous field variables as in the work of Herrmann and Al-Yassin (1978). With fiber displacement or slip as an unknown, one can account for bond breakdown and still ensure compatible inter-element fiber displacements. The use of dilation as a field variable is less straightforward; it is selected as an unknown as it simplifies implementation of the nonlinear bond model. It is recognized that for the linear elastic case it could be condensed out at the element level if one were willing to sacrifice dilation inter-element compatibility. This may not be a bad assumption in light of other approximations made in the micro-mechanics material model.

Given the composite constitutive relations and nodal unknown definitions, one can use well-established finite element formulation techniques such as the principle of virtual work or minimization of potential energy to develop a composite continuum finite element. It is also shown that this work can be extended to the nonlinear case of an elastic-plastic bond model using the same basic framework. Details of this development are discussed.

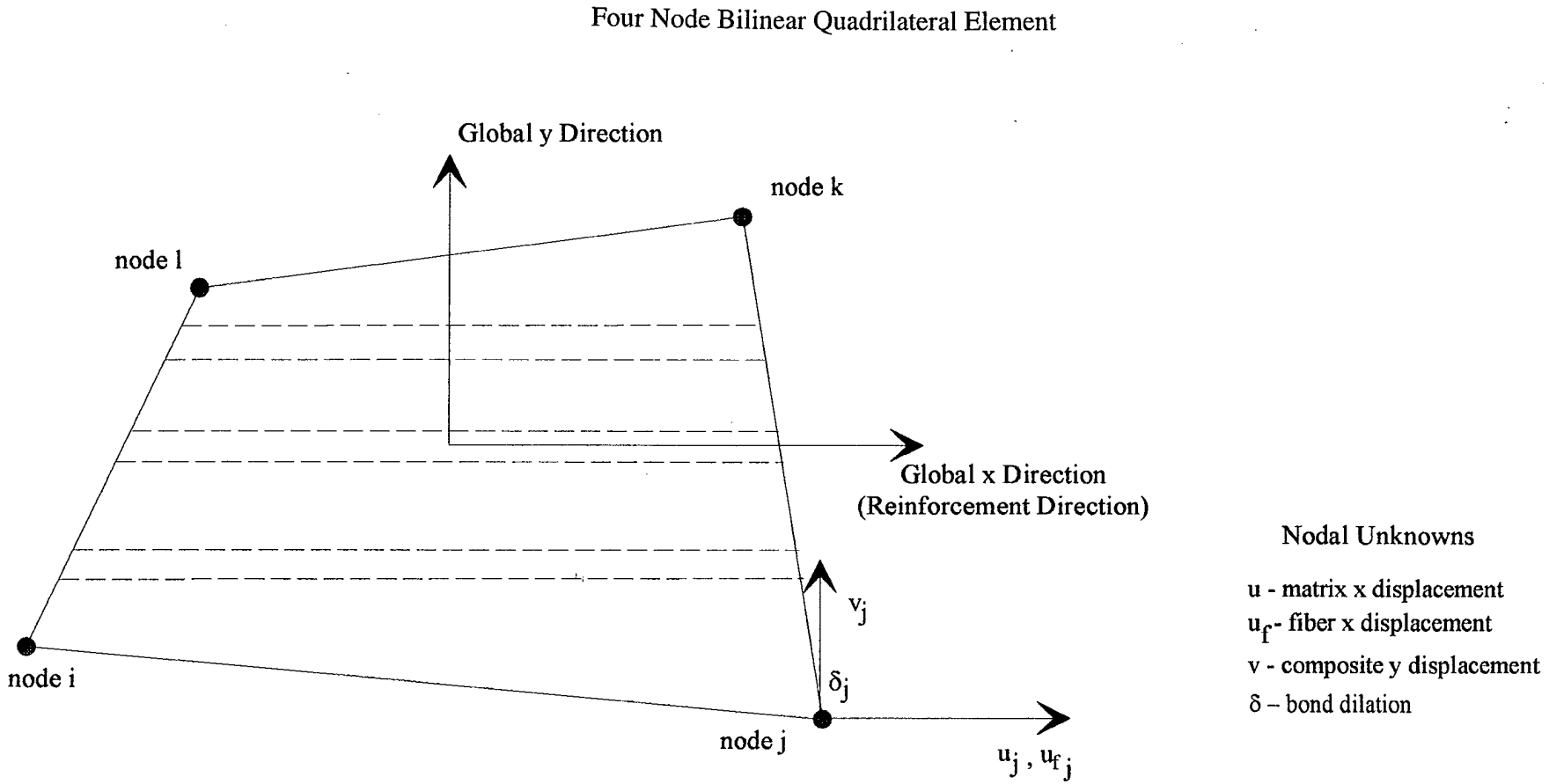

Figure 4. - Composite Plane Strain Global Unknowns

4. DEVELOPMENT OF LINEAR-EQUIVALENT HOMOGENEOUS COMPOSITE PROPERTIES INCLUDING BOND

The finite element scheme requires an equivalent homogeneous material model as discussed in Section 3. The basic goal is to find effective elastic moduli of the reinforced material in terms of the constituents elastic moduli and their geometry. The details of the development of a composite material model that consists of linear-elastic fiber, matrix, and bond follow.

Aboudi (1991), Bienveniste (1985), and others have performed micro-mechanics analyses with imperfect interfaces or elastic tangential slip. The micro-mechanics analysis of this study is different in that it includes the bond dilation effect in addition to slip.

The general method used is an extension of Hashin and Rosen's (1964) work. Deformation states of a representative volume element of material, whose strain energies are uncoupled, are examined. In each case, homogeneous properties are obtained by equating the virtual work of the composite system to that of the constituents. The virtual work approach is selected over equating strain energies because it is more general, allowing for a nonsymmetrical bond model, and it is also easily extended to the case of a nonlinear inelastic bond response, which is discussed later.

4.1 Hexagonal Pack Representative Volume Element

The fiber and matrix are assumed to be arranged in hexagonal pack as shown in Figure 5. This packing assumption was introduced by Hashin and Rosen. It allows one to consider the response of a single cylindrical representative volume element (RVE), which is a sample of the composite material that represents the composite on average. It contains the three phases of interest: fiber, bond, and matrix. The RVE is large compared to the constituent micro-structure, but small relative to the entire structure. This allows one to use continuum theories for scales larger than the RVE. Because the fiber lengths are much greater than the fiber diameters, the analysis can be further simplified by examining a very long cylindrical sample of material.

At this point, the response of the fiber, matrix, and bond is assumed to be linear elastic, thus the constituent material properties for the micro-mechanics model are:

E_m, ν_m - Young's modulus and Poisson's ratio for matrix material

E_f, ν_f - Young's modulus and Poisson's ratio for reinforcing fiber material

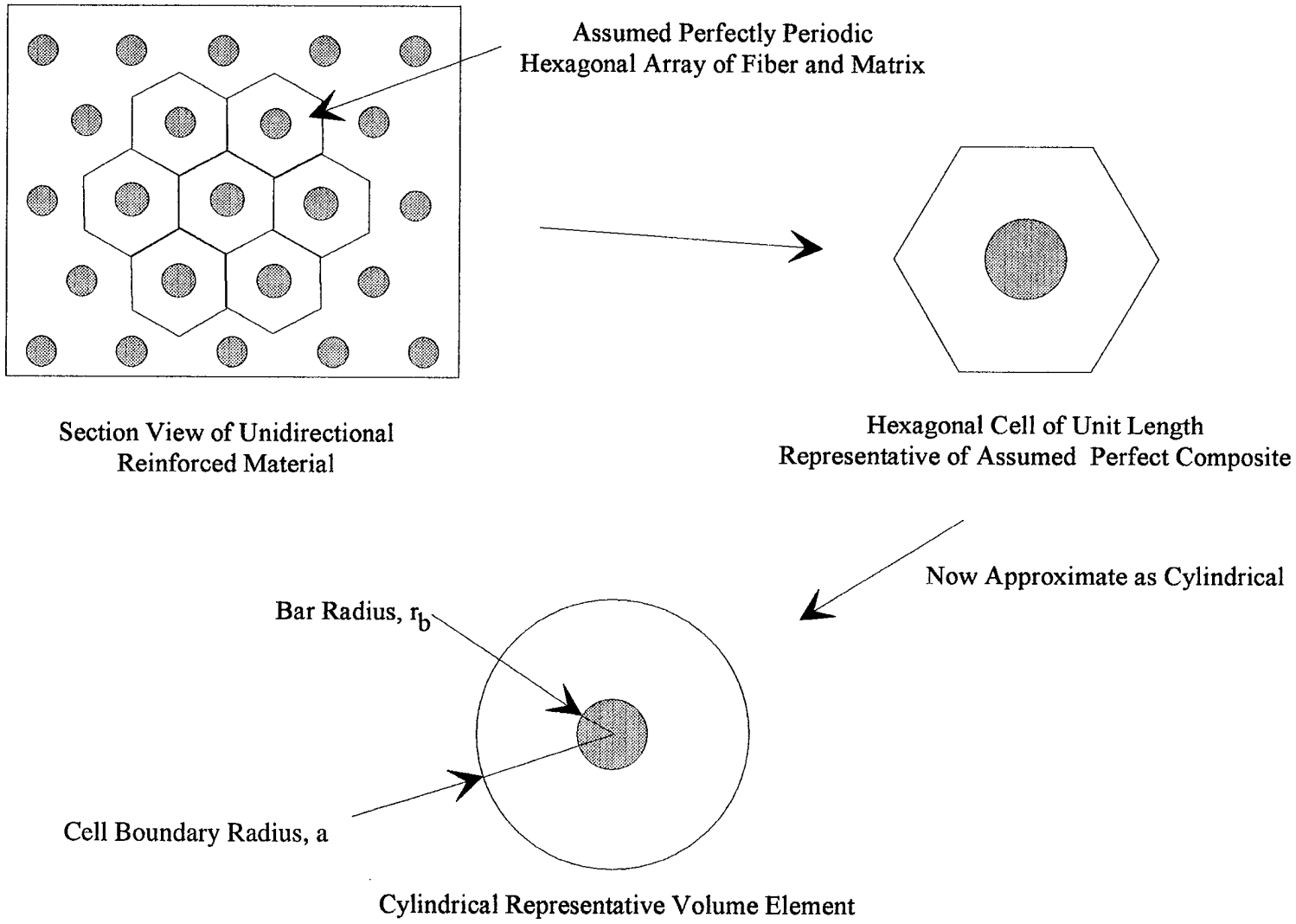

Figure 5. - Assumed Hexagonal Packed Composite

[D] - stress-strain matrix for the composite with elastic bond behavior

The composite section geometry parameter is defined using the fiber volume fraction

$$\rho = \frac{\pi r_b^2}{\pi a^2} \tag{4.1}$$

for the representative volume element, where r_b is the fiber radius and "a" is the outer diameter of the RVE. The ratio of the RVE outer radius to fiber radius is also used in the development and is defined as

$$\alpha = \frac{a}{r_b} \tag{4.2}$$

4.2 Unit Cell Deformations, Strain and Stress Definitions

Because of the peculiarities of the analysis that include bond slip and dilation, it is important to carefully define the RVE deformations that are shown in Figure 6. The displacements are:

u,v - average transverse displacement
w - average matrix displacement in the fiber direction
u_f - fiber displacement
s - slip
δ - average dilation of the bond zone

The composite strains that result from the micro-mechanics analysis are:

$\varepsilon_x, \varepsilon_y, \gamma_{xy}, \gamma_{xz}, \gamma_{yz}$ - composite strains

ε_z - average matrix strain (fiber direction)

ε_f - average axial fiber strain

q_1 - average slip strain

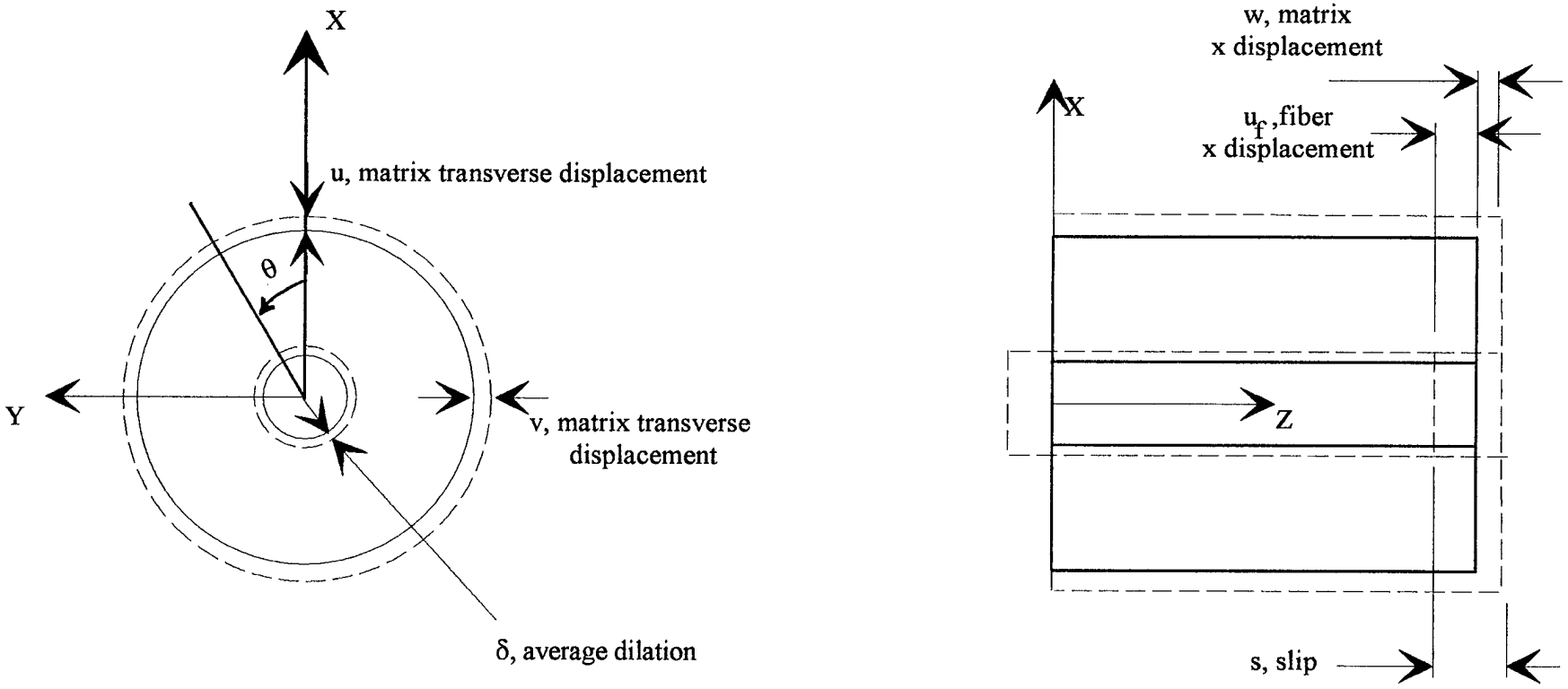

Figure 6. - RVE, Unit Cell Deformations

q_2 - average dilation strain

The conjugate stresses are:

$\sigma_x, \sigma_y, \tau_{xy}, \tau_{xz}, \tau_{yz}$ - composite stresses

σ_z - average matrix stress (fiber direction)

σ_f - average axial fiber stress

τ - average bond zone shear stress

σ - average bond zone normal stress

σ^* - fiber-bond-matrix equilibrium stress

The average stresses and strains are for one constituent, but are averaged over the entire unit cell. The composite properties are also average values, but are representative of the combination of constituents. Six deformation cases are used to determine the effective elastic constants in the matrix [D]. In each of these, a deformation is applied that results in a strain energy that is uncoupled. These deformations are used to determine boundary conditions for the field problems to be solved for the RVE. The solutions of these problems are used when equating the virtual work of the homogeneous material to that of the constituents.

4.3 Case A - XZ Shear

The first deformation case examined yields η_0, an effective shear modulus for pure shear of the RVE in the xz plane. Since no strain energy is developed at the bond surface, bond stress and strain does not enter this case. This deformation is shown in Figure 7. For the composite

$$\tau_{xz} = \eta_0 \gamma_{xz} \tag{4.3}$$

where τ_{xz} and γ_{xz} are composite stress and strain; the variable η_0 is the effective shear modulus sought.

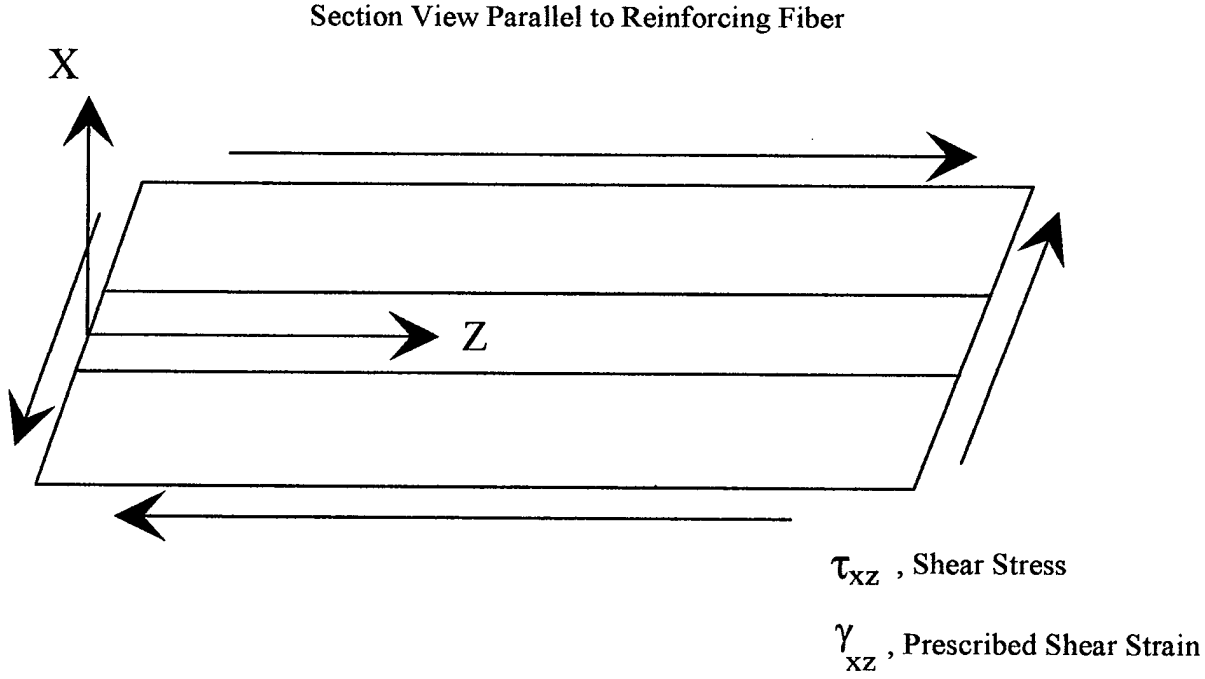

Figure 7. - Case A, Pure Shear in XZ Plane

The prescribed deformation is γ_{xz}, while all other strains are zero for this case. The axial displacement, u_z , at the boundary is approximated as:

$$u_{z|r=a} = f(a) \cos(\theta) \tag{4.4}$$

and similarly the fiber and matrix z direction displacements are written as:

$$u_{z_f} = f_f(r) \cos(\theta) \tag{4.5}$$

$$u_{z_m} = f_m(r) \cos(\theta) \tag{4.6}$$

The subscript "f" denotes fiber and "m" matrix. The above boundary condition, Equation 4.4, is applied to u_{zm} which results in :

$$f_m(a) = a\,\gamma_{xz} \tag{4.7}$$

Fiber and matrix interface compatibility and equilibrium require:

$$f_f(r_b) = f_m(r_b) \tag{4.8}$$

$$\tau_{xz_m}(r_b) = \tau_{xz_f}(r_b) \tag{4.9}$$

The deformation for either fiber or matrix, Equations 4.5 and 4.6, is written as:

$$u_{z_i} = f_i(r) \cos(\theta) \tag{4.10}$$

where i is either m or f. The strain-displacement relations in cylindrical coordinates reduce to:

$$\varepsilon_{rr_i} = \varepsilon_{\theta\theta_i} = \varepsilon_{zz_i} = \gamma_{rz_i} = 0 \tag{4.11}$$

$$\gamma_{rz_i} = \frac{df_i}{dr} \cos\theta \tag{4.12}$$

$$\gamma_{\theta z_i} = \frac{-f_i}{r} \sin\theta \tag{4.13}$$

Hooke's law for the fiber and matrix materials is written as:

$$\tau_{rz_i} = G_i \gamma_{rz_i} \tag{4.14}$$

$$\tau_{\theta z_i} = G_i \gamma_{\theta z_i} \tag{4.15}$$

The equilibrium equation reduces to:

$$\frac{\partial \tau_{rz_i}}{\partial r} + \frac{1}{r} \frac{\partial \tau_{\theta z_i}}{\partial \theta} + \frac{1}{r} \tau_{rz_i} = 0 \tag{4.16}$$

Equations 4.12, 4.13, 4.14, 4.15, and 4.16 form a complete set of elasticity equations. The solution to these equations is of the form

$$f_i = r^c \tag{4.17}$$

and is subject to the boundary conditions of Equations 4.7, 4.8, and 4.9, and the further condition that the result is finite at $r = 0$. The displacement solutions are:

$$u_{z_f} = A_f \; r\cos\theta \tag{4.18}$$

$$u_{z_m} = (A_m r + \frac{B_m}{r}) \cos\theta \tag{4.19}$$

where the arbitrary constants A_f, A_m, and B_m are found from the given boundary conditions. The results are found to be:

$$A_m = K_1 \gamma_{x_z} \tag{4.20}$$

$$B_m = a^2 K_2 \gamma_{x_z} \tag{4.21}$$

$$A_f = K_3 \gamma_{xz} \tag{4.22}$$

where

$$K_1 = \frac{(G_m/G_f+1)\alpha^2}{(\alpha^2-1)+(1+\alpha^2)G_m/G_f} \tag{4.23}$$

$$K_2 = (1 - K_1) \tag{4.24}$$

$$K_3 = [\alpha^2 (1 - K_1) + K_1] \tag{4.25}$$

with α defined previously in Equation 4.2 as the ratio of the matrix radius to fiber radius. G_m and G_f are the elastic shear moduli for the matrix and fiber, respectively. Given the displacement solution, one can determine strains and stresses for each constituent using Equations 4.12, 4.13, 4.14, and 4.15. To derive an expression for the desired effective homogeneous shear modulus, the virtual work of the equivalent composite homogeneous material is equated to that of the constituent materials, i.e.,

$$W_c = W_m + W_f \tag{4.26}$$

where W_c, the composite virtual work, is defined as:

$$W_c = \int_o^a \int_o^{2\pi} \tau_{xz} \Delta\gamma_{xz} \, r dr \, d\theta \tag{4.27}$$

and where $\Delta\gamma_{xz}$ is a virtual strain applied to the composite RVE. Likewise for the matrix and fiber:

$$W_m = \int_{r_b}^a \int_o^{2\pi} [\tau_{rz_m} \Delta\gamma_{rz_m} + \tau_{\theta z_m} \Delta\gamma_{\theta z_m}] r \, dr \, d\theta \tag{4.28}$$

$$W_f = \int_a^{r_b} \int_o^{2\pi} [\tau_{rz_f} \Delta\gamma_{rz_f} + \tau_{\theta z_f} \Delta\gamma_{\theta z_f}] r \, dr \, d\theta \tag{4.29}$$

The $\Delta\gamma_{rz_f}$, $\Delta\gamma_{\theta z_f}$, $\Delta\gamma_{rz_m}$, and $\Delta\gamma_{\theta z_m}$ virtual strains are written in terms of $\Delta\gamma_{xz}$. It has also been shown that τ_{rz_f}, $\tau_{\theta z_f}$, τ_{rz_m}, and $\tau_{\theta z_m}$ can be written in terms of γ_{xz} and the elastic constants from

the elasticity solution. Equating virtual work, as described in Equation 4.26, one can obtain the desired composite shear modulus, η_0:

$$\eta_0 = \frac{G_f K_3^3}{\alpha^2} + G_m \left[K_1^2 \left(1 - \frac{1}{\alpha^2}\right) + K_2^2(\alpha^2 - 1)\right] \tag{4.30}$$

Note that this homogeneous or composite shear modulus is a function of the elastic constants of the constituents and the volume fraction of each in the RVE.

4.4 Case B - YZ Shear

The next deformation case examined is pure shear in the yz plane. Because of the axisymmetry of the RVE, the results of this case are the same as for Case A

$$\tau_{yz} = \eta_0 \gamma_{yz} \tag{4.31}$$

where η_0 is given by equation Equation 4.30. Bond stress and slip are absent from this case also.

4.5 Case C - Change in Volume with Slip and Dilation

The next case considers the following deformations:

- s - slip
- δ - dilation
- ε_f - fiber axial strain
- ε_z - matrix strain (in fiber direction)
- ε_x - transverse strain
- ε_y - transverse strain

where $\varepsilon_x = \varepsilon_y = \varepsilon_1/2$, which corresponds to a change in diameter of the RVE. The deformation state is pictured in Figure 8. Recall how the strain for homogeneous isotropic materials may be decomposed into hydrostatic and deviatoric components. The present deformation case is analogous to the hydrostatic, or change in volume, component.

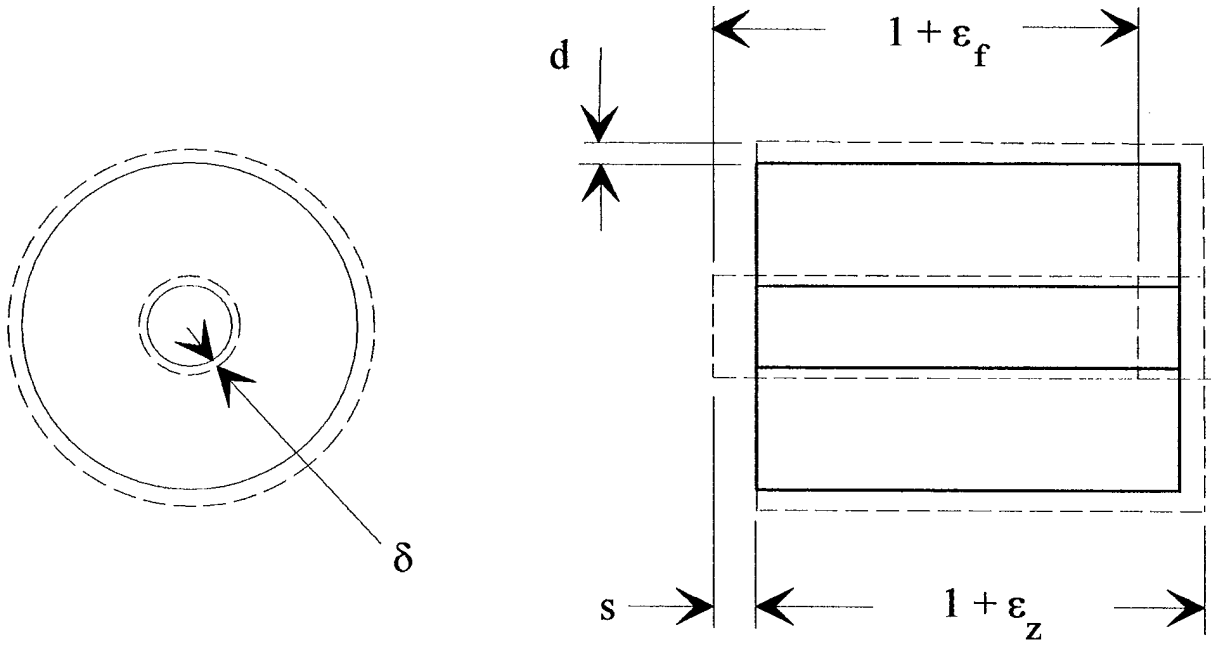

Figure 8. - Case C, Change in Volume with Slip and Dilation

The inclusion of dilation as a global degree of freedom requires that one of the constituent relations developed in this deformation case be a statement of equilibrium at the interface. A fictitious interface stress, σ^*, is introduced conjugate to the dilation strain. To aid in understanding this procedure, a simple analogous one-dimensional example is reviewed prior to introducing the much more complicated case (see Figure 9). For this simple bar problem, the dilation of the interface at the top of the bar, δ, and the deflection of the end of the bar, u, are the displacement unknowns. Virtual work is used to find the constitutive relations for F* and F, the conjugate stress quantities. If one then studies F*, it is seen that it is an equilibrium expression for the interface.

The bar strain and virtual strain are written as:

$$\varepsilon = (u - \delta)/l \tag{4.32}$$

$$\Delta\varepsilon = (\Delta u - \Delta\delta)/l \tag{4.33}$$

For simplicity, the bar's area is assumed to be unity and the interface constitutive relation is taken to be:

$$F_b = K_b\,\delta \tag{4.34}$$

The composite virtual work is equated to that of the constituents as is in the more complicated case,

$$W_c = W_{bar} + W_{bond}$$

$$W_c = F\Delta u + F^*\,\Delta\delta$$

$$W_{bar} = \int_0^l \Delta\varepsilon\, E\varepsilon\, dx$$

$$W_{bond} = K_b\,\delta\,(\Delta\delta)$$

where E is Young's modulus for the bar.

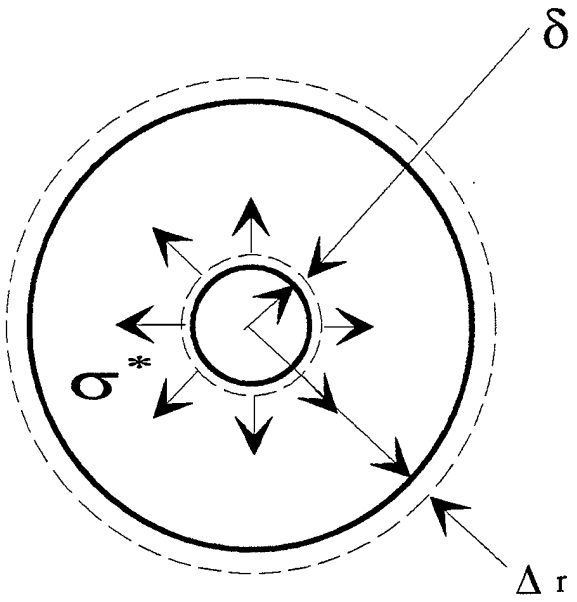

Dilation and Fictitious Interface Stress, σ^*

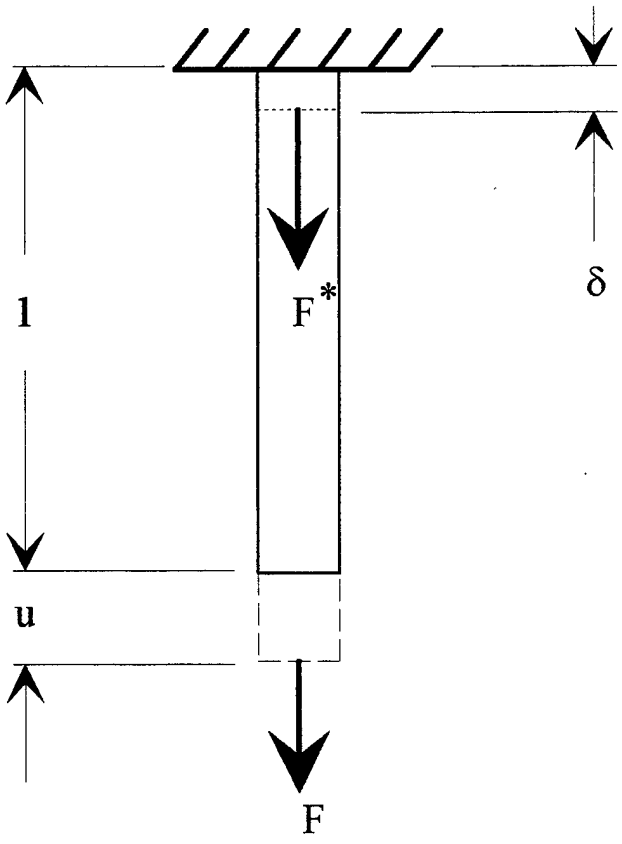

Figure 9. - Simple Bar Interface Example

Combining the above expressions, simplifying the results, and substituting the appropriate strain expressions, one finds:

$$[F - \frac{E}{l}(u-\delta)]\Delta u + [F^* + \frac{E}{l}(u-\delta) - K_b\,\delta]\Delta\delta = 0 \tag{4.35}$$

For arbitrary Δu and $\Delta\delta$, it follows that:

$$F = \frac{E}{l}(u-\delta) \tag{4.36}$$

which is the constitutive relation for the bar portion of the composite in terms of u and δ, and

$$F^* = E\,\frac{(u-\delta)}{l} - K_b\,\delta \tag{4.37}$$

which upon inspection reveals that F* should be zero for equilibrium at the interface. One may question where to set F* to zero to ensure equilibrium if the constituent relations of Equations 4.36 and 4.37 were to be used in a finite element scheme. To show how this is achieved, one simply writes the expression for potential energy for the bar-interface composite, and the resulting energy minimization process accompanying the finite element development results in F* being set to zero. (Recall that the finite element equations are derived by taking derivatives of the potential energy with respect to u and δ.)

Having introduced the concept of a fictitious stress at the interface, we may now proceed with analyzing the deformation case pictured in Figure 8. The prescribed RVE deformations are s, δ, ε_f, ε_z and

$$\varepsilon_x = \varepsilon_y = \varepsilon_1/2 \tag{4.38}$$

The fiber displacement is $u_f = w - s$, and the fiber strain is:

$$\varepsilon_f = \varepsilon_z - \frac{ds}{dz} \tag{4.39}$$

In the radial displacement of the boundary of the RVE, d needs to be related to the prescribed strain in the x and y directions given above. To calculate d, one equates the changes in volume:

$$\pi a^2 (\varepsilon_x + \varepsilon_y) = 2\pi a(d) \tag{4.40}$$

Using Equation 4.38, one finds

$$d = a \frac{\varepsilon_1}{2} \tag{4.41}$$

which is the desired boundary displacement in terms of the radial strain.

As in Case A, one uses the elasticity relations for a long axisymmetric cylinder to calculate each constituent's stress and strain that result from the prescribed RVE deformations.

Conditions of axisymmetric deformation and the RVE being long lead to the assumptions of no changes in the θ and z direction. Radial direction equilibrium then gives:

$$\frac{\partial \sigma_r}{\partial r} + \frac{\sigma_r - \sigma_\theta}{r} = 0 \tag{4.42}$$

The strain displacement relations (with constant ε_z) are:

$$\varepsilon_r = \frac{du}{dr}, \quad \varepsilon_\theta = \frac{u_r}{r} \tag{4.43}$$

Hooke's Law for the assumed linear-elastic, isotropic material is:

$$\begin{aligned} \sigma_r &= (\lambda + 2\mu)\varepsilon_r + \lambda \varepsilon_\theta + \lambda \varepsilon_z \\ \sigma_\theta &= (\lambda + 2\mu)\varepsilon_\theta + \lambda \varepsilon_r + \lambda \varepsilon_z \end{aligned} \tag{4.44}$$

The displacement formulation is obtained by substituting Equations 4.43 into 4.44 and then the subsequent results into the equilibrium Equation 4.42

$$\frac{d^2 u_r}{dr^2} + \frac{1}{r}\frac{du_r}{dr} - \frac{u_r}{r^2} = 0 \tag{4.45}$$

which holds for either matrix, m, or fiber, f. This second order, ordinary differential equation has a general solution of the form:

$$u_r = c_1 r + \frac{c_2}{r} \tag{4.46}$$

The radial displacement for the matrix is:

$$u_{r_m} = c_{1_m} r + c_{2_m} \frac{1}{r} \tag{4.47}$$

The radial displacement for the fiber reduces to:

$$u_{r_f} = c_{1_f} \; r \tag{4.48}$$

because the solution must be bounded at r = 0. The strain displacement relations are written in terms of these displacement functions and the prescribed axial deformations. For the matrix:

$$\varepsilon_{r_m} = c_{1_m} - c_{2_m} \frac{1}{r^2}$$

$$\varepsilon_{\theta_m} = c_{1_m} + c_{2_m} \frac{1}{r^2} \tag{4.49}$$

$$\varepsilon_{z_m} = \varepsilon_z$$

and for the fiber:

$$\varepsilon_{r_f} = c_{1_f}$$

$$\varepsilon_{\theta_f} = c_{1_f} \tag{4.50}$$

$$\varepsilon_{z_f} = \varepsilon_f = \varepsilon_z - \frac{ds}{dz}$$

The boundary and interface conditions are now defined to complete the elasticity problem. For the boundary of the RVE from Equation 4.41:

$$u_{r_m}\big|_a = d = a \; \frac{\varepsilon_1}{2} \tag{4.51}$$

For the interface, equilibrium and continuity yield:

$$\sigma_{r_m}\big|_{r_b} = \sigma_{r_f}\big|_{r_b}$$

$$u_{r_m}\big|_{r_b} = u_{r_f}\big|_{r_b} + \delta \tag{4.52}$$

where δ is the average RVE bond dilation.

This elasticity problem is now solved for c_{1m}, c_{2m}, and c_{1f}. Mathematica (1995) was employed to check the algebra involved in the solutions with the following results:

$$\begin{aligned} c_{1f} &= K_6\varepsilon_1 + K_7\delta/r_b + K_8\varepsilon_z + K_9\varepsilon_f \\ c_{1m} &= K_{10}\varepsilon_1 + K_{11}\delta/r_b + K_{12}\varepsilon_z + K_{13}\varepsilon_f \\ c_{2m} &= a^2(K_{14}\varepsilon_1 - K_{11}\delta/r_b - K_{12}\varepsilon_z - K_{13}\varepsilon_f) \end{aligned} \tag{4.53}$$

where

$$\begin{aligned} K_4 &= (\mu_m(\alpha^2+1) + \lambda_m)/(\alpha^2-1) \\ K_5 &= 1/(2(K_4 + \mu_f + \lambda_f)) \\ K_6 &= \alpha^2\,(K_4 - \mu_m)K_5 \\ K_7 &= -2\,K_4K_5 \\ K_8 &= \lambda_m\,K_5 \\ K_9 &= -\lambda_f\,K_5 \end{aligned} \tag{4.54}$$

$$K_{10} = \frac{\alpha^2-2K_6}{2(\alpha^2-1)}$$

$$K_{11} = \frac{-(1+K_7)}{(\alpha^2-1)}$$

$$\begin{aligned} K_{12} &= -K_8/(\alpha^2-1) \\ K_{13} &= -K_9/(\alpha^2-1) \\ K_{14} &= \frac{1}{2} - K_{10} \end{aligned}$$

The algebra makes these expressions appear complicated but once again they are simply functions of the constituent elasticity constants λ and μ, and the quantity α which is related to the volume fraction of each of the constituents.

What remains is to equate the virtual work of the desired composite model to that of the constituents. For this case:

$$W_{comp} = W_{fiber} + W_{matrix} + W_{bond} \tag{4.55}$$

For the composite, the work is:

$$W_{comp} = \pi a^2 \{\sigma_x \Delta\varepsilon_x + \sigma_y \Delta\varepsilon_y +$$

$$(1-\rho)\sigma_z \Delta\varepsilon_z + \rho\sigma_f \Delta\varepsilon_f + \frac{2\pi r_b}{\pi a^2} (\tau \Delta s + \sigma^* \Delta\delta)\} \tag{4.56}$$

Some important things to note in the preceding equation are the volume fraction quantities in front of the matrix, fiber, and bond terms and that the x and y subscripted terms are for the composite. Note the inclusion of σ^*, the fictitious composite bond stress, introduced previously with the help of the simple bar example. Recall that $\varepsilon_x = \varepsilon_y = \varepsilon_1/2$, and so Equation 4.56 now is written as:

$$W_{comp} = \pi a^2 \{\sigma_1 \Delta\varepsilon_1 + (1-\rho)\sigma_z \Delta\varepsilon_z + \rho\sigma_f \Delta\varepsilon_f + \frac{2\pi r_b}{\pi a^2} (\tau \Delta s + \sigma^* \Delta\delta)\} \tag{4.57}$$

The fiber virtual work is written as:

$$W_{fiber} = \int_0^{r_b} \int_0^{2\pi} (\sigma_{rf} \Delta\varepsilon_{rf} + \sigma_{\theta f} \Delta\varepsilon_{\theta f} + \sigma_f \Delta\varepsilon_f)\, r dr d\theta \tag{4.58}$$

The bond virtual work is:

$$W_{bond} = 2\pi r_b (\tau \Delta s + \sigma \Delta\delta) \tag{4.59}$$

The matrix virtual work is:

$$W_{matrix} = \int_{r_b}^{a} \int_{o}^{2\pi} (\sigma_{r_m} \Delta\varepsilon_{r_m} + \sigma_{\theta_m} \Delta\varepsilon_{\theta_m} + \sigma_{z_m} \Delta\varepsilon_{z_m})\, r dr d\theta \tag{4.60}$$

The constituent virtual strains in these expressions are found using the strain relations of Equations 4.49 and 4.50. For example, for the radial strain in the matrix, one finds:

$$\Delta\varepsilon_{r_m} = \Delta c_{1m} - \Delta c_{2m} \frac{1}{r^2}$$

$$\Delta c_{1_m} = K_{10}\, \Delta\varepsilon_1 + K_{11} \frac{\Delta\delta}{r_b} + K_{12}\, \Delta\varepsilon_z + K_{13}\, \Delta\varepsilon_f$$

$$\Delta c_{2_m} = a^2 (K_{14}\, \Delta\varepsilon_1 - K_{11} \frac{\Delta\delta}{r_b} - K_{12}\, \Delta\varepsilon_z - K_{13}\, \Delta\varepsilon_f)$$

and so on and so forth for $\Delta\varepsilon_{\theta_m}$, $\Delta\varepsilon_{r_f}$, and $\Delta\varepsilon_{\theta_f}$.

Mathematica was once again employed to do the algebra and find the resulting constitutive relations; details are to be found in Mello (1996). The final results are:

$$\sigma_1 = \eta_1\, \varepsilon_1 + \eta_2\, \varepsilon_z + \eta_3\, \varepsilon_f + \eta_4\, \delta/r_b \tag{4.61}$$

$$\sigma_z = \frac{1}{(1-\rho)} [\eta_2\, \varepsilon_1 + \eta_5\, f_z + \eta_6\, \varepsilon_f + \eta_7\, \delta/r_b] \tag{4.62}$$

$$\sigma_f = \frac{1}{\rho} [\eta_3\, \varepsilon_1 + \eta_6\, \varepsilon_z + \eta_8\, \varepsilon_f + \eta_9\, \delta/r_b] \tag{4.64}$$

$$\tau = [d_{11}\, s/r_b + d_{12}\, \delta/r_b] \tag{4.65}$$

$$\sigma^* = \frac{2}{\alpha^2} [\eta_4\, \varepsilon_1 + \eta_7\, \varepsilon_z + \eta_8\, \varepsilon_f + \eta_{10}\, \delta/r_b] + [d_{21}\, s/r_b + d_{22}\, \delta/r_b] \tag{4.66}$$

As explained before, the quantity σ^* is an equilibrium equation for the interface and is set to zero during the process of developing the finite element equations for the composite element based on these material relations. The η's are the desired effective moduli; detailed expressions are to be found in the Mathematica Notebook given in Mello (1996). (The expressions are in FORTRAN

format and were pasted directly from Mathematica into the FORTRAN finite element program.) The expression for η_1 given below is representative of these results:

$$\begin{aligned}\eta_1 = \; & 4\,(\mu_m K_{10}^2 - \mu_m K_{14}^2 + \lambda_m K_{10}^2 \\ & + a^2 \mu_m K_{14}^2 / r_b^2 - r_b^2 \mu_m K_{10}^2 / a^2 \\ & + r_b^2 \mu_f K_6^2 / a^2 + r_b^2 \lambda_f K_6^2 / a^2 \\ & - r_b^2 \lambda_m K_{10}^2 / a^2\end{aligned}$$

The parameter η_1 given above, as are all the others, is a function of μ_m, λ_m, μ_f, λ_f, r_b and "a" only.

Finally, note that Equation 4.61 relates the composite stress, σ_1, to the composite deformations. Recall that σ_1 and ε_1 are the radial stress and strain. What is desired ultimately are σ_x and σ_y. These are found by superimposing the results of Cases C and D, which follow.

4.6 Case D - Cross Section Distortion

The next deformation case is shown in Figure 10; for this case the fiber strain, ε_f, and the matrix strain (in the fiber direction), ε_z, are zero, which also implies no slip. The dilation is also taken to be zero. Recall that this is the average value for the RVE. The cross section is distorted such that

$$\varepsilon_x = -\varepsilon_y = \varepsilon_2/2 \tag{4.67}$$

where ε_2 is the imposed strain, and the deflections in the x and y directions are:

$$u_x = \frac{\varepsilon_2}{2}\, x$$

$$u_y = -\frac{\varepsilon_2}{2}\, y \tag{4.68}$$

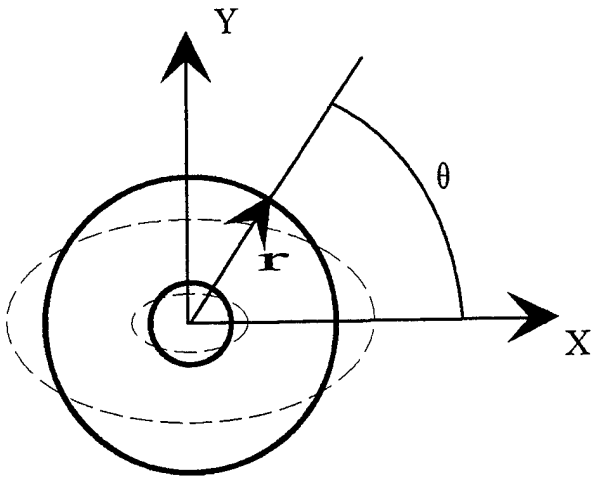

Figure 10. - Case D, Cross Section Distortion

This deformation is similar to the direct components of deviatoric strain when a material response is divided into hydrostatic and deviatoric components. Recall that Case C was analogous to a change in volume strain. This deformation of the RVE is the nonaxisymmetric plane strain behavior of a thick cylinder. In terms of cylindrical coordinates, it is observed that the radial displacement, u_r, is a symmetrical function of θ and the tangential displacement, u_θ, is an antisymmetric function of θ. For this type of periodic behavior one seeks solutions of the form

$$u_r = f(r)\cos(n\theta)$$

$$u_\theta = g(r)\sin(n\theta) \qquad (0 \le \theta \le 2\pi) \tag{4.69}$$

where $n = 2$. The deflection at the boundary of the RVE likewise is approximated as:

$$u_r\big|_a = f(a)\cos(2\theta)$$

$$u_\theta\big|_a = g(a)\sin(2\theta) \tag{4.70}$$

The u_r and u_θ displacements are expressed in terms of the x and y coordinates and the prescribed deformations of Equation 4.68 with the appropriate transformation to cylindrical coordinates, which is:

$$x = r\cos(\theta)$$

$$y = r\sin(\theta) \tag{4.71}$$

The radial displacement is written as:

$$u_r = \frac{\varepsilon_2}{2} r\cos(2\theta) \tag{4.72}$$

using the appropriate substitutions and trigonometric identities. For the outer boundary of the RVE at r = a, one finds

$$u_r\big|_a = \frac{\varepsilon_2}{2} a\cos(2\theta) \tag{4.73}$$

which implies that

$$f(a) = \frac{\varepsilon_2}{2} a \tag{4.74}$$

on the boundary. One can likewise show that:

$$u_\theta = -\frac{\varepsilon_2}{2} r\sin 2\theta \tag{4.75}$$

and

$$g(a) = -\frac{\varepsilon_2}{2} a \tag{4.76}$$

The equilibrium equations for fiber and matrix for the elasticity problem associated with this deformation case are:

$$\frac{\partial \sigma_r}{\partial r} + \frac{1}{r} + \frac{\partial \tau_r \theta}{\partial \theta} + \frac{\sigma_r - \sigma_\theta}{r} = 0.0 \tag{4.77}$$

$$\frac{\partial \tau_r}{\partial r} + \frac{1}{r}\frac{\partial \sigma_\theta}{\partial \theta} + \frac{2}{r}\tau_{r\theta} = 0.0 \tag{4.78}$$

Likewise the strain-displacement relations are:

$$\varepsilon_r = \frac{\partial u_r}{\partial r} \qquad \varepsilon_\theta = \frac{1}{r}\frac{\partial u_\theta}{\partial \theta} + \frac{u_r}{r}$$

$$\gamma_{r\theta} = \frac{1}{r}\frac{\partial u_r}{\partial \theta} + \frac{\partial u_\theta}{\partial r} - \frac{u_\theta}{r}$$

$$\varepsilon_z = \gamma_{\theta z} = \gamma_{rz} = 0 \tag{4.79}$$

for both the fiber and the matrix. The constitutive relations are:

$$\sigma_r = \frac{E}{(1+\nu)(1-2\nu)}\left[(1-\nu)\varepsilon_r + \nu\,\varepsilon_\theta\right]$$

$$\sigma_\theta = \frac{E}{(1+\nu)(1-2\nu)}\left[(1-\nu)\varepsilon_\theta + \nu\,\varepsilon_r\right]$$

$$\sigma_z = \frac{E}{(1+\nu)(1-2\nu)}\left[\nu\,(\varepsilon_r + \varepsilon_\theta)\right]$$

$$\tau_{r\theta} = \frac{E}{2(1+\nu)}\gamma_{r\theta}$$

$$\tau_{\theta z} = \tau_{rz} = 0 \tag{4.80}$$

where E and ν are the appropriate Young's modulus and Poisson's ratio for fiber or matrix depending on the solution sought. The displacement solution for the matrix is found to be:

$$f_m = C_{1_m} r^3 + C_{2_m} r + C_{3_m}\frac{1}{r} + C_{4_m}\frac{1}{r^3}$$

$$g_m = -\left(\frac{3-2\nu}{2\nu}\right) C_{1_m} r^3 - C_{2_m} r + \frac{2\nu-1}{2(1-\nu)} C_{3_m} \frac{1}{r} + C_{4_m} \frac{1}{r^3} \tag{4.81}$$

and for the fiber whose solution must be bounded at r=0:

$$f_f = C_{1_f} r^3 + C_{2_f} r$$

$$g_f = -\left(\frac{3-2\nu}{2\nu}\right) C_{1_f} r^3 - C_{2_f} r \tag{4.82}$$

The boundary condition at the RVE outer radius "a" is from Equations 4.74 and 4.76:

$$f_m(a) = a \frac{\varepsilon_2}{2}$$

$$g_m(a) = -a \frac{\varepsilon_2}{2} \tag{4.83}$$

Assuming perfect bond, the interface conditions are:

$$u_{r_f}(r_b) = u_{r_m}(r_b)$$

$$u_{\theta_f}(r_b) = u_{\theta_m}(r_b)$$

$$\sigma_{r_f}(r_b) = \sigma_{r_m}(r_b)$$

$$\tau_{r\theta_f}(r_b) = \tau_{r\theta_m}(r_b) \tag{4.84}$$

These conditions result in six equations which are used to solve for the constants C_{1_m}, C_{2_m}, C_{3_m}, C_{4_m}, C_{1_f}, and C_{2_f} of the displacement solution given in Equations 4.81 and 4.82.

Attempts to solve this set algebraically with the symbolic program Mathematica resulted in terribly complicated algebra. Since all results are to be implemented numerically, in a FORTRAN program, it was decided to leave the solution of this system to a numerical linear algebra technique such as Gaussian elimination.

As in the other cases previously studied, the effective elastic moduli are obtained by equating the composite virtual work to that of the constituents for the prescribed deformation:

$$W_c = W_f + W_m \tag{4.85}$$

For the composite

$$W_c = \pi a^2 [\sigma_x \Delta\varepsilon_x + \sigma_y \Delta\varepsilon_y]$$

or

$$W_c = \pi a^2 \sigma_2 \frac{\Delta\varepsilon_2}{2} \tag{4.86}$$

for the deformation prescribed, where Δ again denotes virtual quantities. For the fiber the virtual work is:

$$W_f = \int_o^{r_b} \int_o^{2\pi} [\sigma_{r_f} \Delta\varepsilon_{r_f} + \sigma_{\theta_f} \Delta\varepsilon_{\theta_f} + \tau_{r\theta_f} \Delta\gamma_{r\theta_f}] \, r dr d\theta \tag{4.87}$$

and for the matrix:

$$W_m = \int_{r_b}^{a} \int_o^{2\pi} [\sigma_{r_m} \Delta\varepsilon_{r_m} + \sigma_{\theta_m} \Delta\varepsilon_{\theta_m} + \tau_{r\theta_m} \gamma_{r\theta_m}] \, r dr d\theta \tag{4.88}$$

Equating the virtual work is carried out in terms of the six arbitrary constants (which are determined numerically). The result is:

$$\sigma_2 = \eta_{11} \varepsilon_2 \tag{4.89}$$

where η_{11} is the effective modulus sought for this deformation case. The modulus η_{11} is found to be:

$$\begin{aligned} \eta_{11} = \; & (\beta_1 C1_m^2 + \beta_2 C1_m C2_m + \beta_3 C1_m C2_m \\ & + \beta_4 C1_f^2 + \beta_5 C1_f C2_f + \beta_6 C2_f^2 \\ & + \beta_7 C3_m C4_m + \beta_8 C4_m^2 + \beta_9 C3_m^2 \\ & + \beta_{10} C2_m^2)/D \end{aligned} \tag{4.90}$$

where D is

$$D = 2\alpha^8 \nu_f^2 (1 + \nu_f)(\nu_m - 1)^2 \nu_m^2 (1 + \nu_m) \tag{4.91}$$

and the betas are

$$\beta_1 = 3\alpha^6 (-1 + \alpha^6)E_m \nu_f^2 (1 + \nu_f)(3 - 2\nu_m)(-1 + \nu_m)^2$$

$$\beta_2 = 12\alpha^6 (-1 + \alpha^4)E_m \nu_f^2 (1 + \nu_f)(-1 + \nu_m)^2 \nu_m$$

$$\beta_3 = 6\alpha^6 (-1 + \alpha^2)E_m \nu_f^2 (1 + \nu_f) \nu_m (1 - 3\nu_m + 2\nu_m^2)$$

$$\beta_4 = 3\alpha^6 E_f (3 - 2\nu_f)(-1 + \nu_m)^2 \nu_m^2 (1 + \nu_m)$$

$$\beta_5 = 12\alpha^6 E_f \nu_f (-1 + \nu_m)^2 \nu_m^2 (1 + \nu_m)$$

$$\beta_6 = 8\alpha^6 E_f \nu_f^2 (-1 + \nu_m)^2 \nu_m^2 (1 + \nu_m)$$

$$\beta_7 = 12\alpha^2 (-1 + \alpha^4)E_m \nu_f^2 (1 + \nu_f)(1 - \nu_m) \nu_m^2$$

$$\beta_8 = 24 (-1 + \alpha^6)E_m \nu_f^2 (1 + \nu_f)(-1 + \nu_m)^2 \nu_m^2$$

$$\beta_9 = \alpha^4 (-1 + \alpha^2)E_m \nu_f^2 (1 + \nu_f)(3 - 2\nu_m) \nu_m^2$$

$$\beta_{10} = 8\alpha^6(-1 + \alpha^2)E_m \nu_f^2(1 + \nu_f)(-1 + \nu_m)^2 \nu_m^2 \tag{4.92}$$

which are basically the coefficients of the arbitrary constant C's. The six equations that result from Equations 4.81 and 4.82 are:

$$C_{1_f} + C_{2_f} = C_{1_m} + C_{2_m} + C_{3_m} + C_{4_m} \tag{4.93a}$$

$$C_{1_f} - C_{2_f} - 3\,C_{1_f}\,/\,2\nu_f =$$

$$- C_{2_m} + C_{4_m} + C_{1_m}\,(-3 + 2\,\nu_m)/2\nu_m$$

$$+ C_{3_m}\,(-1 + 2\nu_m)\,/\,(2 - 2\,\nu_m) \qquad (4.93b)$$

$$C_{2_f}\,E_f\,/\,(1 + \nu_f) =$$

$$E_m\,(-C_{2_m} + C_{3_m} + 3C_{4_m} + C_{2_m}\,\nu_m - 3\,C_{4_m}\,\nu_m)\,/\,(-1 + \nu_m^2) \qquad (4.93c)$$

$$-E_f\,(3\,C_{1_f} + 2C_{2_f}\,\nu_f)\,/\,(2\,\nu_f\,(1 + \nu_f)) =$$

$$E_m\,(-3\,C_{1_m} + 3\,C_{1_m}\,\nu_m - 2\,C_{2_m}\,\nu_m - C_{3_m}\,\nu_m$$

$$- 6\,C_{4_m}\,\nu_m + 2\,C_{2_m}\,\nu_m^2 + 6\,C_{4_m}\,\nu_m^2)\,/\,(2\,\nu_m - 2\,\nu_m^3) \qquad (4.93d)$$

$$a\,C_{2_m} + a^3\,C_{1_m}/r_b^2 + r_b^2\,C_{3_m}/a + r_b^4\,C_{4_m}/a^3 = a\,\varepsilon_2/2 \qquad (4.93e)$$

$$-a\,C_{2_m} + r_b^4\,C_{4_m}/a^3 + a^3\,C_{1_m}(-3 + 2\,\nu_m)/(2r_b^2\,\nu_m)$$

$$+ C_{3_m}\,r_b^2\,(-1 + 2\,\nu_m)/(2a - 2a\,\nu_m) = -\frac{a\,\varepsilon_2}{2} \qquad (4.93f)$$

In summary, to obtain η_{11}, the desired effective modulus for this particular case, the procedure is:

- Substitute the appropriate numerical values into Equations 4.93 and solve for the C's using an appropriate equation solver.
- Calculate values for β.
- Evaluate η_{11}.

The details for the development of Equations 4.92 and 4.93 were carried out using Mathematica, and are to be found in Mello (1996).

4.7 Case E - Composite Stresses σ_x and σ_y

The deformations of this case are found by superposing the results of Cases C and D examined previously (see Figure 11). Analysis of this case yields the effective moduli for determining σ_x and σ_y. This superposition is analogous to adding the hydrostatic and deviatoric stresses to obtain total stress. Recall for Case C that the prescribed x and y strains are:

$$\varepsilon_x = \frac{\varepsilon_1}{2} \qquad \varepsilon_y = \frac{\varepsilon_1}{2}$$

and for Case D

$$\varepsilon_x = \frac{\varepsilon_2}{2} \qquad \varepsilon_y = -\frac{\varepsilon_2}{2}$$

so for the linear combination

$$\varepsilon_x = \frac{\varepsilon_1}{2} + \frac{\varepsilon_2}{2}$$

$$\varepsilon_y = \frac{\varepsilon_1}{2} - \frac{\varepsilon_2}{2} \tag{4.94}$$

for Case E. Now inverting one finds:

$$\varepsilon_1 = \varepsilon_x + \varepsilon_y$$

$$\varepsilon_2 = \varepsilon_x - \varepsilon_y \tag{4.95}$$

The x and y composite stresses are similarly found:

$$\sigma_x = \sigma_1 + \sigma_2$$

$$\sigma_y = \sigma_1 - \sigma_2 \tag{4.96}$$

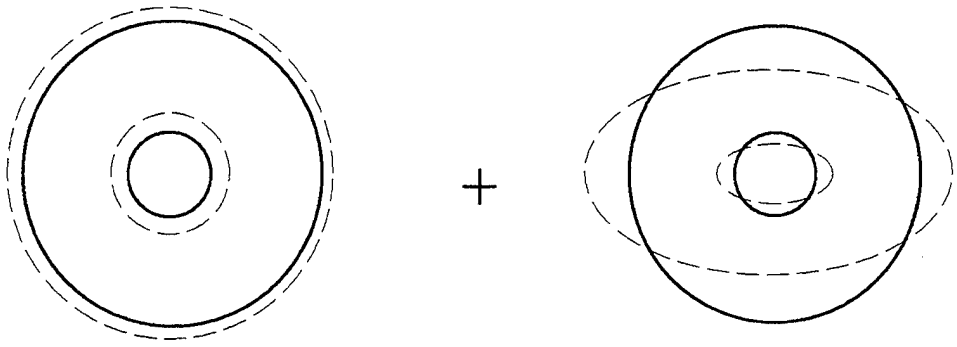

Case C - Change in Volume with Slip and Dilation

Case D - Cross Section Distortion

Figure 11. - Case E Deformation

Now from Case C, Equation 4.61, we have

$$\sigma_1 = \eta_1 \varepsilon_1 + \eta_2 \varepsilon_2 + \eta_3 \varepsilon_f + \eta_4 \frac{\delta}{r_b}$$

and from Case D, Equation 4.89:

$$\sigma_2 = \eta_{11} \varepsilon_2$$

Substituting Equation 4.95 into the above and putting the results into Equation 4.96, one obtains expressions for the x and y stresses which are:

$$\sigma_x = (\eta_1 + \eta_{11})\varepsilon_x + (\eta_1 - \eta_{11})\varepsilon_y + \eta_2 \varepsilon_z + \eta_3 \varepsilon_f + \eta_4 \frac{\delta}{r_b} \qquad (4.97)$$

and

$$\sigma_y = (\eta_1 - \eta_{11})\varepsilon_x + (\eta_1 + \eta_{11})\varepsilon_y + \eta_2 \varepsilon_z + \eta_3 \varepsilon_f + \eta_4 \frac{\delta}{r_b} \qquad (4.98)$$

which yields the desired composite elastic moduli. The remaining effective stress-strain equations, arising from the superposition of Cases C and D, are found by substituting Equation 4.95 into Equations 4.62 to 4.66 of Case C. These are:

$$\sigma_z = \frac{1}{(1-\rho)} \left[\eta_2 \varepsilon_x + \eta_2 \varepsilon_y + \eta_5 \varepsilon_z + \eta_6 \varepsilon_f + \eta_7 \frac{\delta}{r_b}\right] \tag{4.99}$$

$$\sigma_f = \frac{1}{\rho} \left[\eta_3 \varepsilon_x + \eta_3 \varepsilon_y + \eta_6 \varepsilon_z + \eta_8 \varepsilon_f + \eta_9 \frac{\delta}{r_b}\right] \tag{4.100}$$

$$\tau = d_{11} \frac{s}{r_b} + d_{12} \frac{\delta}{r_b} \tag{4.101}$$

$$\sigma^* = \frac{\alpha^2}{2} \left[\eta_4 \varepsilon_x + \eta_4 \varepsilon_y + \eta_7 \varepsilon_z + \eta_9 \varepsilon_f + \eta_{10} \frac{\delta}{r_b}\right] + d_{21} \frac{s}{r_b} + d_{22} \frac{\delta}{r_b} \tag{4.102}$$

This leaves only one more composite elastic relation to be developed.

4.8 Case F - XY Shear

The final deformation case considered is shear in the xy plane, shown in Figure 12. The prescribed deformation is γ_{xy}. Recall Case D which examined the distortion of the cross section (see Figure 10). Because of the axisymmetric nature of the RVE, we may find the desired relations for the present case by rotating (transforming) the results of Case D by 45 degrees (recall the simple Mohr's circle type stress-strain transformation). The transformation relations are:

$$\tau_{xy} = -\left(\frac{\sigma_{x'} - \sigma_{y'}}{2}\right) \sin(2\theta) + \tau_{x'y'} \cos(2\theta)$$

and

$$\frac{\gamma_{xy}}{2} = -\left(\frac{\varepsilon_{x'} - \varepsilon_{y'}}{2}\right) \sin(2\theta) + \frac{\gamma_{x'y'}}{2} \cos(2\theta)$$

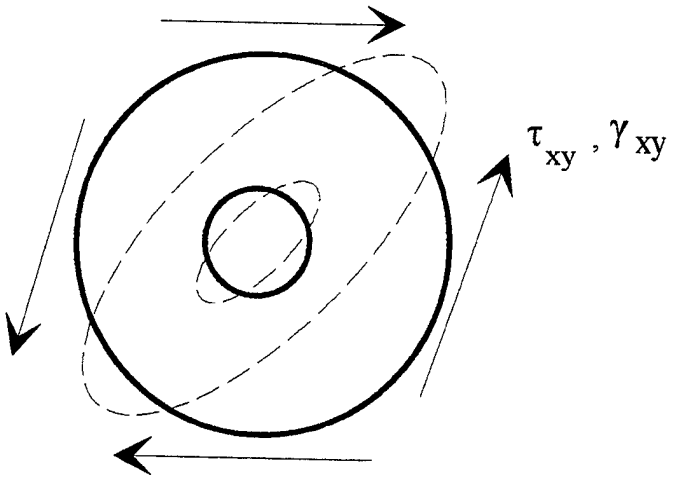

Figure 12. - Case F, XY Shear Deformation

where the primed quantities are from Case D. For θ of 45 degrees and $\tau_{x'y'}$ and $\frac{\gamma_{x'y'}}{2}$ equal to zero as defined in Case D, one obtains:

$$\tau_{xy} = \frac{\sigma_{x'} - \sigma_{y'}}{2} \tag{4.103}$$

$$\gamma_{xy} = \varepsilon_{x'} - \varepsilon_{y'} \tag{4.104}$$

To find $\sigma_{x'}$ and $\sigma_{y'}$ for Case D deformation we use Equations 4.97 and 4.98, now written as primed variables

$$\sigma_{x'} = (\eta_1 + \eta_{11})\varepsilon_{x'} + (\eta_1 - \eta_{11})\varepsilon_{y'}$$

$$\sigma_{y'} = (\eta_1 - \eta_{11})\varepsilon_{x'} + (\eta_1 + \eta_{11})\varepsilon_{y'}$$

which are substituted into Equation 4.103 to get, after some algebraic manipulation:

$$\tau_{xy} = \eta_{11} (\varepsilon_{x'} - \varepsilon_{y'}) \tag{4.105}$$

Substituting the result of Equation 4.104 into the above equation leads to the final results:

$$\tau_{xy} = \eta_{11}\,\gamma_{xy} \tag{4.106}$$

4.9 Composite Properties

The results of Cases A through E are now summarized and organized into the desired three-dimensional, homogeneous, constituent relations. The equations that result are:

$$\sigma_x = (\eta_1 + \eta_{11})\,\varepsilon_x + (\eta_1 - \eta_{11})\,\varepsilon_y + \eta_2\,\varepsilon_z + \eta_3\,\varepsilon_f + \eta_4\,\frac{\delta}{r_b}$$

$$\sigma_y = (\eta_1 - \eta_{11})\,\varepsilon_x + (\eta_1 + \eta_{11})\,\varepsilon_y + \eta_2\,\varepsilon_z + \eta_3\,\varepsilon_f + \eta_4\,\frac{\delta}{r_b}$$

$$\sigma_z = \frac{1}{(1-\rho)}\,[\eta_2\,\varepsilon_x + \eta_2\,\varepsilon_y + \eta_5\,\varepsilon_z + \eta_6\,\varepsilon_f + \eta_7\,\frac{\delta}{r_b}]$$

$$\sigma_f = \frac{1}{\rho}\,[\eta_3\,\varepsilon_x + \eta_3\,\varepsilon_y + \eta_6\,\varepsilon_z + \eta_8\,\varepsilon_f + \eta_9\,\frac{\delta}{r_b}]$$

$$\tau_{xy} = \eta_{11}\,\gamma_{xy}$$

$$\tau_{xz} = \eta_0\,\gamma_{xz}$$

$$\tau_{yz} = \eta_0\,\gamma_{yz}$$

$$\tau = d_{11}\,\frac{s}{r_b} + d_{12}\,\frac{\delta}{r_b}$$

$$\sigma^* = \frac{\alpha^2}{2}\,[\eta_4\,\varepsilon_x + \eta_4\,\varepsilon_y + \eta_7\,\varepsilon_z + \eta_9\,\varepsilon_f + \eta_{10}\,\frac{\delta}{r_b}]$$

$$+ d_{21}\,\frac{s}{r_b} + d_{22}\,\frac{\sigma}{r_b} \tag{4.107}$$

For implementation into a finite element scheme, it is convenient to write these equations in matrix form

$$\{ \sigma \} = [D] \{ \varepsilon \} \tag{4.108}$$

where

$$\{\sigma\}^T = \{\sigma_x, \sigma_y, (1-\rho)\sigma_z, \tau_{xy}, \tau_{yz}, \tau_{xz}, \rho\sigma_f, 2_\rho\tau, 2_\rho\sigma^*\} \tag{4.109}$$

$$\{\varepsilon\}^T = \{\varepsilon_x, \varepsilon_y, \varepsilon_z, \gamma_{xy}, \gamma_{yz}, \gamma_{xz}, \varepsilon_f, \frac{s}{r_b}, \frac{\delta}{r_b}\} \tag{4.110}$$

$$D = \begin{bmatrix}
\eta_1+\eta_{11} & \eta_1-\eta_{11} & \eta_2 & 0 & 0 & 0 & \eta_3 & 0 & \eta_4 \\
\eta_1-\eta_4 & \eta_1+\eta_{11} & \eta_2 & 0 & 0 & 0 & \eta_3 & 0 & \eta_4 \\
\eta_2 & \eta_2 & \eta_5 & 0 & 0 & 0 & \eta_6 & 0 & \eta_7 \\
0 & 0 & 0 & \eta_{11} & 0 & 0 & 0 & 0 & 0 \\
0 & 0 & 0 & 0 & \eta_0 & 0 & 0 & 0 & 0 \\
0 & 0 & 0 & 0 & 0 & \eta_0 & 0 & 0 & 0 \\
\eta_3 & \eta_3 & \eta_6 & 0 & 0 & 0 & \eta_8 & 0 & \eta_9 \\
0 & 0 & 0 & 0 & 0 & 0 & 0 & 2\rho d_{11} & 2\rho d_{12} \\
\eta_4 & \eta_4 & \eta_7 & 0 & 0 & 0 & \eta_9 & 2\rho d_{21} & \eta_{10}+2\rho d_{22}
\end{bmatrix} \tag{4.111}$$

The finite element code developed around this composite material model is limited to plane strain conditions and it is standard to consider the x-y plane in such an analysis. The above results are thus transformed into this coordinate system and specialized to plane strain :

$$\{\sigma\} = [D] \{\varepsilon\} \tag{4.112}$$

$$\{\sigma\}^T = \{(1-\rho)\sigma_x, \sigma_y, \tau_{xy}, \rho\sigma_f, 2\rho\tau, 2\rho\sigma^*\} \tag{4.113}$$

$$\{\varepsilon\}^T = \{\varepsilon_x, \varepsilon_y, \gamma_{xy}, \varepsilon_f, \frac{s}{r_b}, \frac{\delta}{r_b}\} \tag{4.114}$$

$$[D] = \begin{bmatrix} \eta_5 & \eta_2 & 0 & \eta_6 & 0 & \eta_7 \\ \eta_2 & \eta_1+\eta_{11} & 0 & \eta_3 & 0 & \eta_4 \\ 0 & 0 & \eta_0 & 0 & 0 & 0 \\ \eta_6 & \eta_3 & 0 & \eta_8 & 0 & \eta_9 \\ 0 & 0 & 0 & 0 & 2\rho d_{11} & 2\rho d_{12} \\ \eta_7 & \eta_4 & 0 & \eta_9 & 2\rho d_{21} & \eta_{10}+2\rho d_{22} \end{bmatrix} \tag{4.115}$$

where the x direction is now the fiber direction (see Figure 13).

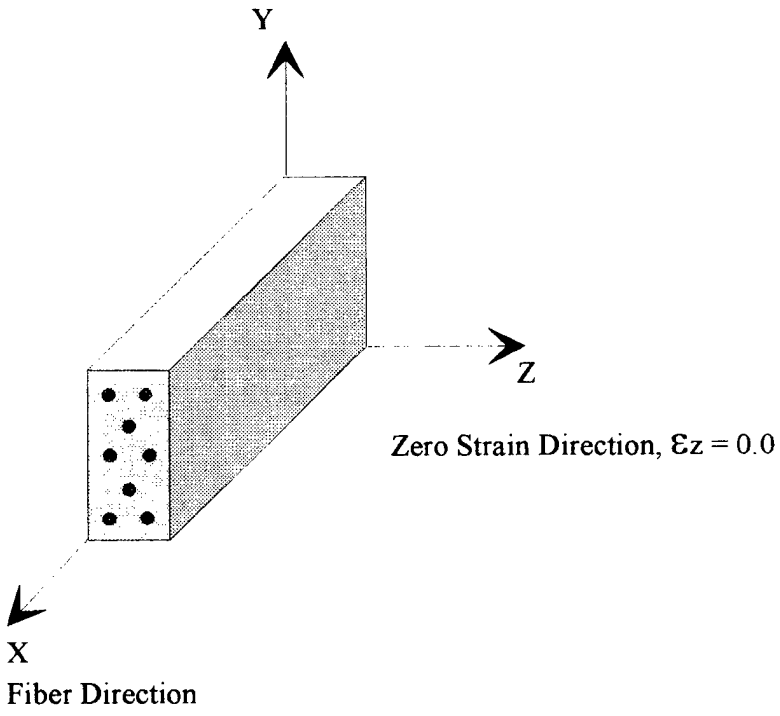

Figure 13. - Composite Material Orientation for Plane Strain Analysis

5. LINEAR COMPOSITE FINITE ELEMENT DEVELOPMENT

The composite finite element was introduced in Section 3. Recall that the scope of its applicability is limited to plane strain, linear isotropic fiber/matrix, unidirectional reinforcement, and small deformations. For the finite element development in this section, the bond response is also limited to linear-elastic behavior. Bond nonlinearity and its implementation is presented in subsequent sections. The element employs four degrees of freedom per node as discussed previously (see Figure 4). The composite material relations developed in the previous section are coupled with the four nodal unknowns to form a specialized finite element scheme.

The element is based on what has become a standard: a bilinear displacement-based, four-node quadralateral, two-dimensional, isoparametric formulation. The details for such an element can be found in many sources such as Cook (1981) or Zienkiewicz (1989). The steps used in deriving this element will now be briefly discussed. Details will be given where the element differs from the norm because of the added nodal unknowns or its peculiar constitutive relations.

The finite element equations for a linear static analysis can be posed in terms of minimizing potential energy, equating of virtual work, or Galerkin's method of weighted residuals, with the same results. This work will be extended later to the case of nonlinear inelastic material analysis; therefore, either Galerkin's method or virtual work must be used since minimizing potential energy is limited to elasticity. Virtual work will be used in this development for the sake of brevity. It is recognized that this method is less general than Galerkin's method, however, Zienkiewicz has shown that for problems in solid mechanics it is exactly the same as the weak form of the equilibrium equations.

The general governing equation derived from virtual work is written in matrix form as:

$$\int_V \{\Delta\varepsilon\}^T \{\sigma\} dV = \int_A \{\Delta u\}^T \{T\} dA + \int_V \{\Delta u\}^T \{q\} dV + \{f\} \{\Delta u\} \tag{5.1}$$

where $\{T\}$ are tractions, $\{q\}$ body forces, and $\{f\}$ discrete loads. Nodal loads are the only loads considered presently. The displacements $\{u\}$, strains $\{\varepsilon\}$, and stresses $\{\sigma\}$ are defined in vector form by:

$$\{u\}^T = \{u, v, u_f, \delta\} \tag{5.2}$$

$$\{\Delta u\}^T = \{\Delta u, \Delta v, \Delta u_f, \Delta\delta\} \tag{5.3}$$

$$\{\varepsilon\}^T = \{\varepsilon_x,\ \varepsilon_y,\ \gamma_{xy}, \varepsilon_f, q_1, q_2\} \tag{5.4}$$

$$\{\Delta\varepsilon\}^T = \{\Delta\varepsilon_x, \Delta\varepsilon_y, \Delta\gamma_{xy}, \Delta\varepsilon_f, \Delta q_1, \Delta q_2\} \tag{5.5}$$

$$\{\sigma\}^T = \{(1-\rho)\sigma_x, \sigma_y, \tau_{xy}, \rho\sigma_f, 2\rho\tau, 2\rho\sigma^*\} \tag{5.6}$$

The virtual quantities are denoted by Δ. The stresses and strains are taken from the constitutive Equation 4.107 of the previous section. Note that these definitions differ significantly from that seen in a common homogenous finite element formulation. The displacement vector contains fiber displacement and bond dilation. It is important to emphasize and review what each of these vector's represent. The displacements are:

- u - average matrix displacement in the fiber direction (x-direction)
- v - average transverse (to the fiber) displacement (y-direction) for both fiber and matrix
- u_f - average fiber displacement (x-direction)
- δ - average bond dilation

As mentioned previously, this analysis is limited to reinforcement in the x-direction only. The strains are:

- ε_x - average matrix strain in the fiber direction
- ε_y - average transverse strain
- γ_{xy} - average in-plane shear strain
- q_1 - average slip strain, s/r_b
- q_2 - average dilation strain, δ/r_b

where the relative movement of the fiber and matrix (slip) is

$$s = u - u_f$$

The stress quantities are:

- $(1-\rho)\sigma_x$ - average matrix stress in the fiber direction
- σ_y - average transverse stress
- τ_{xy} - average in-plane shear stress

$\rho\sigma_f$ - average fiber stress

$2\rho\tau$ - average bond shear stress

$2\rho\sigma^*$ - average equilibrium stress

Recall that ρ represents the fiber volume fraction and that the quantity σ^* is used to impose equilibrium at the bond interface when dilation is used as an unknown in the composite micro-mechanics analysis. This quantity is set to zero in the virtual work process thus enforcing the required equilibrium.

For small deformations the strain displacement relations may be written as:

$$\{\varepsilon\} = [A]\,\{u\} \tag{5.7}$$

or

$$\begin{Bmatrix} \varepsilon_x \\ \varepsilon_y \\ \gamma_{xy} \\ \varepsilon_f \\ q_1 \\ q_2 \end{Bmatrix} = \begin{bmatrix} \frac{\partial}{\partial x} & 0 & 0 & 0 \\ 0 & \frac{\partial}{\partial y} & 0 & 0 \\ \frac{\partial}{\partial y} & \frac{\partial}{\partial x} & 0 & 0 \\ 0 & 0 & \frac{\partial}{\partial x} & 0 \\ \frac{1}{r_b} & 0 & \frac{-1}{r_b} & 0 \\ 0 & 0 & 0 & \frac{1}{r_b} \end{bmatrix} \begin{Bmatrix} u \\ v \\ u_f \\ \delta \end{Bmatrix} \tag{5.8}$$

where [A] is sometimes called the differential operator matrix.

For a displacement-based finite element scheme, the body is approximated as an assembly of discrete finite elements connected at node points. The unknowns at the nodes define the global displacement vector $\{u\}$,

$$\{u\}^T = \{u_1\ v_1\ u_{f_1}\ \delta_1\ u_2\ v_2 \ldots \delta_N\} \tag{5.9}$$

Within an element, m, the displacements are approximated in terms of shape functions and the nodal displacements:

$$\{u\}_m = [N]_m\,\{u\} \tag{5.10}$$

Thus, for this element the extra degrees of freedom, slip and dilation, are interpolated exactly as the x-y displacement components of a standard two-dimensional homogeneous element. Thus, although the displacement variables and constitutive law are very different for this element, only simple extensions of an existing finite element code are required for its implementation.

The strains and virtual strains are expressed in the usual fashion as:

$$\{\varepsilon\}_m = [B]_m \{u\} \tag{5.11}$$

$$\{\Delta\varepsilon\}_m = [B]_m \{\Delta u\} \tag{5.12}$$

where [B] is the strain-displacement matrix and is given later.

The usual virtual work process leads to the general governing equation written in terms of element contributions

$$\sum_{m=1}^{nelem} \int_v [B]_m^+ \{\sigma\} dv = \sum_{m=1}^{nelem} \int_{v_m} [N]_m^T \{q\} \tag{5.13}$$

where the only element loads are due to body forces. For the current restriction of linear elastic material response, one writes

$$\{\sigma\} = [D] \{\varepsilon\} \tag{5.14}$$

where [D] is given in Equation 4.15 of the previous section. Using this expression leads to writing the element stiffness matrix in the standard form:

$$[k]_m = \int_{v_m} [B]_m^T [D]_m [B]_m \, dv \tag{5.15}$$

The form here is such that the element stiffness can be formed using an existing finite element code, given the new stress-strain [D] and strain-displacement [B] matrices for the composite material and the four degrees of freedom (per node) element.

A general FORTRAN finite element code, Mish (1992), for two-dimensional heat transfer, HEAT2D, was used as a basis for developing this specialized composite code, hereafter referred to as COMP2D. HEAT2D was an attractive starting point as it contained parameter statements

governing the dimensions of all the global arrays and came with user-friendly graphical post-processing routines. In COMP2D, as in HEAT2D and most finite element codes, the element stiffness matrix is calculated in terms of four sub-matrices. The four degrees of freedom per node of the composite element results in a sub-matrix 4 by 4 in size. For the i,j (i,j = 1,4) sub-matrix, the elements are written as

$$k_{ij} = \int \int_A [B]_i^T [D] [B]_j \, dA \tag{5.16}$$

The shape functions are written in sub-matrix form as:

$$[N]_j = \begin{bmatrix} N_j & & & \\ & N_j & & \\ 0 & & N_j & \\ & & & N_j \end{bmatrix} \tag{5.17}$$

The strain-displacement matrix is found by multiplying the differential operator matrix by the shape functions

$$[B]_j = [A] [N]_j \tag{5.18}$$

or

$$[B]_j = \begin{bmatrix} \frac{\partial N_j}{\partial x} & 0 & 0 & 0 \\ 0 & \frac{\partial N_j}{\partial y} & 0 & 0 \\ \frac{\partial N_j}{\partial y} & \frac{\partial N_j}{\partial x} & 0 & 0 \\ 0 & 0 & \frac{\partial N_j}{\partial x} & 0 \\ \frac{N_j}{r_b} & 0 & \frac{-N_j}{r_b} & 0 \\ 0 & 0 & 0 & \frac{N_j}{r_b} \end{bmatrix} \tag{5.19}$$

The stiffness terms for the i,j sub-matrix terms are now calculated by doing the appropriate matrix multiplications in Equation 5.16. For example, one gets

$$k_{11}^{m} = \int \int_{A_m} [\, \frac{\partial N_s}{\partial x} \frac{\partial N_s}{\partial x} D_{11} + \frac{\partial N_i}{\partial y} \frac{\partial N_j}{\partial y} D_{44} + \frac{N_i N_j}{r_b^2} D_{88}] \, dA$$

for the integrand of the upper left-hand corner term of this sub-matrix. The integration over the element is performed numerically using a four-point gauss quadrature scheme.

At this point, no element loading due to either surface tractions or body forces is built into COMP2D, as the prescription of discrete nodal loads and displacements are adequate to test the code. The basic changes made in creating COMP2D from a general two-dimensional heat transfer code are:

- Global and elemental arrays increased to accommodate four degrees of freedom per node as needed.
- A composite material algorithm created to calculate [D], the new constitutive law, using the relations derived from the micro-mechanics analysis.
- A new 16 by 16 element-stiffness matrix formed using [D] and the strain-displacement relations, [B], for the four degree of freedom element.
- A composite stress computation algorithm at the Gauss points based on the new constitutive law, using [D].
- Input/output and format changes.

6. BOND PLASTICITY MODEL

The ultimate objective of this work is to implement an elastic-plastic bond model in a composite element. In this section the elastic-plastic bond model is described. The numerical algorithm to evaluate this analytical model and the associated nonlinear finite element scheme are presented in Section 7.

A comprehensive plasticity bond model was developed by Herrmann and Cox (1992), as stated previously. The model can be applied to both monotonic and cyclic loading and is based on classic nonassociative, elasticity-plasticity theory. As previously noted, the primary goal of this work was to demonstrate that a bond model that includes dilation may be successfully implemented in a composite finite element scheme. In this section the model of Herrmann and Cox will be restricted to monotonic loading and simplified somewhat to facilitate this initial implementation. These restrictions may be removed in future development. The complications that would need to be added impact the material model and its associated numerical algorithm and not the overall theory used in embedding the bond model within a composite representation.

The bond model has four main components: an elastic law, yield function, hardening law, and flow rule. The reader is referred to Herrmann and Cox (1992) for the detailed development of each of these components. The simplified version used in this work is presented below.

6.1 Elastic Law

The bond elastic law was introduced previously in Section 3 but is repeated here for completeness and is now written in terms of compliance:

$$\begin{Bmatrix} q_1 \\ q_2 \end{Bmatrix} = [\,A\,] \begin{Bmatrix} \tau \\ \sigma \end{Bmatrix} \tag{6.1}$$

Herrmann and Cox found the components of the compliance matrix to be proportional to the reciprocal of the concrete modulus in the following fashion:

$$[A] = [a] / E_c \tag{6.2}$$

where E_c = concrete modulus

and

$$\begin{aligned} a_{11} &= 20.0 \\ a_{12} &= 0.86 \\ a_{21} &= 0.86 \\ a_{22} &= 28.6 \end{aligned} \tag{6.3}$$

Note that these values are twice those reported by Herrmann and Cox, due to the fact that in their work the slip and dilation strains were normalized with respect to the bar diameter as compared to the bar radius here.

6.2 Yield Function

Consistent with classical plasticity models, a yield function or surface is used to define the limits of elasticity. For the behavior of concrete bond, this function must harden and soften as damage occurs. The yield function of Herrmann and Cox simplifies to the form:

$$F = \frac{\tau}{F_t} - C(D)\alpha_1 \left(\frac{-\sigma}{F_t}\right)^{\alpha_2} \tag{6.4}$$

where

F_t = concrete tensile strength

$C(D)$ = hardening law which is a function of damage, D (to be discussed subsequently)

α_1, α_2 = parameters introduced by Herrmann and Cox

This function is plotted in Figure 14 for the case of no damage, which should be compared to Herrmann and Cox's Figure 19. This power law yield surface is a simplification of the blended power law-exponential function used by Herrmann and Cox. This simplification is made in part to allow for the use of a nonassociative flow rule that is simply related to the yield surface. A discussion of this follows the definition of the flow rule. Because of this simplification, the fidelity of the predictions to experimental results is less than that achieved by Herrmann and Cox when there is significant damage combined with low confinement (bond normal stress).

The damage, D, serves as the internal variable governing the evolution of the yield surface and the resulting plastic flow. Herrmann and Cox found the best damage measure to be:

$$D = \frac{q_1^{pl} r_b}{S_L \cos\phi} \tag{6.5}$$

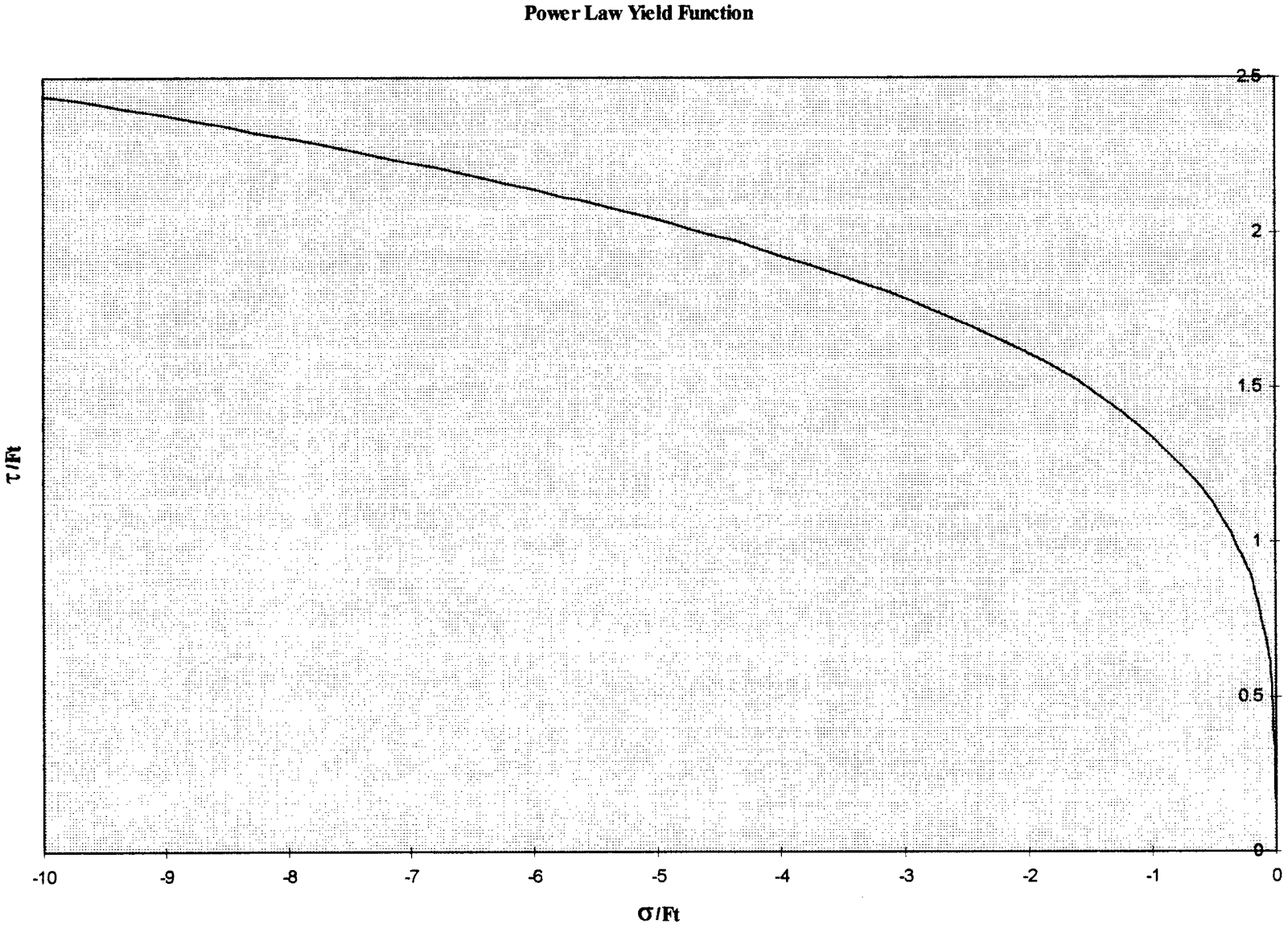

Figure 14. - Bond Model Yield Function

where

q_1^{pl} = plastic slip strain

r_b = reinforcement radius

S_L = reinforcement lug spacing

ϕ = reinforcement lug angle

Thus, damage is essentially a function of the plastic slip.

6.3 Hardening Law

The hardening and softening, or changing size, of the yield surface is controlled by the value of the C(D) term in Equation 6.4. The hardening law of Herrmann and Cox was given as a differential equation in damage, D. This is simplified in this work to the following functional relation:

$$C(D) = \alpha_3 + \alpha_4 (1 - e^{-\alpha_5 D}) - \alpha_6 (1 - e^{-\alpha_7 D}) \tag{6.6}$$

This is accomplished by numerically solving the ordinary differential equation of Herrmann and Cox and fitting the parameters α_3 - α_7 to best match their results. This was accomplished using Mathematica. The details of this process can be found in Mello (1996). Figure 15 compares the two results.

6.4 Nonassociative Flow Rule

The nonassociative flow rule which governs the relation between plastic slip and plastic dilation strains was defined by Herrmann and Cox in terms of function g, where:

$$g = \frac{\dot{q}_2^{pl}}{\dot{q}_1^{pl}} \tag{6.7}$$

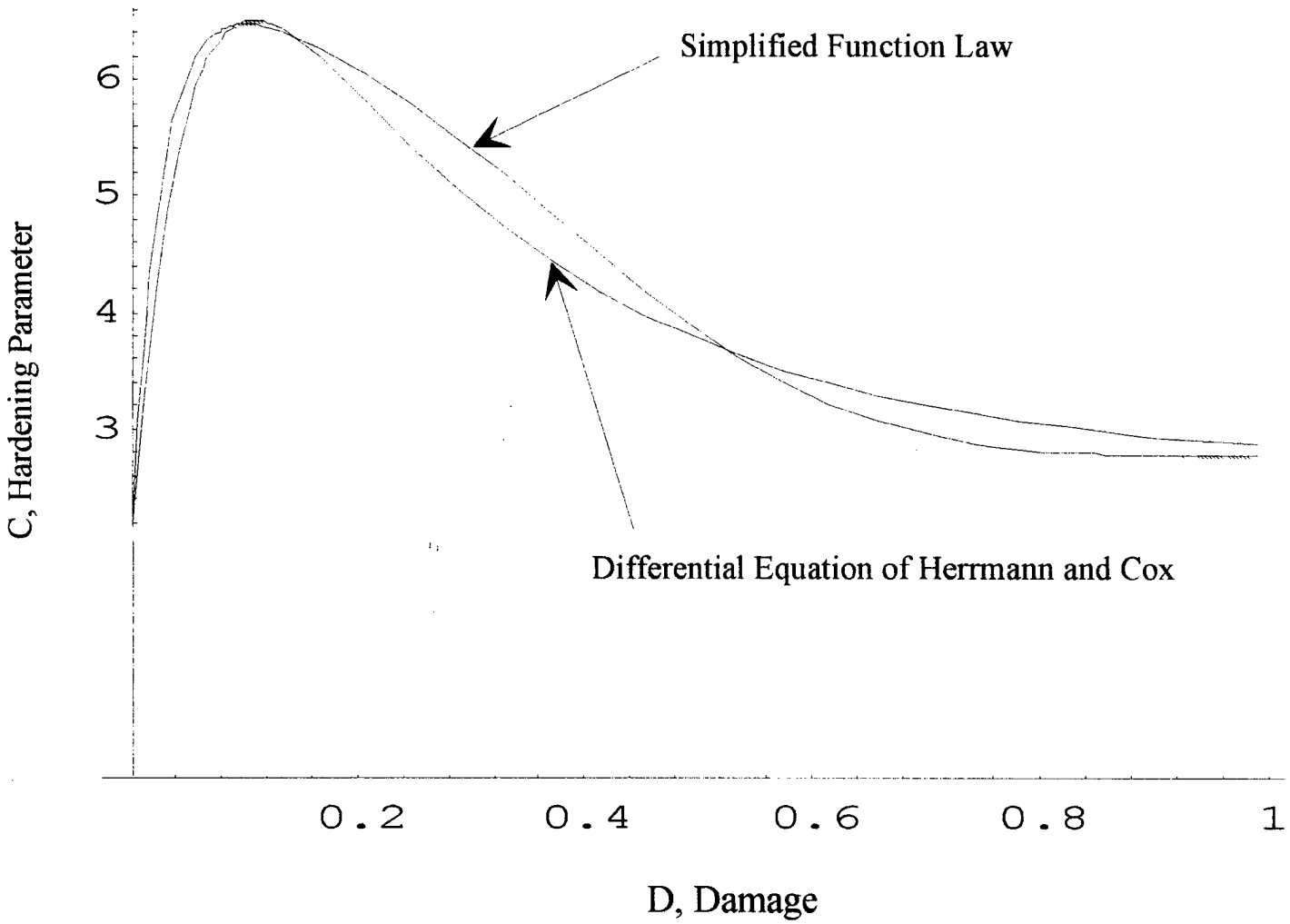

Figure 15. - Bond Model Hardening Law

Herrmann and Cox found g to be a complex function of bond normal stress, damage, plastic dilation, and nearly a dozen parameters. Once again this relation is simplified. A less complex flow rule is derived by rotating back a prescribed constant angle θ_r from the normal to the yield surface as defined by Equation 6.4 (the angle is a calibrated quantity). This is shown in Figure 16. Using this assumption

$$g = \frac{\dot{q}_2^{pl}}{\dot{q}_1^{pl}} = \tan\theta \tag{6.8}$$

where θ is the angle between the flow direction and the τ axis

$$\theta = \theta^* - \theta_r \tag{6.9}$$

and

$$\theta^* = \tan^{-1}\left(\frac{\partial F}{\partial \sigma} \Big/ \frac{\partial F}{\partial \tau}\right) \tag{6.10}$$

letting

$$h = \frac{\partial F}{\partial \sigma} \Big/ \frac{\partial F}{\partial \tau} \tag{6.11}$$

it is easy to show that:

$$g = \frac{h - \tan\theta_r}{1 + h\,\tan\theta_r} \tag{6.12}$$

The only parameter to be determined in this case is the rotation angle, θ_r, assuming the yield surface and its associated derivatives have been defined.

The calibration of θ_r is done using the simplified yield surface Equation 6.4, its derivatives, the damage function C(D) of Equation 6.6, and the experimental results of Gambarova as reported in Figure 30 of Herrmann and Cox (1992). The angle was adjusted so

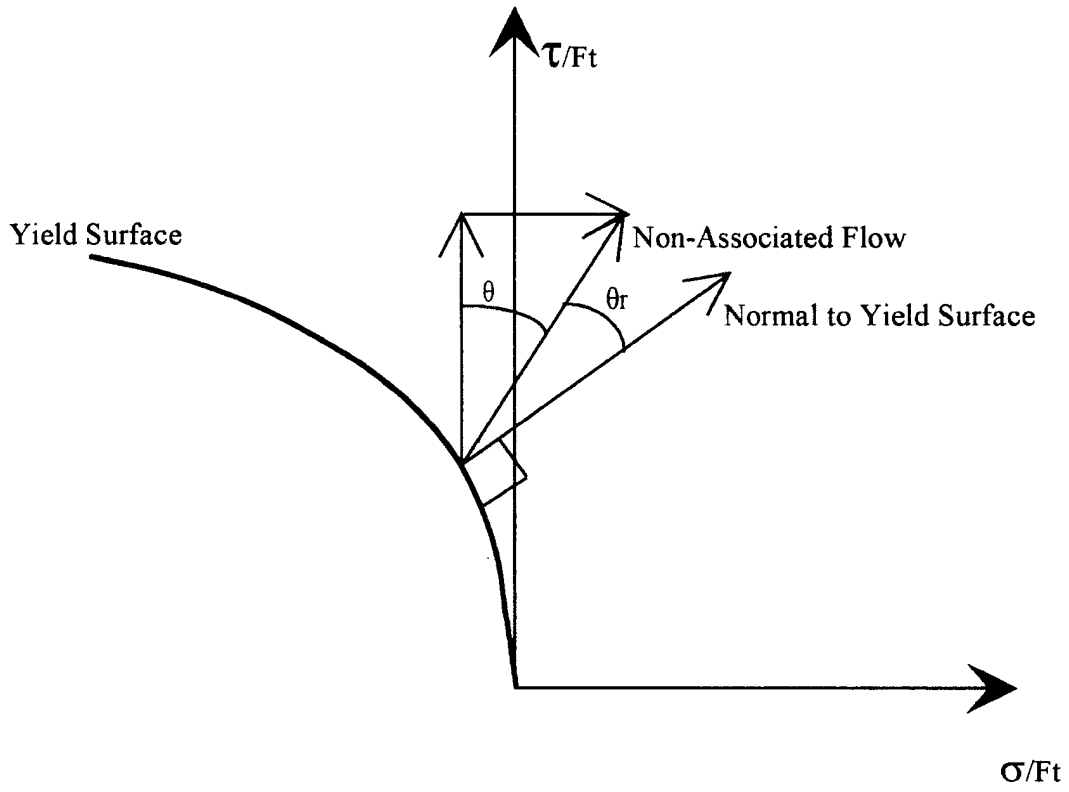

Figure 16. - Bond Model Flow Rule

that the results for g best match those of Herrmann and Cox given in their Figure 25. Details are given in Mello (1996). The best fit is found to be:

$$\theta_r = 0.21 \text{ rad} \tag{6.13}$$

The analytical yield function, hardening law, and flow rule are implemented in a numerical nonlinear material algorithm that evaluates the bond stress state, given a strain history. Details of this algorithm and its implementation in the global composite finite element scheme follow in the next section.

7. NONLINEAR BOND FINITE ELEMENT IMPLEMENTATION

The incorporation of the simplified elastic-plastic bond model into the composite finite element scheme is detailed in this section. First, the finite element solution of nonlinear plasticity problems is discussed in general terms. The process is outlined briefly to understand what is required of the bond model and composite material algorithm. There are many references in the area of nonlinear finite element analysis. Those used most here are Zienkiewicz and Taylor (1991), Owen and Hinton (1980), and Bathe (1982).

7.1 Nonlinear Finite Element Solution

The source of nonlinearity for this study is limited to the elastic-plastic behavior of the bond. It is recognized that the behavior of the matrix and reinforcing fibers may be nonlinear also, but in this study the goal is the initial implementation of a plasticity bond model including dilation effects. Because the analysis also assumes small deformations, no reformulation of the strain-displacement relations is required.

An incremental Newton-Raphson iterative method is used to solve the nonlinear problem. As in the linear case, the problem is formulated in terms of unknown nodal displacements. The global residual is defined for a load increment as:

$$\{R(u_{n+1})\} = \{P(u_{n+1})\} - \{f_{n+1}\} \tag{7.1}$$

where $\{f\}$ are the applied forces and

$$\{P\} = \int_v [B]^T \{\sigma\}_{n+1} \, dv \tag{7.2}$$

is the vector of internal forces. The vector {P} is a nonlinear function of displacement as a result of the bond nonlinearity. An iterative solution to the problem is sought and found when the residual, {R}, of Equation 7.1 is near zero. For a Newton-Raphson iterative scheme, Equation 7.1 is written as a truncated Taylor series and set to zero, making the residual small:

$$\{R(u_{n+1}^{i+1})\} \approx \{R(u_{n+1}^{i})\} + \{ \frac{\partial R}{\partial (u_{n+1}^{i})} \} \, \delta u_{n+1}^{i+1} = 0 \tag{7.3}$$

where

$$J_{n+1}^{i} = [\frac{\partial R}{\partial u}]_{n+1}^{i}$$

is the global Jacobian. Note the superscripts are the iteration counters. The iterative correction is desired and is found by solving

$$[J]_{n+1}^{i} \{\delta u\}_{n+1}^{i+1} = - \{R\}_{n+1}^{i} \tag{7.4}$$

which is identical in form to the system of equations that occurred for the linear-elastic case. The displacement approximation is updated each iteration in the following manner:

$$\{u\}_{n+1}^{i+1} = \{u\}_{n+1}^{i} + \{\delta u\}_{n+1}^{i+1} \tag{7.5}$$

where u_n is the displacement at the end of the last load increment. The Newton-Raphson iterative process is repeated until convergence, that is, until some norm of the residual is sufficiently small. With this procedure, most of the structure of a linear-elastic finite element code is used. The important new components on the global level are the global residual and Jacobian.

7.1.1 Global Residual. Recall the global residual is:

$$\{R\} = \int_{vol} [B]^T \{\sigma\}\, dv - \{f\}$$

This requires knowing the composite stress state $\{\sigma\}$ for the given displacement estimate and resulting strains. Obtaining the stresses for this composite scheme is a two-step process:

1. A suitable numerical algorithm is used to determine bond model stresses for a given bond strain history.

2. The material micro-mechanics model is then used to determine the composite stresses given the bond stresses and the composite strains.

The second step is addressed first, as it is simple compared to the task of determining the bond stresses in Step 1.

The composite stress relations for a nonlinear bond stress model are obtained by returning to deformation Case C of Section 4 which involves the bond. Instead of substituting the linear-elastic bond stiffness in the constituent virtual work expression for this deformation mode, it is left in terms of the bond stresses. Equation 4.66 is now:

$$\sigma^* = \frac{\alpha^2}{2} [\eta_4 \varepsilon_1 + \eta_7 \varepsilon_2 + \eta_8 \varepsilon_f + \eta_{10} \frac{\delta}{r_b}] + \sigma \tag{7.6}$$

The virtual work of the composite and constituents is equated as before but now the composite stress-strain relations that result are in terms of the bond stresses as well as the strains. These resulting composite stress-strain relations for a nonlinear bond stress model are:

$$\sigma_x = \frac{1}{(1-\rho)} [\eta_5 \varepsilon_x + \eta_2 \varepsilon_y + \eta_6 \varepsilon_f + \eta_7 \frac{\delta}{r_b}] \tag{7.7}$$

$$\sigma_y = \eta_2 \varepsilon_x + (\eta_1 + \eta_{11}) \varepsilon_y + \eta_3 \varepsilon_f + \eta_4 \frac{\delta}{r_b} \tag{7.8}$$

$$\tau_{xy} = \eta_0 \gamma_{xy} \tag{7.9}$$

$$\sigma_f = \frac{1}{\rho} [\eta_6 \varepsilon_x + \eta_c \varepsilon_y + \eta_8 \varepsilon_f + \eta_a \frac{\delta}{r_b}] \tag{7.10}$$

$$\tau = \tau \tag{7.11}$$

$$\sigma^* = \frac{1}{2\rho} [\eta_7 \varepsilon_x + \eta_4 \varepsilon_y + \eta_9 \varepsilon_f + \eta_{10} \frac{\delta}{r_b}] + \sigma \tag{7.12}$$

where τ and σ are the nonlinear bond stresses determined in Step 1 from a numerical evaluation algorithm for the bond model.

The first step in determining the bond stresses turns out to be quite difficult due to the nonassociative plasticity and a yield function that is not defined for tensile stresses. Before developing an algorithm to determine the bond stresses from the bond model, we must determine what additional information the global solution scheme requires from such an algorithm.

7.1.2 Global Jacobian. Recall the global Jacobian equation was defined as:

$$[J]^{i}_{n+1} = [\frac{\partial R}{\partial u}]^{i}_{n+1}$$

which, for constant loads and small deformations is written as:

$$J = \int_v [B]^T [\frac{\partial \sigma}{\partial \varepsilon}] [B] \, dv \tag{7.13}$$

The global Jacobian, [J], which can be thought of as a consistent stiffness matrix in the tangent direction, is built up from the global material Jacobian or consistent tangent material stiffness and the linear strain-displacement matrix. The global material Jacobian for the composite is found by substituting the bond material Jacobian

$$J_{BG} = \begin{bmatrix} \frac{\partial \tau}{\partial q_1} & \frac{\partial \tau}{\partial q_2} \\ \\ \frac{\partial \sigma}{\partial q_1} & \frac{\partial \sigma}{\partial q_2} \end{bmatrix} \tag{7.14}$$

into the composite material relations in place of the elastic bond matrix. Thus, the two items required and yet to be derived are the bond stresses and the bond material Jacobian.

7.2 Numerical Implementation of the Bond Model

To complete the implementation of the nonlinear bond model, a numerical material algorithm is required. This algorithm must use the yield function, hardening law, and flow rule for the bond model, as given in Section 6, to calculate the bond stress state and material Jacobian for a given strain history.

7.2.1 Cutting-Plane Algorithm. The cutting-plane algorithm of Hughes (1987) was initially selected and used. This procedure uses a return mapping algorithm to integrate the inelastic constitutive equations. The algorithm worked adequately for problems where significant bond confinement pressure existed but had numerical difficulties with more general bond states. The trouble resulted from the fact that the algorithm's iterative process employed an elastic trial stress. Using the bond elastic law, the trial stress (when no initial confinement existed) resulted in a positive bond normal stress. Positive normal stresses are not defined mathematically or physically for the bond model. A variety of remedies were attempted. The most promising used a new yield surface with a fictitious extension of the surface in the positive stress region blended to the desired power law. This is shown in Figure 17. This fix worked for most situations but had stability problems in the case of little or no confinement, which occurs at the start of most practical problems.

The solution to the above dilemma was the development of a new more robust algorithm. The algorithm is based on recent work by Herrmann (1996). His Reduced-Newton algorithm had been used successfully on complicated soil material models that were mathematically similar to the bond model. The details of the application of this algorithm to the bond model follow.

7.2.2 Reduced-Newton Material. The basic idea of this algorithm is to analytically reduce the model equations to a minimum number of equations and unknowns. In this case, two pair of nonlinear ordinary differential equations were obtained. These equations are expressed in terms of the bond stresses which are, in turn, functions of a pseudo-time variable, t, representing the history of the strain increment. These equations are solved using a fully implicit (or backward difference) time-marching scheme, and because the equations are nonlinear, a Newton-Raphson iteration as well.

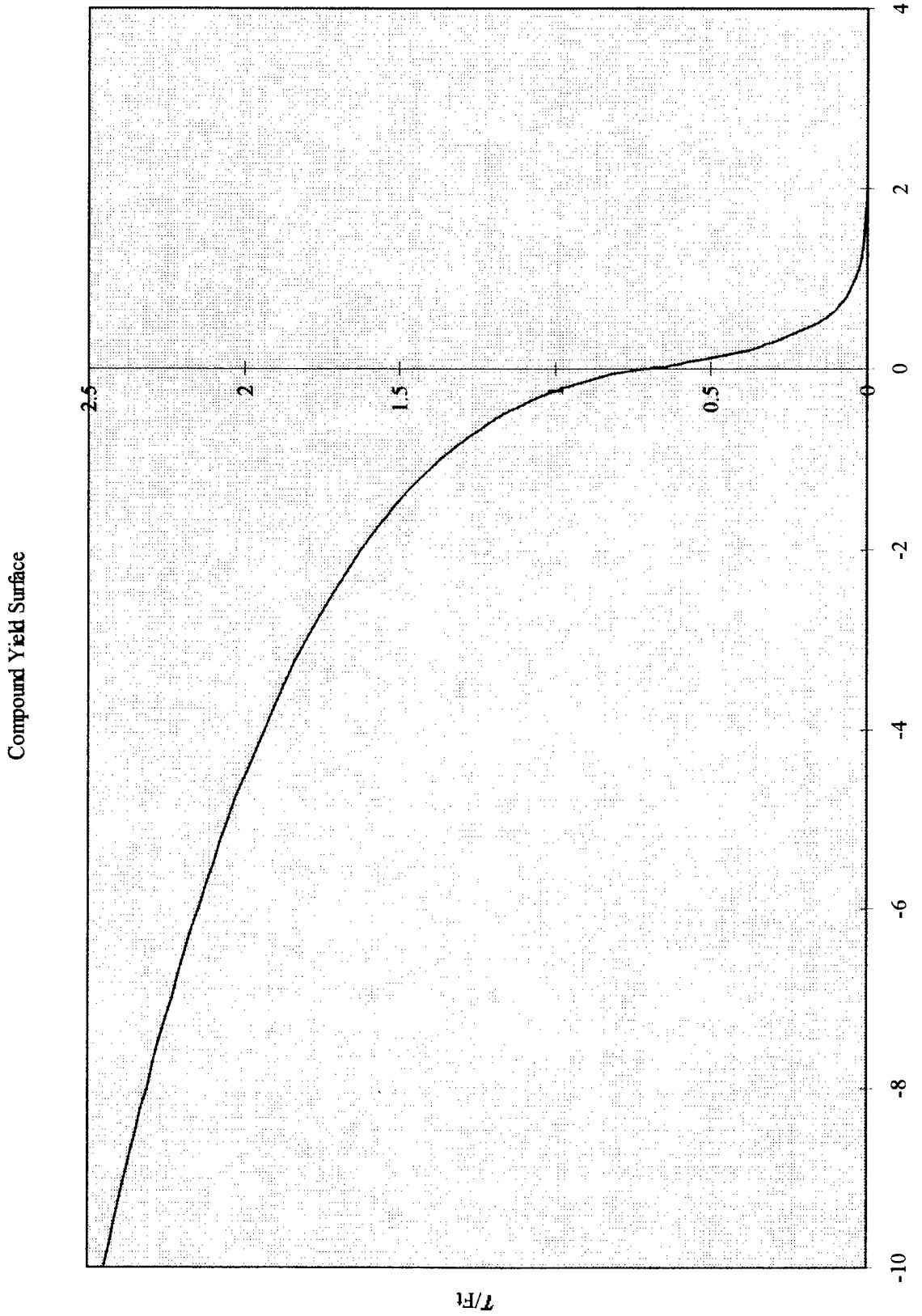

Figure 17. - Yield Function Including Fictitious Bond Tension

Material Algorithm Input/Output

Input to the algorithm is derived from the solution for the previous solution step and the current estimate of the displacement increment:

$\{\Delta q_1 \quad \Delta q_2\}$ - estimate of strain increment for current step (seeking stress at the end of this increment)

$\{q_{1b} \quad q_{2b}\}$ - total strain at the end of the last step

$\{q_{1_b}^{pl}\}$ - plastic slip strain at the end of the last step

$\{\tau_b \quad \sigma_b\}$ - total stress at the end of the last step

Required output from the material algorithm is:

$\{\tau_n \quad \sigma_n\}$ - new stress state (to be used in the global residual)

$\{q_{1_n}^{pl}\}$ - new plastic slip strain

$\{J_{BG}\}$ - bond material Jacobian

Time Stepping

The application of the given strain increment is defined in terms of a pseudo-time variable within the increment or step as shown in Figure 18. The quantities known at the beginning of the increment, or t=0, are designated by the b subscript while the n denotes those to be found at the end of the increment (t=1). Thus, the strain over the given increment is written as a function of time,

$$q_1(t) = q_{1_b} + \Delta q_1 \; t$$

$$q_2(t) = q_{2_b} + \Delta q_2 \; t \qquad (7.15)$$

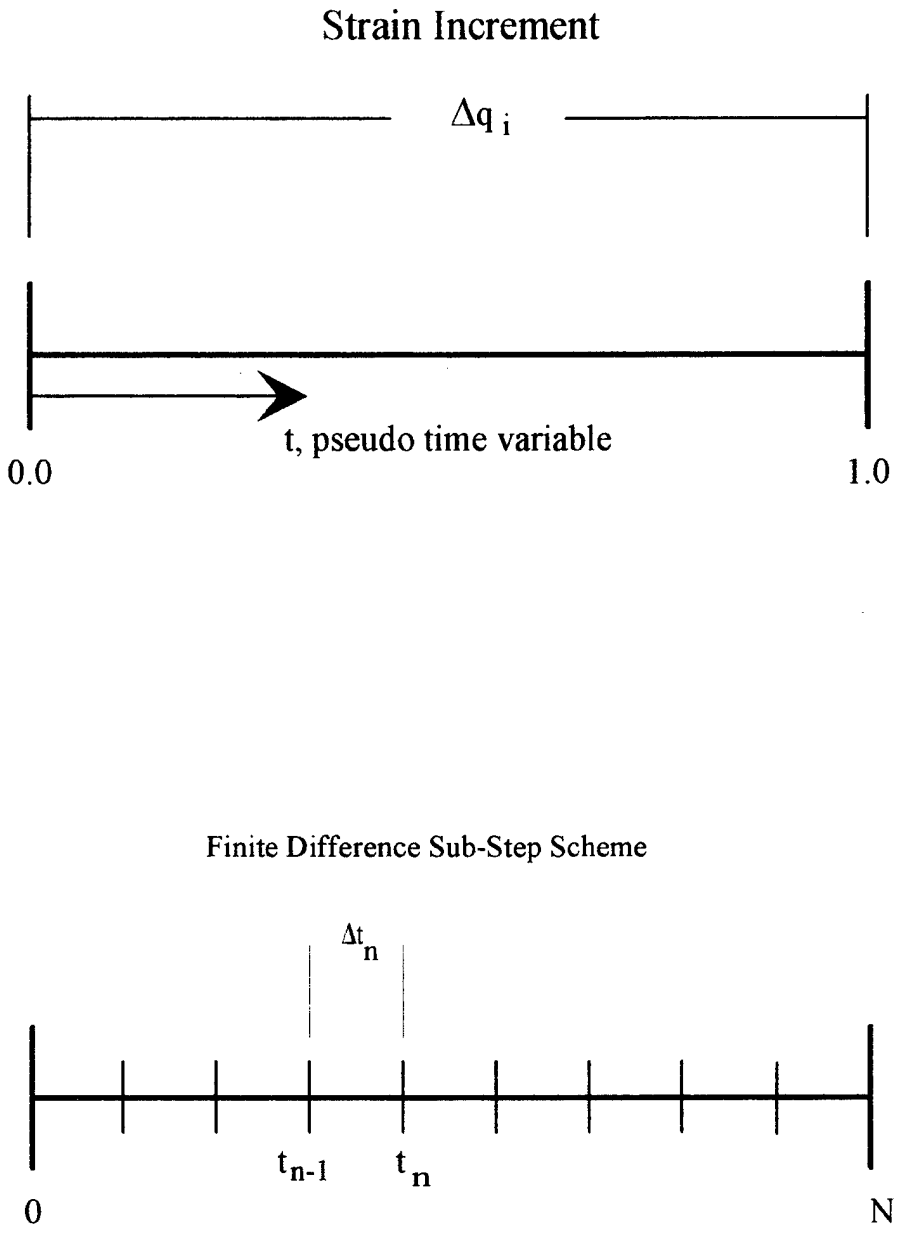

Figure 18.- Strain Increment Time Variable and Sub-Stepping

with the underlying assumption that the strain increments are sufficiently small so that the strain histories are proportional over the increment. Now one gets the strain rates by taking the time derivatives of the above expressions,

$$\frac{dq_1}{dt} = \Delta q_1$$

$$\frac{dq_2}{dt} = \Delta q_2 \tag{7.16}$$

The dot (•) notation is employed so that the rates are written:

$$\dot{q}_1 = \Delta q_1 \qquad \dot{q}_2 = \Delta q_2 \tag{7.17}$$

The development that follows is limited to plastic loading, that is the initial stress state, designated by b, is initially on the yield surface and a strain increment results in plastic flow, evolution of the yield surface, and resulting stresses on a new yield surface.

Elastic Law

The bond model elastic law given in Equation 6.1 is written in equation form as:

$$q_1^e = A_{11}\,\tau + A_{12}\,\sigma$$

$$q_2^e = A_{12}\,\tau + A_{22}\,\sigma \tag{7.18}$$

Plastic Strain

The elastic strain rates are found by differentiating the above expression to get

$$\dot{q}_1^e = A_{11}\,\dot{\tau} + A_{12}\,\dot{\sigma}$$

$$\dot{q}_2^e = A_{12}\,\dot{\tau} + A_{22}\,\dot{\sigma} \tag{7.19}$$

During yielding, the material will behave partly elastic and partly plastic. Thus, during any increment of stress, the changes in strain are assumed to be divisible into elastic and plastic parts,

$$\dot{q}_1 = \dot{q}_1^e + \dot{q}_1^{pl}$$

$$\dot{q}_2 = \dot{q}_2^e + \dot{q}_2^{pl} \tag{7.20}$$

One then solves for the plastic strain rates by substituting the elastic rates which are given in Equation 7.17,

$$\dot{q}_1^{pl} = \Delta q_1 - A_{11}\,\dot{\tau} - A_{12}\,\dot{\sigma}$$

$$\dot{q}_2^{pl} = \Delta q_2 - A_{12}\,\dot{\tau} - A_{22}\,\dot{\sigma} \tag{7.21}$$

Hardening Law

Since the hardening law that controls evolution of the yield surface is in terms of the total plastic slip, it is necessary to integrate the above rate equations,

$$\int_o^t \dot{q}_1^{pl}\, dt' = \dot{q}_1^{pl}(t) - q_{1_b}^{pl} \tag{7.22}$$

Performing this integration and solving for the plastic slip at time, t, results in the following:

$$q_1^{pl}(t) = q_{1_1}^{pl} + \Delta q_1 t - A_{11}(\tau(t) - \tau b) - A_{12}(\sigma(t) - \sigma_b) \tag{7.23}$$

The hardening law is finally written as:

$$C_D(t) = \alpha_3 + \alpha_4 (1 - e^{-\alpha_5 D_N q_1^{pl}(t)}) - \alpha_6 (1 - e^{-\alpha_7 D_N q_1^{pl}(t)}) \tag{7.24}$$

where

$$D_N = \frac{r_b}{(S_L \cos\phi)} \tag{7.25}$$

is the coefficient that normalizes plastic slip to obtain damage.

Yield Function

The yield function of Equation 6.4 is rearranged algebraically and is treated as a residual R_1 in the numerical algorithm,

$$R_1 = \left(\frac{\tau(t)}{F_t}\right)^{\beta} + \left(C_D(t)\,\alpha_1\right)^{\beta} \left(\frac{\sigma(t)}{F_t}\right) \tag{7.26}$$

The β power is:

$$\beta = \frac{1}{\alpha_2} \tag{7.27}$$

This form of the yield surface is numerically the same as given in Equation 6.4 but has the advantage that it may be evaluated for initial values of τ and σ that are zero, which is the case for most real-world problems. This equation is cast as a residual, thus, if the unknowns, stress at time t, are such that they converge to the yield surface, then this residual is zero.

Flow Rule

The flow rule of Equations 6.7, 6.11, and 6.12 is treated as a second residual and is written as:

$$R_2 = \frac{h(t)+\tan\theta_r}{\Delta - h(t)\tan\theta_r} - \frac{\dot{q}_1^{pl}(t)}{\dot{q}_2^{pl}(t)} \tag{7.28}$$

where

$$h(t) = \frac{\beta \left(\frac{\tau(t)}{F_t} \right)^{(\beta-1)}}{(C_D(t)\alpha_1)^{\beta}} \tag{7.29}$$

This form of the residual had division by zero problems in some cases and thus was rearranged so as to be mathematically well defined:

$$R_2 = \dot{q}_2^{pl} (h(t) + \tan\theta_r) - \dot{q}_1^{pl} (1 - h(t) \tan\theta_r) \tag{7.30}$$

The plasticity equations of Section 6 thus reduce to Equations 7.26 and 7.30 with the appropriate substitutions. These form a coupled set of nonlinear, ordinary differential equations in the unknown stresses τ and σ that are solved as functions of the pseudo-time variable t.

Finite Difference Scheme

A finite difference method is used to solve the coupled nonlinear, ordinary differential equations that define the plasticity model. To accomplish this, the time step is divided into uniform sub-steps, as shown in Figure 18. Using a backward difference scheme (Kreyszig, 1983), the unknown stresses and associated first derivatives are written as:

$$\tau(t) = \tau_n \qquad \sigma(t) = \sigma_n$$

$$\dot{\tau} = \frac{\tau_n - \tau_{n-1}}{\Delta t_n}$$

$$\dot{\sigma} = \frac{\sigma_n - \sigma_{n-1}}{\Delta t_n} \tag{7.31}$$

These difference relations are substituted into the equations that make up the residuals R_1 and R_2, the coupled ordinary differential equations of yield and flow. The result is a pair of nonlinear algebraic equations for τ_n and σ_n.

Newton-Raphson Iteration

A Newton-Raphson iterative scheme is used to solve the nonlinear algebraic equations for each time step. The unknown stresses for this process are written in iterative form for time, t_n, as:

$$\begin{Bmatrix} \tau_n \\ \sigma_n \end{Bmatrix}_{(I)} = \begin{Bmatrix} \tau_n \\ \sigma_n \end{Bmatrix}_{(I-1)} + \begin{Bmatrix} \delta\tau_n \\ \delta\sigma_n \end{Bmatrix}_{(I)} \tag{7.32}$$

Expanding the residuals in a truncated Taylor series and making the (I) residuals small, one gets in the normal Newton-Raphson fashion,

$$0 = R_{1(I-1)} + \frac{\partial R_1}{\partial \tau_n}_{(I-1)} \delta\tau_{n(I)} + \frac{\partial R_1}{\partial \sigma_n}_{(I-1)} \delta\sigma_{n(I)} \tag{7.33}$$

$$0 = R_{2(I-1)} + \frac{\partial R_2}{\partial \tau_n}_{(I-1)} \delta\tau_{n(I)} + \frac{\partial R_2}{\partial \sigma_n}_{(I-1)} \delta\sigma_{n(I)}$$

which results in a system of equations for the Newton-Raphson stress corrections:

$$\begin{bmatrix} \frac{\partial R_1}{\partial \tau_n} & \frac{\partial R_1}{\partial \sigma_n} \\ \frac{\partial R_2}{\partial \tau_n} & \frac{\partial R_2}{\partial \sigma_n} \end{bmatrix}_{(I-1)} \begin{Bmatrix} \delta\tau_n \\ \delta\sigma_n \end{Bmatrix}_{(I)} = - \begin{Bmatrix} R_1 \\ R_2 \end{Bmatrix}_{(I-1)} \tag{7.34}$$

or

$$\begin{bmatrix} J_{11} & J_{12} \\ J_{21} & J_{22} \end{bmatrix} \begin{Bmatrix} \delta\tau_n \\ \delta\sigma_n \end{Bmatrix} = - \begin{Bmatrix} R_1 \\ R_2 \end{Bmatrix} \tag{7.35}$$

The J_{ij} is the Jacobian used for solving for the stress corrections above.

The first residual equation is now:

$$R_1 = \left(\frac{\tau_n}{F_t}\right)^{\beta} + \left(C_{D_n}\,\alpha_1\right)^{\beta} \left(\frac{\sigma_n}{F_t}\right) \tag{7.36}$$

where

$$C_{D_n}\,\alpha_3 + \alpha_4\left(1 - e^{-\alpha_5 D_N\, q1_n^{pl}}\right) - \alpha_6\left(1 - e^{-\alpha_7 D_N\, q1_n^{pl}}\right) \tag{7.37}$$

$$q1_n^{pl} = q1_b^{pl} + \Delta q1 t_n - A_{11}(\tau_n - \tau_b) - A_{12}(\sigma_n - \sigma_b) \tag{7.38}$$

The J_{11} and J_{12} Jacobian terms are found by taking the derivatives of this first residual equation. For the J_{11} term,

$$J_{11} = \frac{\partial R_1}{\partial \tau_n} \tag{7.39}$$

where

$$\frac{\partial R_1}{\partial \tau_n} = \frac{\beta}{F_t}\left(\frac{\tau_n}{F_t}\right)^{(\beta-1)} + \beta\alpha_1\left(C_{D_n}\,\alpha_1\right)^{(\beta-1)} \frac{\partial C_{D_n}}{\partial \tau_n} \frac{\sigma_n}{F_t} \tag{7.40}$$

$$\frac{\partial C_{D_n}}{\partial \tau_n} = \left[\alpha_4\alpha_5 e^{-\alpha_5 D_N q1_n^{pl}} - \alpha_6\alpha_7 e^{-\alpha_7 D_N q1_n^{pl}}\right] \frac{\partial q1_n^{pl}}{\partial \tau_n} \tag{7.41}$$

$$\frac{\partial q1_n^{pl}}{\partial \tau_n} = - A_{11} \tag{7.42}$$

For the J_{12} term,

$$J_{12} = \frac{\partial R_1}{\partial \sigma_n} \tag{7.43}$$

where

$$\frac{\partial R_1}{\partial \sigma_n} = \beta \alpha_1 (C_{D_n} \alpha_1)^{(\beta-1)} \frac{\sigma_n}{F_t} \frac{\partial C_{D_n}}{\partial \sigma_n} + (C_{D_n} \alpha_1)^{\beta} \frac{1}{F_t} \tag{7.44}$$

$$\frac{\partial C_{D_n}}{\partial \sigma_n} = [\alpha_4 \alpha_5 e^{-\alpha_5 D_N q_n^{pl}} - \alpha_6 \alpha_7 e^{-\alpha_7 D_N q_n^{pl}}] \frac{\partial q1_n^{pl}}{\partial \sigma_n} \tag{7.45}$$

$$\frac{\partial q1_n^{pl}}{\partial \sigma_n} = - A_{12} \tag{7.46}$$

The second residual equation is:

$$R_2 = \dot{q}_{2n}^{pl} (h_n + \tan\theta_r) - \dot{q}_{1n}^{pl} (1 - h_n \tan\theta_r) \tag{7.47}$$

where

$$h_n = \beta \left(\frac{\tau_n}{F_t}\right)^{(\beta-1)} / (C_{D_n} \alpha_1)^{\beta} \tag{7.48}$$

$$\dot{q}_{1n}^{pl} = \Delta q_1 - A_{11} \left(\frac{\tau_n - \tau_{n-1}}{\Delta t_n}\right) - A_{12} \left(\frac{\sigma_n - \sigma_{n-1}}{\Delta t_n}\right) \tag{7.49}$$

$$\dot{q}_{2n}^{pl} = \Delta q_2 - A_{12} \left(\frac{\tau_n - \tau_{n-1}}{\Delta t_n}\right) - A_{22} \left(\frac{\sigma_n - \sigma_{n-1}}{\Delta t_n}\right) \tag{7.50}$$

The associated Jacobian terms J_{21} and J_{22} are now found. For the J_{21} term,

$$J_{21} = \frac{\partial R_2}{\partial \tau_n} \tag{7.51}$$

where

$$\frac{\partial R_2}{\partial \tau_n} = \frac{\partial h_n}{\partial \tau_n} \left(\dot{q}_{1n}^{pl} \tan\theta_r + \dot{q}_{2n}^{pl} \right) + \frac{\partial \dot{q}_{2n}^{pl}}{\partial \tau_n} \left(h_n + \tan\theta_r \right)$$

$$- \frac{\partial \dot{q}_{1n}^{pl}}{\partial \tau_n} \left(1 - h_n \tan\theta_r \right) \tag{7.52}$$

$$\frac{\partial h_n}{\partial \tau_n} = \frac{(C_{D_n} \alpha_1)^{\beta} \frac{\beta(\beta-1)}{F_t} \left(\frac{\tau_n}{F_t} \right)^{\beta-2} - \beta^2 \left(\frac{\tau_n}{F_t} \right)^{(\beta-1)} \alpha_1 (C_{D_n} \alpha_1)^{(\beta-1)}}{\left((C_{D_n} \alpha_1)^{\beta} \right)^2} \frac{\partial C_{D_n}}{\partial \tau_n} \tag{7.53}$$

$$\frac{\partial \dot{q}_{1n}^{pl}}{\partial \tau_n} = - \frac{A_{11}}{\Delta t_n} \tag{7.54}$$

$$\frac{\partial \dot{q}_{2n}^{pl}}{\partial \tau_n} = - \frac{A_{12}}{\Delta t_n} \tag{7.55}$$

For the J_{22} term,

$$J_{22} = \frac{\partial R_2}{\partial \sigma_n} \tag{7.56}$$

where

$$\frac{\partial R_2}{\partial \sigma_n} = \frac{\partial h_n}{\partial \sigma_n} \left(\partial \dot{q}_{1n}^{pl} \tan\theta_r + \partial \dot{q}_{2n}^{pl} \right) + \frac{\partial \dot{q}_{2n}^{pl}}{\partial \sigma_n} \left(h_n + \tan\theta_r \right)$$

$$- \frac{\partial \dot{q}_{1n}^{pl}}{\partial \sigma_n} \left(1 - h_n + \tan\theta_r \right) \tag{7.57}$$

$$\frac{\partial h_n}{\partial \sigma_n} = - \beta^2 \left(\frac{\tau_n}{F_t} \right)^{(\beta-1)} \alpha_1 \left(C_{D_n} \alpha_1 \right)^{(-\beta-1)} \frac{\partial C_{D_n}}{\partial \sigma_n} \tag{7.58}$$

$$\frac{\partial \dot{q}_{1n}^{pl}}{\partial \sigma_n} = - \frac{A_{12}}{\Delta t_n} \tag{7.59}$$

$$\frac{\partial \dot{q}_{2n}^{pl}}{\partial \sigma_n} = - \frac{A_{22}}{\Delta t_n} \tag{7.60}$$

These equations are used to solve for τ_n and σ_n using Newton-Raphson iteration for each time step.

Bond Material Jacobian

Recall that in addition to the new bond stresses, the global finite element routine requires the bond material Jacobian in order to form the global Jacobian. The material Jacobian is:

$$[J_{BG}] = \begin{bmatrix} \frac{\partial \tau}{\partial q_1} & \frac{\partial \tau}{\partial q_2} \\ \frac{\partial \sigma}{\partial q_1} & \frac{\partial \sigma}{\partial q_2} \end{bmatrix} = \begin{bmatrix} J_{G11} & J_{G12} \\ J_{G21} & J_{G22} \end{bmatrix} \tag{7.61}$$

which for the particular increment of strain is written:

$$\begin{bmatrix} \frac{\partial \tau_n}{\partial \Delta q_1} & \frac{\partial \tau_n}{\partial \Delta q_2} \\ \frac{\partial \sigma_n}{\partial \Delta q_1} & \frac{\partial \sigma_n}{\partial \Delta q_2} \end{bmatrix} \tag{7.62}$$

To derive these Jacobian terms we return to the two residual equations of the yield surface and the flow rule, Equations 7.36, 7.47. Now, for the assumed plastic loading,

$$\frac{\partial R_1}{\partial \Delta q_1} = 0$$

$$\frac{\partial R_1}{\partial \Delta q_2} = 0 \tag{7.63}$$

that is, the stress state remains on the yield surface for an increment of strain. Likewise,

$$\frac{\partial R_2}{\Delta q_1} = 0 \quad , \quad \frac{\partial R_2}{\partial \Delta q_2} = 0 \tag{7.64}$$

the flow rule must be satisfied.

Implicit partial differentiation of the residual equations and the chain rule are used to form Equations 7.63 and 7.64:

$$\frac{\partial R_{1n}}{\partial \Delta q_1} + \frac{R_{1n}}{\partial \tau_n}\left(\frac{\partial \tau_n}{\partial \Delta q_1}\right) + \frac{\partial R_{1n}}{\partial \sigma_n}\left(\frac{\partial \sigma_n}{\partial \Delta q_1}\right) = 0$$

$$\frac{\partial R_{1n}}{\partial \Delta q_2} + \frac{R_{1n}}{\partial \tau_n}\left(\frac{\partial \tau_n}{\partial \Delta q_2}\right) + \frac{\partial R_1}{\partial \sigma_n}\left(\frac{\partial \sigma_n}{\partial \Delta q_2}\right) = 0$$

$$\frac{\partial R_{2n}}{\partial \Delta q_1} + \frac{R_{2n}}{\partial \tau_n}\left(\frac{\partial \tau_n}{\partial \Delta q_1}\right) + \frac{\partial R_2}{\partial \sigma_n}\left(\frac{\partial \sigma_n}{\partial \Delta q_1}\right) = 0$$

$$\frac{\partial R_{2n}}{\partial \Delta q_2} + \frac{R_{2n}}{\partial \tau_n}\left(\frac{\partial \tau_n}{\partial \Delta q_2}\right) + \frac{\partial R_2}{\partial \sigma_n}\left(\frac{\partial \sigma_n}{\partial \Delta q_2}\right) = 0 \tag{7.65}$$

The results are four simultaneous equations in the desired global material Jacobian terms. Note that some of these terms are identical to the Jacobian of Equation 7.35. Additionally, the derivatives of the residual equations with respect to the strain increments Δq_1 and Δq_2 need to be derived. The four new terms that result are:

$$\frac{\partial R_1}{\partial \Delta q_1} = \alpha_1 \beta (C_{D_n} \alpha_1)^{(\beta-1)} \frac{\partial C_{D_n}}{\partial \Delta q_1} \left(\frac{\sigma_n}{F_t}\right) \tag{7.66}$$

$$\frac{\partial C_{D_n}}{\partial \Delta q_1} = [\alpha_4 \alpha_5 D_n e^{-\alpha_5 D_N q_{1_n}^{pl}} - \alpha_6 \alpha_7 D_n e^{-\alpha_7 D_N q_{1_n}^{pl}}] \frac{\partial q_{1_n}^{pl}}{\partial \Delta q_1} \tag{7.67}$$

$$\frac{\partial q_{1_n}^{pl}}{\partial \Delta q_1} = t_n \tag{7.68}$$

and

$$\frac{\partial R_1}{\partial \Delta q_2} = 0 \tag{7.69}$$

and

$$\frac{\partial R_2}{\partial \Delta q_1} = \frac{\partial h_n}{\partial \Delta q_1} (\dot{q}_{1n}^{pl} \tan\theta_r + \dot{q}_{2n}^{pl}) + \frac{\partial \dot{q}_{2n}^{pl}}{\partial \Delta q_2} (h_n + \tan\theta_r) - \frac{\partial \dot{q}_{1n}^{pl}}{\partial \Delta q_1} (1 - h_n \tan\theta_r) \tag{7.70}$$

$$\frac{\partial h_n}{\partial \Delta q_1} = \beta \left(\frac{\tau_n}{F_t}\right)^{(\beta-1)} (-\beta\alpha_1)^{(-\beta-1)} \frac{\partial C_{D_n}}{\partial \Delta q_1} \tag{7.71}$$

$$\frac{\partial \dot{q}_{1n}^{pl}}{\partial \Delta q_1} = 1 + \frac{A_{11}}{\Delta t} \frac{\partial \tau_{n-1}}{\partial \Delta q_1} + \frac{A_{12}}{\Delta t} \frac{\partial \sigma_{n-1}}{\partial \Delta q_1} \tag{7.72}$$

$$\frac{\partial \dot{q}^{pl}_{2n}}{\partial \Delta q_2} = 1 + \frac{A_{12}}{\Delta t}\frac{\partial \tau_{n-1}}{\partial \Delta q_1} + \frac{A_{22}}{\Delta t}\frac{\partial \sigma_{n-1}}{\partial \Delta q_1} \tag{7.73}$$

Note that the derivatives of the stresses at the previous time step will be known for the present time step for which these equations are formulated. The final term is:

$$\frac{\partial R_2}{\partial q_2} = \frac{\partial \dot{q}^{pl}_{2n}}{\partial \Delta q_2}(h_n + \tan\theta_r) - \frac{\partial \dot{q}^{pl}_{1n}}{\partial \Delta q_2}(1 - h_n \tan\theta_r) \tag{7.74}$$

$$\frac{\partial \dot{q}^{pl}_{1n}}{\partial \Delta q_2} = \frac{A_{11}}{\Delta t}\frac{\partial \tau_{n-1}}{\Delta q_2} + \frac{A_{12}}{\Delta t}\frac{\partial \sigma_{n-1}}{\partial \Delta q_2} \tag{7.75}$$

$$\frac{\partial \dot{q}^{pl}_{2n}}{\partial \Delta q_2} = 1 + \frac{A_{12}}{\Delta t}\frac{\partial \tau_{n-1}}{\partial \Delta q_2} + \frac{A_{22}}{\Delta t}\frac{\partial \sigma_{n-1}}{\partial \Delta q_2} \tag{7.76}$$

All the terms required to calculate the bond material Jacobian have been found. The system of equations for the Jacobian is rewritten as:

$$(J_{11})\,J_{G11} + (J_{12})\,J_{G21} = \frac{-\partial R_1}{\partial \Delta q_1}$$

$$(J_{21})\,J_{G11} + (J_{22})\,J_{G21} = \frac{-\partial R_2}{\partial \Delta q_1} \tag{7.77}$$

$$(J_{11})\,J_{G12} + (J_{12})\,J_{G22} = 0$$

$$(J_{21})\,J_{G12} + (J_{22})\,J_{G22} = \frac{-\partial R_2}{\partial \Delta q_2} \tag{7.78}$$

The resulting two pair of equations, each in two unknowns, are solved numerically using Cramer's rule. Note the whole process of calculating the bond material Jacobian is not performed until the converged stresses are determined by appropriate sub-stepping. This is accomplished by saving the converged stress history. Later, the recursive bond material Jacobian equations are solved without iteration given the converged stress history. This saves substantial computation, as this

process must be repeated for each global Newton-Raphson iteration and for each quadrature point in the finite element model. Details of the FORTRAN code used to evaluate the model can be found in Mello (1996).

8. ELEMENT VERIFICATION TESTS

The element, its material model, and FORTRAN code implementation were tested during various stages of development. The three main test sets were linear composite element tests, bond model tests, and structural tests. Examples of each are discussed below.

8.1 Linear Composite Element Tests

This stage of testing was performed after development of the composite material model and the creation of the four degree of freedom linear-elastic element based on the composite material relations. The analyses were aimed at testing the micro-mechanics material model accuracy and verifying that the finite element stiffness matrix and global arrays were modified to handle four degrees of freedom correctly. The results reported here are for no-slip micro-mechanics, uniform slip, and shear-lag problems.

8.1.1 No-Slip Tests. The no-slip micro-mechanics tests were performed to demonstrate that the composite material model would specialize to the case of perfect bonding between fiber and matrix, that is the case of no-slip. This was done in the four degrees of freedom finite element setting using a penalty formulation (Cook, 1981) to constrain the fiber displacement to that of the matrix (no-slip). Additionally, the dilation was set to zero for all nodes in the model. Single and multiple element tests were performed. Three of the tests were uniform displacement in the fiber direction, the transverse direction, and a state of shear in the xy plane (plane of the fibers). These tests are essentially analytical versions of the three basic orthotropic composite material characterization cases. The results were compared to a perfect bonding micro-mechanics material model based on a two-dimensional finite element analysis of a hexagonal packed fiberglass/epoxy composite (Schulz, 1965). A comparison of results is presented below in Table 1. The small differences are due to the approximation of modeling the hexagonal cross section of the unit cell as circular (see Figure 5).

Table 1. No-Slip Micro-Mechanics Test Results

Strain Fiber Direction (x)		
Method	Transverse Strain (in.)	Fiber Direction Stress (psi)
Hex pack. micro-mechanics	-0.00444	87660
Composite finite element	-0.00457	88030
Percentage difference (%)	2.9	0.42
Strain Transverse Direction (y)		
Method	Fiber Dir. Strain (in.)	Transverse Stress (psi)
Hex pack. micro-mechanics	-0.00145	28630
Composite finite element	-0.00146	28080
Percentage difference (%)	0.70	1.9
In-Plane Shear (xy) Fiber-Transverse		
Method	Composite Shear Stress (psi)	
Hex pack. micro-mechanics	7150	
Composite finite element	7043	
Percentage difference (%)	1.5	

These results show the correctness of the composite micro-mechanics model. They also show that the finite element and its embedded linear micro-mechanics material model can specialize to the case of perfect bonding.

8.1.2 Uniform Slip. The uniform slip case tested the implementation of the bond elasticity model by isolating its response. These analyses included one- and four-element models where the transverse, u_y, and matrix, u_x, displacements were set to zero while a fiber displacement or slip was prescribed. For prescribed slip, the dilation and bond stresses that result were compared to simple analytical calculations based on the bond elasticity relations. A comparison of results is given in Table 2. The linear bond model is implemented correctly as shown by these results.

Table 2. Uniform Slip Test Results

Method	Dilation	Bond Shear Stress	Bond Normal Stress
Analytical	5.290×10^{-6}	6652	-6649
Finite Element	5.291×10^{-6}	6653	-6649

8.1.3 Shear-Lag Tests. The shear-lag test case compared a classical shear-lag solution to finite element results. The test and corresponding composite finite element model is shown in Figure 19. This test simulated pulling reinforcement from a fully-fixed prism of concrete.

An approximate analytical solution was found by reducing the problem to an ordinary differential equation in slip. Figure 20 presents a comparison of the analytical and finite element results. The composite element is able to reproduce linear shear-lag behavior that is associated with an edge effect with a very simple mesh.

8.2 Bond Model and Algorithm Tests

Tests were performed on the bond model and its associated numerical algorithm prior to implementation into the composite finite element. Testing was performed by driving the bond model material algorithm with what amounts to a one-gauss point finite element scheme written in terms of strains and stresses. This driver was patterned after a similar one developed by Herrmann and Kaliakin (1987) that was used to evaluate soil material models and algorithms.

Results of two test cases are presented. These results correspond to some of the bond material characterization tests that Herrmann and Cox (1992) used in development of their bond model. The goal of the present tests is to make sure that the simplified bond model gives results that qualitatively match those of Herrmann and Cox and that the numerical algorithm used to implement the bond model perform adequately.

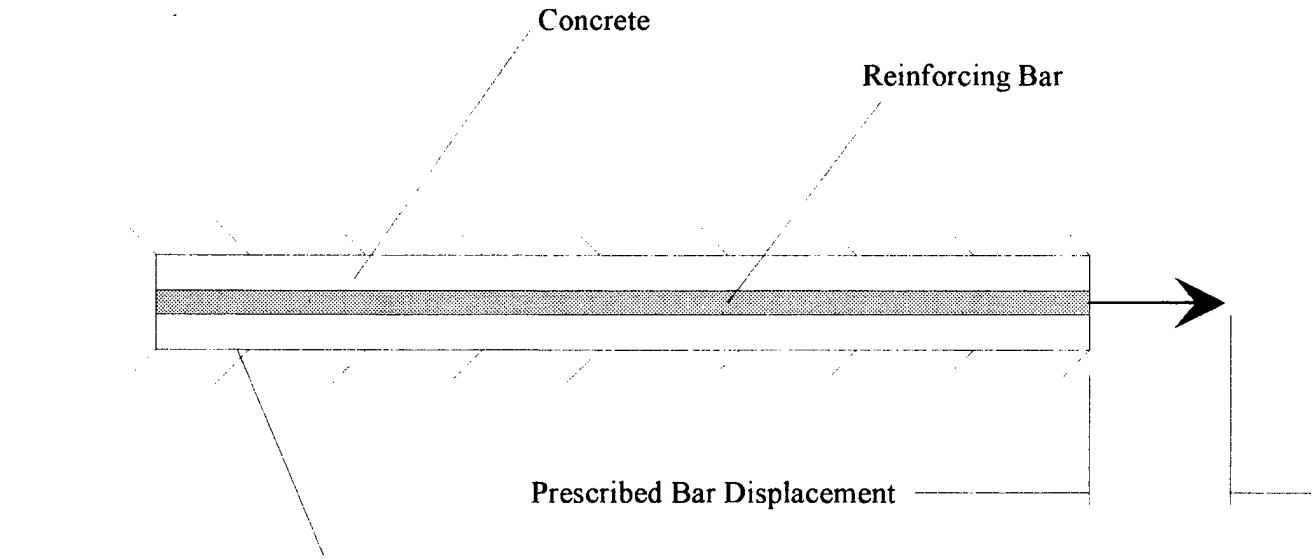

Section View of Reinforced Concrete Prism

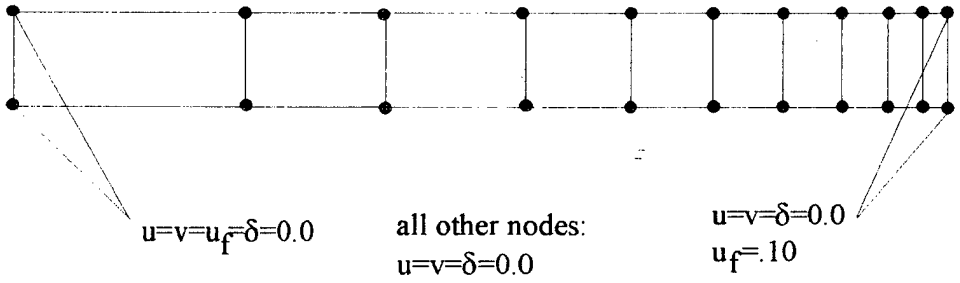

Composite Finite Element Model

Figure 19. - Shear Lag Problem and Finite Element Model

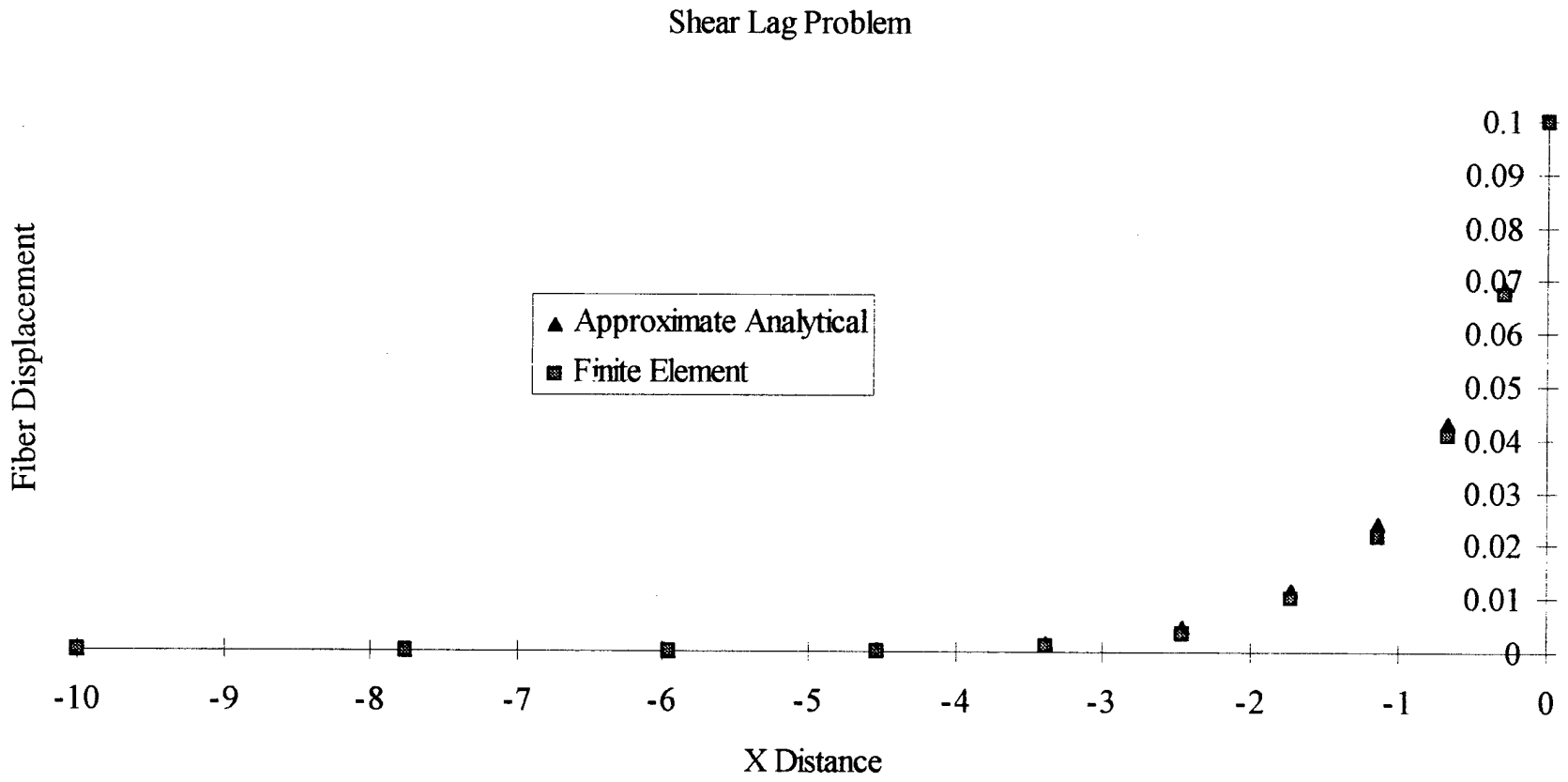

Figure 20. - Shear Lag Problem Results

8.2.1 Simulation of Malvar's Test. In Malvar's (1991) concrete bond tests, confinement pressure was applied to a cylinder of concrete surrounding a single reinforcing bar which was then pulled. The tests yielded bond shear and normal stresses as a function of slip. This test was modeled using the driver program and the simplified bond model described in Sections 6 and 7. Calculated bond shear stress versus slip and dilation are shown in Figures 21 and 22. These can be compared to calculations in Figures 32 and 37 of Herrmann and Cox (1992). A comparison of the plots indicates that the simplified bond model and material algorithm produce results that are qualitatively similar to those of Herrmann and Cox.

8.2.2 Simulation of Gambarova's Test. The Gambarova bond test was somewhat similar to that of Malvar and was also used by Herrmann and Cox in the formulation of their bond model. In this test, a nonsymmetric reinforced prism of concrete was precracked or presplit parallel to the reinforcement. The reinforcement was pulled while normal forces, confinement stresses, were applied to maintain the selected crack width. For more details of the test setup refer to Section 5.3 of Herrmann and Cox or to Gambarova, Rosati, and Zasso (1989).

This test was simulated using the driver program and the simplified bond model. Results are presented in the form of shear and normal stress plots as functions of slip in Figures 23 and 24, which can be compared to Herrmann and Cox's Figures 29 and 30. Once again these results are deemed acceptable as the simplified bond model reproduces the important characteristics of the response.

8.3 Structural Tests

Having verified that the plasticity bond model and algorithm performed adequately, they were implemented in the nonlinear composite finite element code as described in Section 7. Results of a series of tests on this element for a variety of reinforced-concrete structures follow.

8.3.1 Simulation of Bond Tension Tests. A variety of researchers have tested reinforced prisms of concrete to aid in understanding bond effects on a reinforced-concrete structure. Houde and Mirza (1974) have performed tests that attempt to simulate the conditions in the constant moment region of a reinforced beam between tensile cracks. Houde and Mirza instrumented the reinforcement, thus generating good data with which to test the bond model and composite element implementation. The test specimen is shown in Figure 25. The single bar reinforcement was instrumented with strain gages in a cavity machined internally into the bar. Loads were applied to the bar in a tensile test machine. The strain gages allowed the calculation of the bar force distribution as the load was transferred into the concrete prism through the bond.

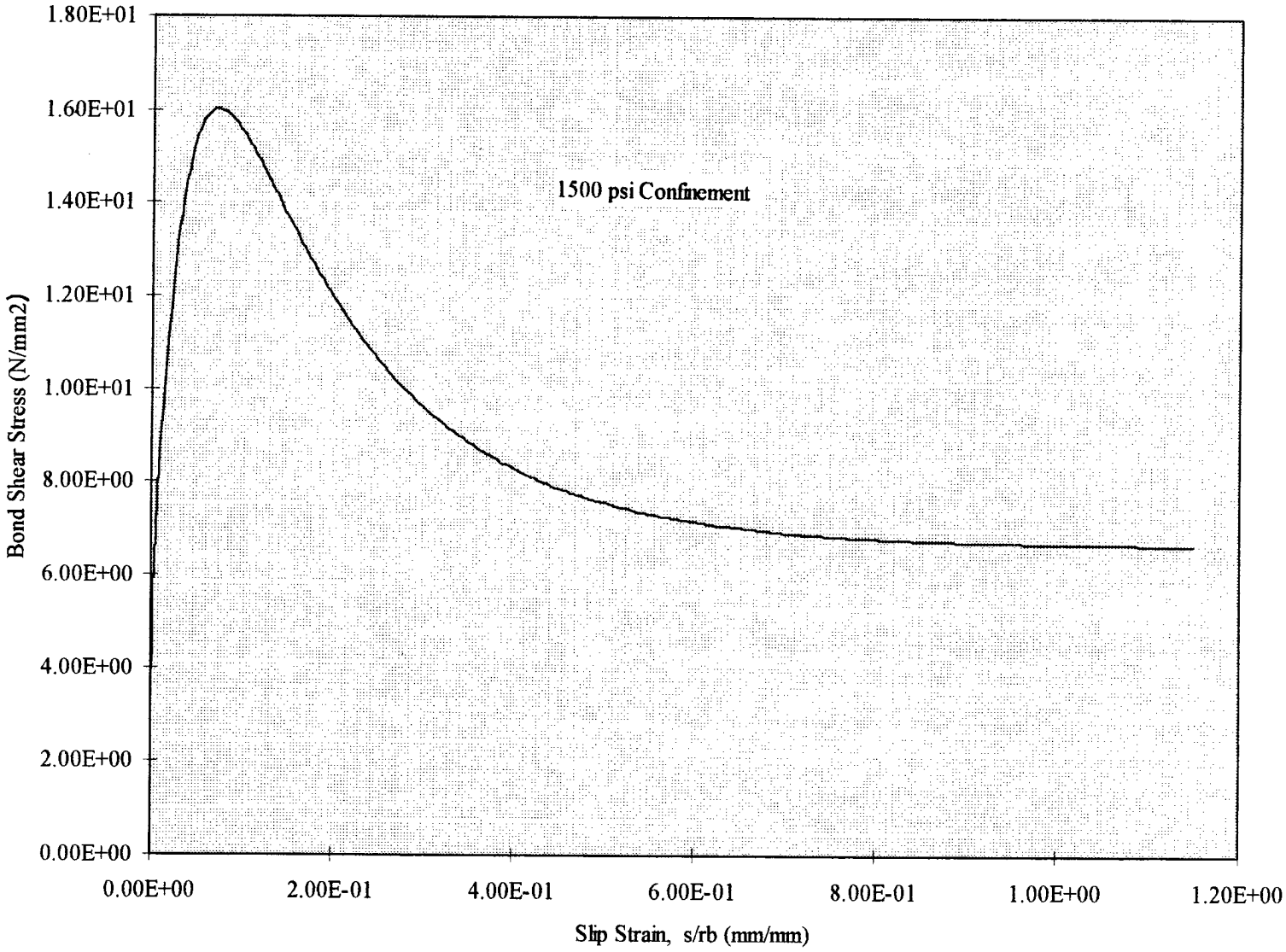

Figure 21. - Malvar Test Simulation, Shear Stress vs. Slip

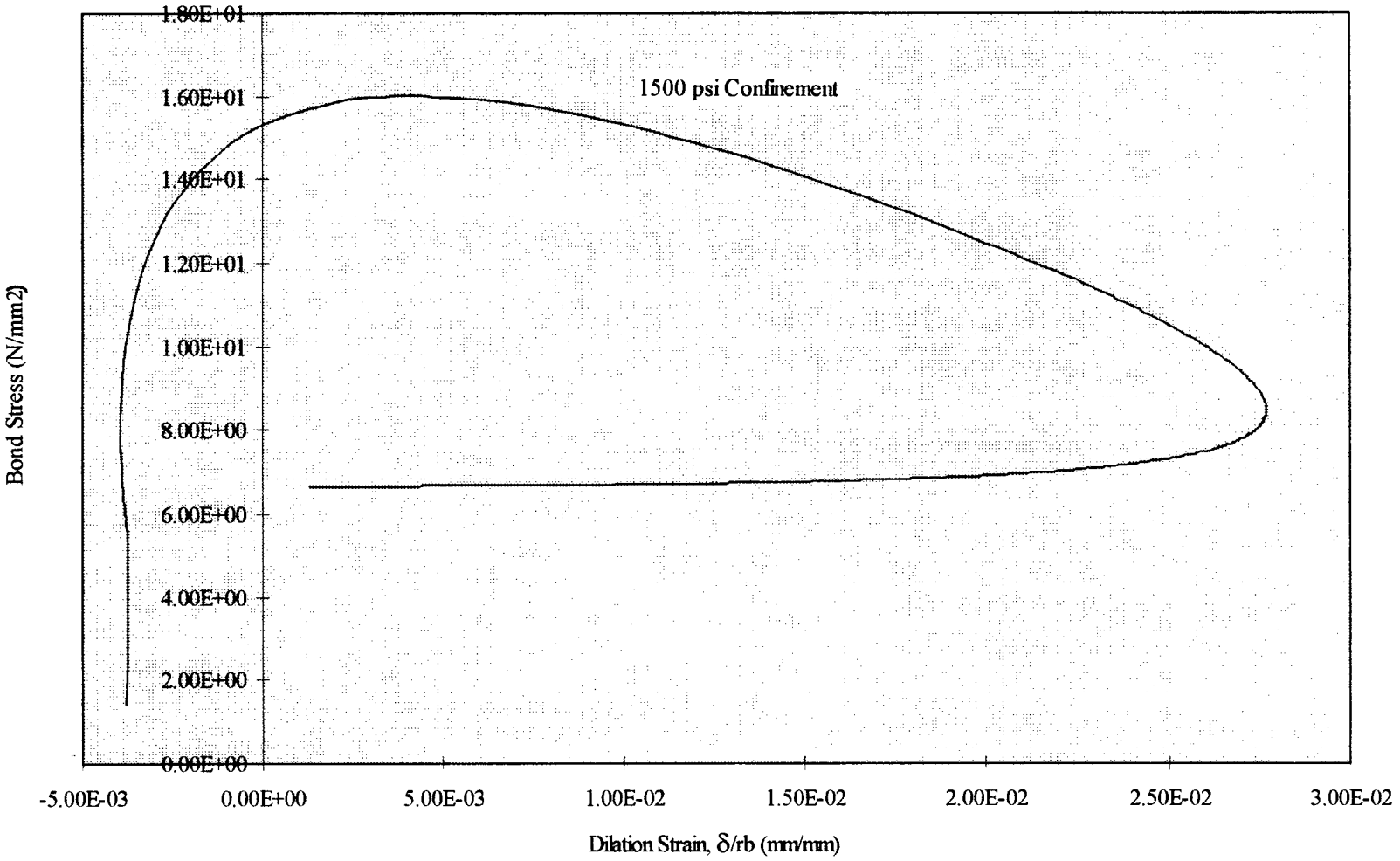

Figure 22. - Malvar Test Simulation, Shear Stress vs. Dilation

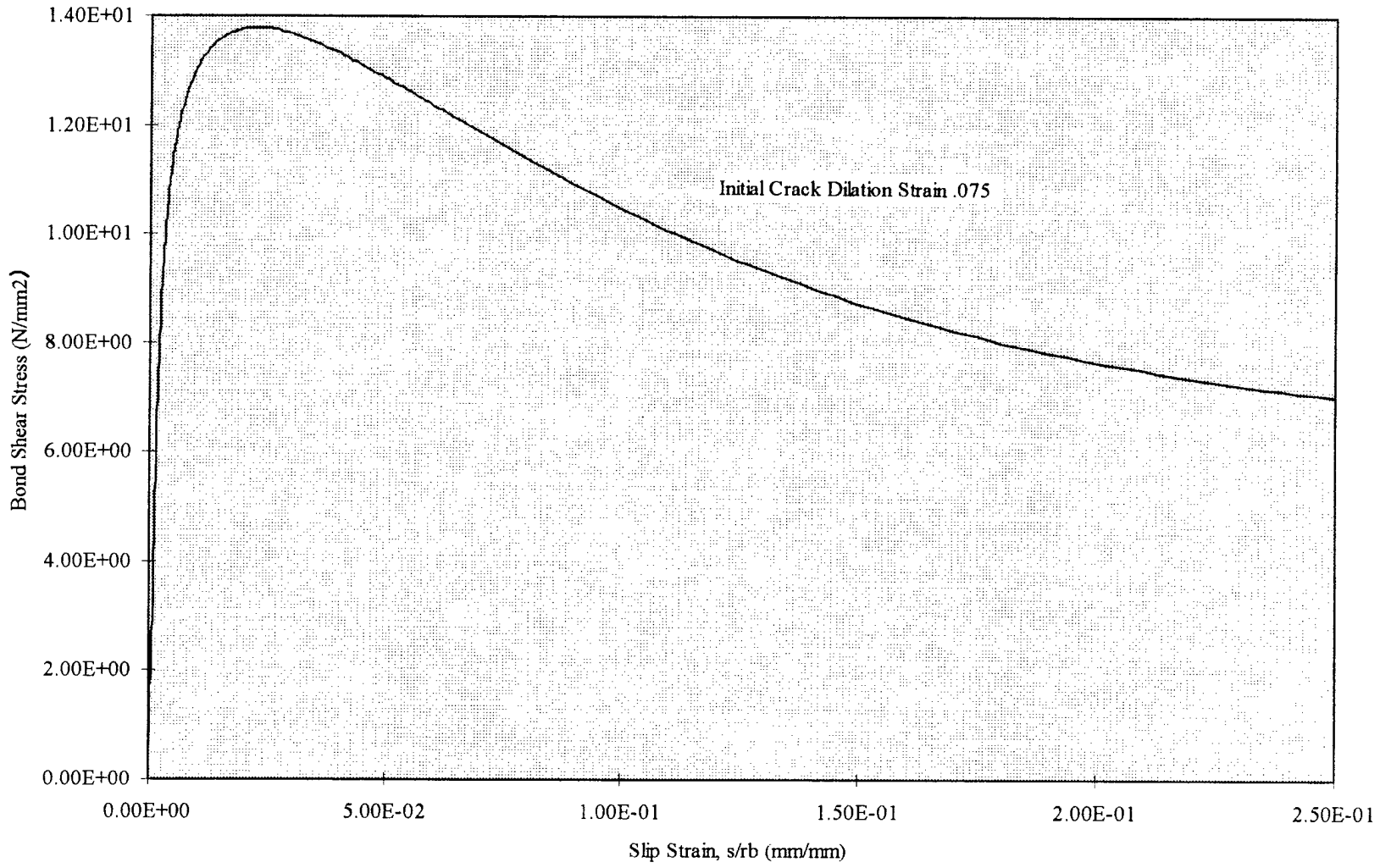

Figure 23. - Gambarova Test Simulation,Shear Stress vs. Slip Strain

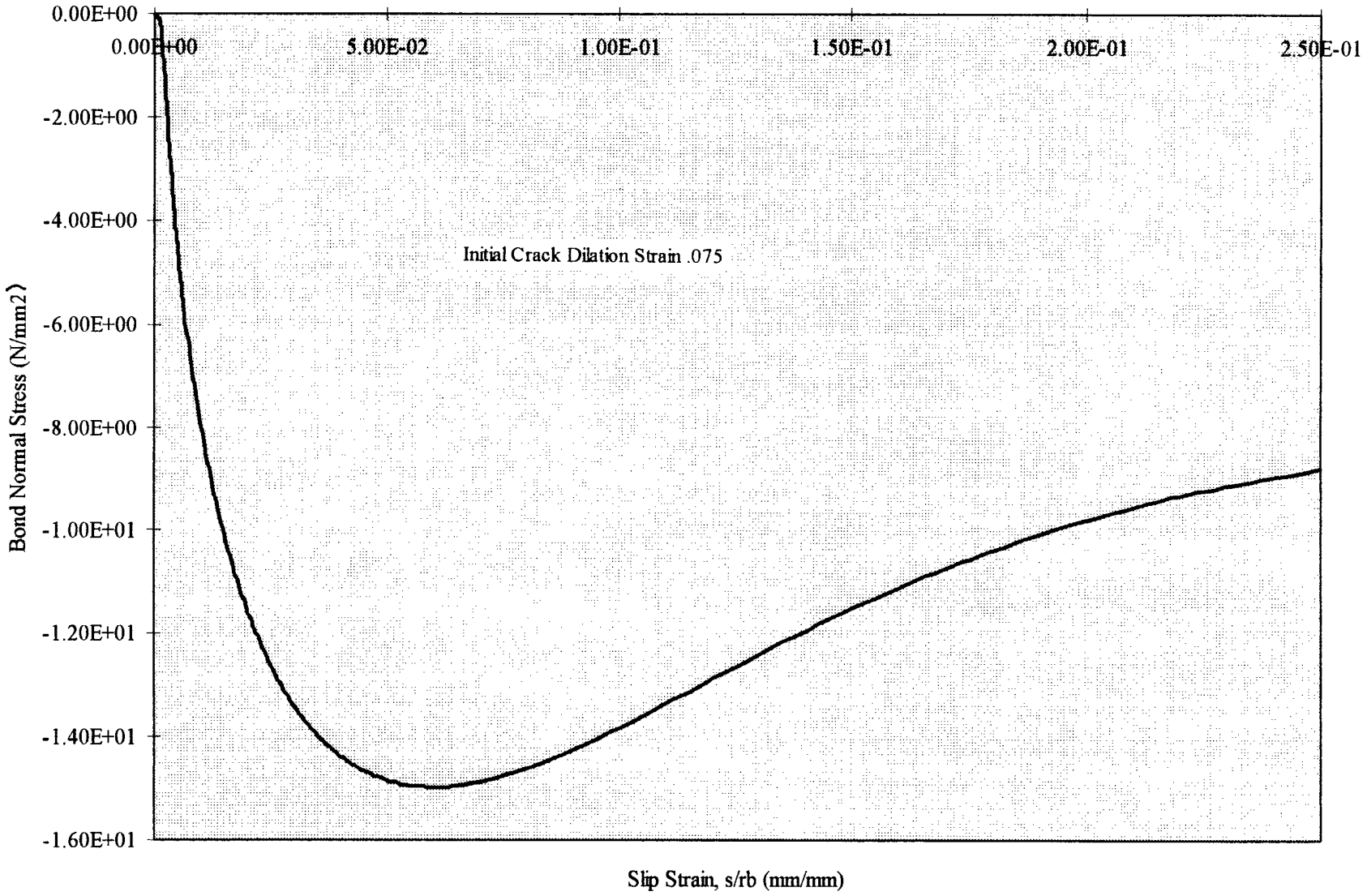

Figure 24. - Gambarova Test Simulation, Normal Stress vs. Slip Strain

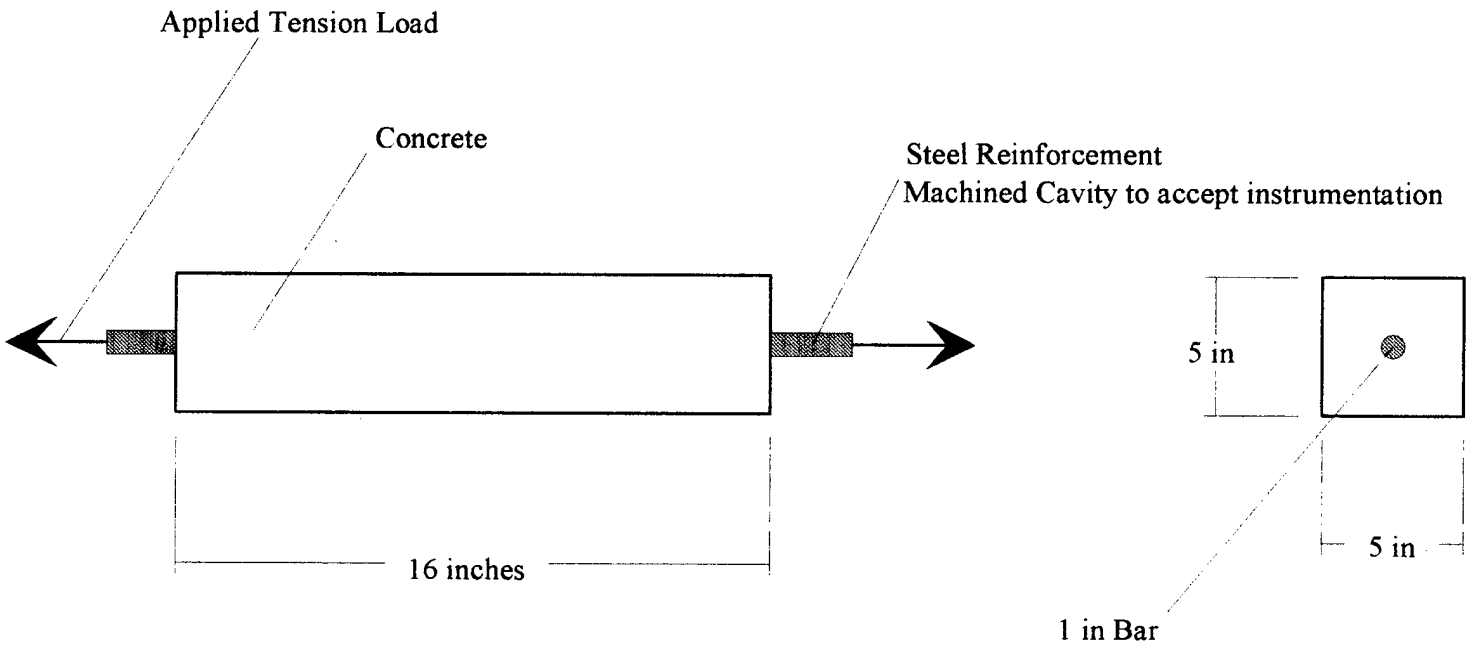

Houde and Mirza
Bond Tension Test No. 19
f 'c = 4955 psi
Esteel = 22.9E6 psi (reduced)
ρ = .040

Bar Instrumentation:
.25 in Strain Gages
.67 in axial spacing in bar cavity

Figure 25. - Houde and Mirza Bond Tension Test

As previously noted, the composite finite element is restricted to plane strain behavior which is better suited to a reinforced slab than a prism. The results, however, can still give a qualitative feel for the bond model and finite element implementation performance. The composite finite element model and boundary conditions for this test are shown in Figure 26. To represent the hollowed bar, the fiber radius and volume fraction were based on the actual bar diameter in order to correctly model the interface in the embedded micro-mechanics model. The lower bar stiffness resulting from the cavity was accounted for by using an artificially-reduced steel modulus. It is important to note the simplicity of the finite element model for this test case. Displacements were prescribed to the fiber degree of freedom simulating the displacement controlled test performed by Houde and Mirza. The model shown is the last in a series of three models in which the mesh size was decreased to check for convergence. Convergence was obtained with one-half of the elements shown.

Resulting predicted bar strains, as a function of distance along the specimen, are plotted for a variety of bar load levels in Figure 27. Similar Houde and Mirza experimental data are given in Figure 28. The model is able to reproduce the qualitative nature of the experimental results. It is not expected to match the quantitative results since the model is plane strain as mentioned earlier. It should also be noted that bar lug spacing and angle which are input parameters for the bond model were not given by Houde and Mirza and are assumed to be similar to those given by other investigators who used bars of similar diameters.

The results are very good in light of the known limitations. The shape of the curves are similar and the strain magnitudes are quite close for common load levels. Note that the composite element predicts detailed bond stresses with a very simple finite element mesh and only basic material parameters.

8.3.2 Simulation of Krefeld and Thurston Cracked-Reinforced Beam. The next reinforced structure analyzed was a cracked-reinforced beam. Krefeld and Thurston (1966) tested a variety of precracked beams to determine how the reinforcing steel contributes to shear resistance. The composite element as implemented in this work cannot model the reinforcement dowel action that Krefeld and Thurston were investigating. To model this effect, it would appear to be necessary to account for finite deformations and the resulting finite length of reinforcement that pulls from the surrounding concrete. This essentially forms a beam spanning the opened crack. In addition, the bending and shear of the reinforcement would need to be accounted for. Krefeld and Thurston's experimental results can still be used to assess the performance of the composite element.

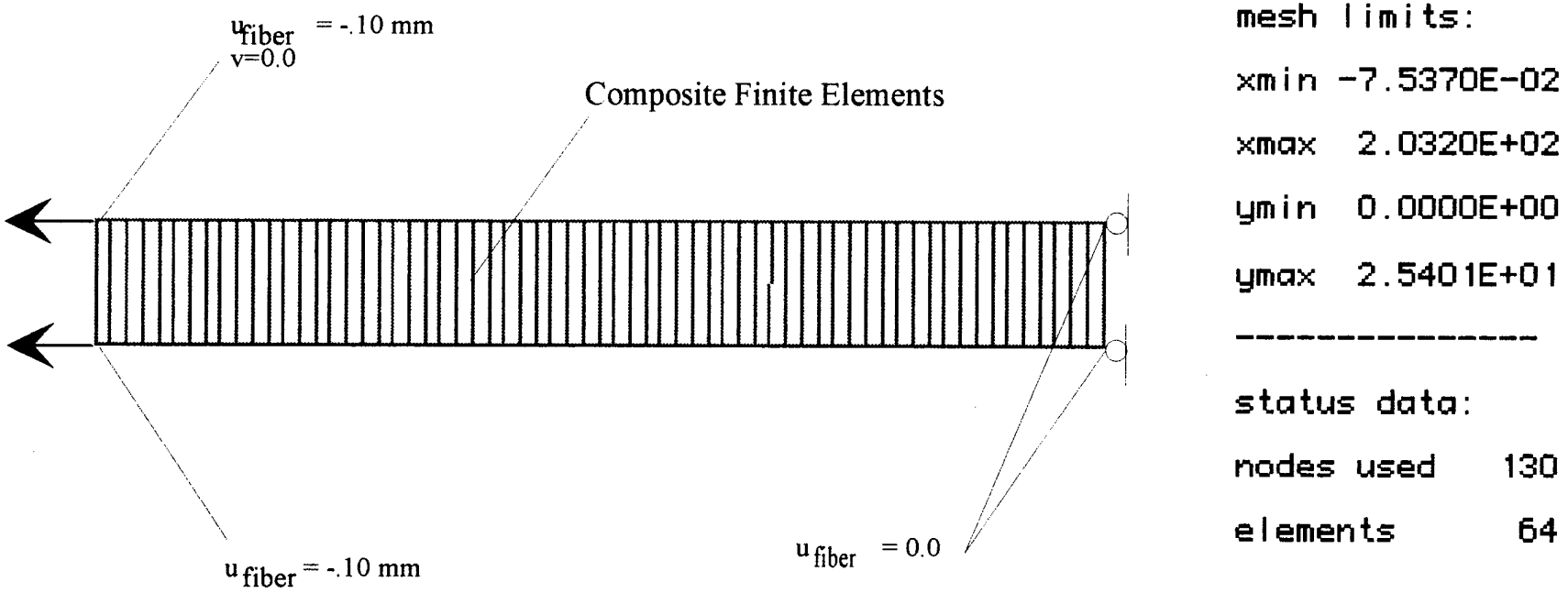

Figure 26. - Houde and Mirza Bond Tension Test Finite Element Model

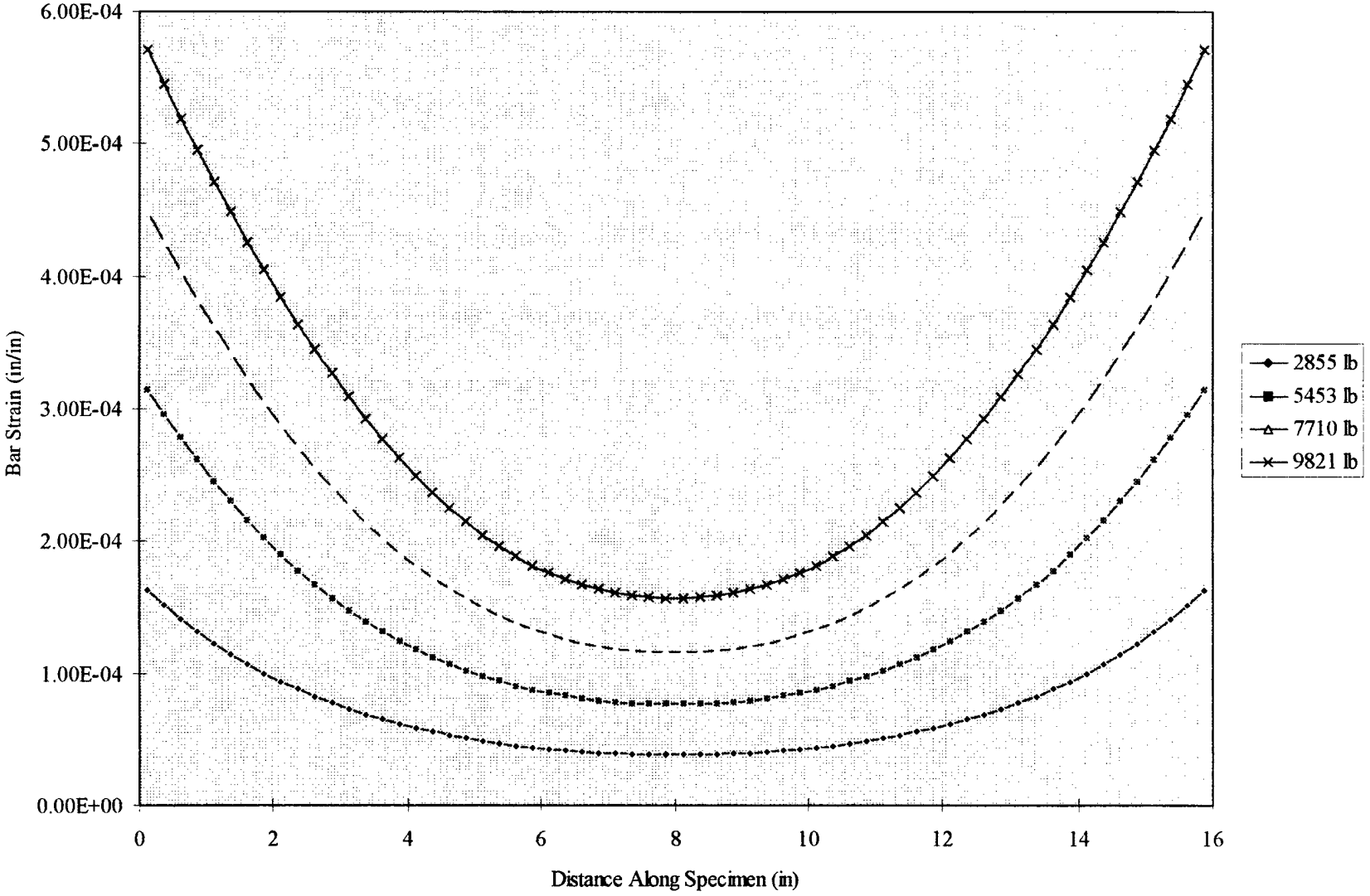

Figure 27. - Houde and Mirza Bond Tension Test, Composite Finite Element Results

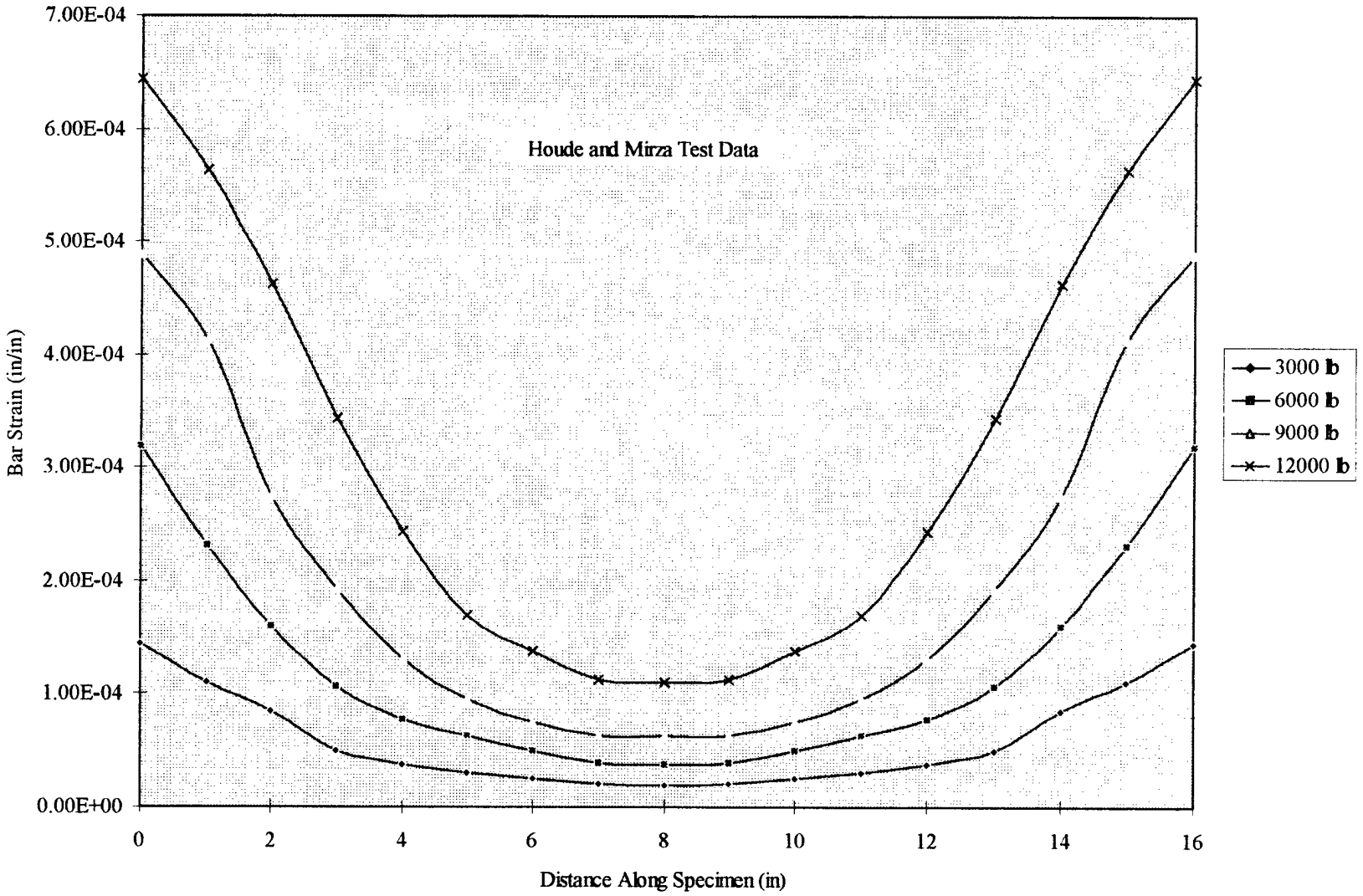

Figure 28. - Houde and Mirza Bond Tension Test Experimental Results

Krefeld and Thurston ran a series of cracked beam tests. Their test, titled DA10, was selected for modeling because the instrumentation included strain gages located on the reinforcement in the crack. The test setup is shown in Figure 29. The corresponding finite element mesh and boundary conditions are shown in Figure 30.

The model employs three different elements. The bottom three rows are composite elements while the upper elements are normal isotropic material elements. The quadrilateral elements in the crack are really truss elements which have stiffness limited to the axial bar response. No shear or bending stiffness was included. As mentioned earlier, the present development is restricted to two-dimensional plane strain and would best model a cracked-reinforced slab. Results again are judged qualitatively rather than quantitatively because of these limitations. (Note that a plane stress implementation could be developed using the three-dimensional material relations given in Equation 4.111. Also a three-dimensional brick element could be developed by adding slip and dilation degrees of freedom to the three global displacement degrees of freedom of a standard 8-node hex element.)

The plane strain model was loaded by prescribing a vertical displacement at the beam's center. The resulting load at the point was accumulated from the global residual before implementation of the essential boundary conditions. Results in the form of a deformed mesh plot are shown in Figure 31. Results are consistent with the boundary conditions and the loss of structure stiffness as a consequence of the crack. Figure 32 is a collection of gray-scale stress contour plots for this model. Figure 32a is the matrix or concrete axial stress. The concrete stress goes to zero in the vicinity of the crack as expected. Figure 32d depicts the fiber, or bar axial stress, while Figures 32e and 32f show the bond stresses for the composite elements. It should be noted that the contour plots were done using averaging across-neighboring elements, which affects the accuracy of stresses at the interface between two material types. A study of these results confirms the expected behavior of a beam cracked in this fashion.

Figure 33 gives experimental results from Krefeld and Thurston (1966) in which the force in the reinforcing bars is plotted versus the applied machine load. Figure 34 is a similar plot using the composite finite element results. The model is not able to predict the nonlinearities present at the higher load levels. These nonlinearities are assumed to be a result of concrete inelastic response due to crushing and cracking and bar yield. Recall that the composite element's nonlinear response is limited to that of the bond and, thus, cannot be expected to predict such behavior. The good quantitative agreement at the lower loads again verifies the composite element approach. Figure 35 presents more finite element results where the bar and machine loads are plotted as a function of the mid-span displacement. Note that, in the case of the machine load, one can see the effects of the bond nonlinearity as the structure softens as a result of slip.

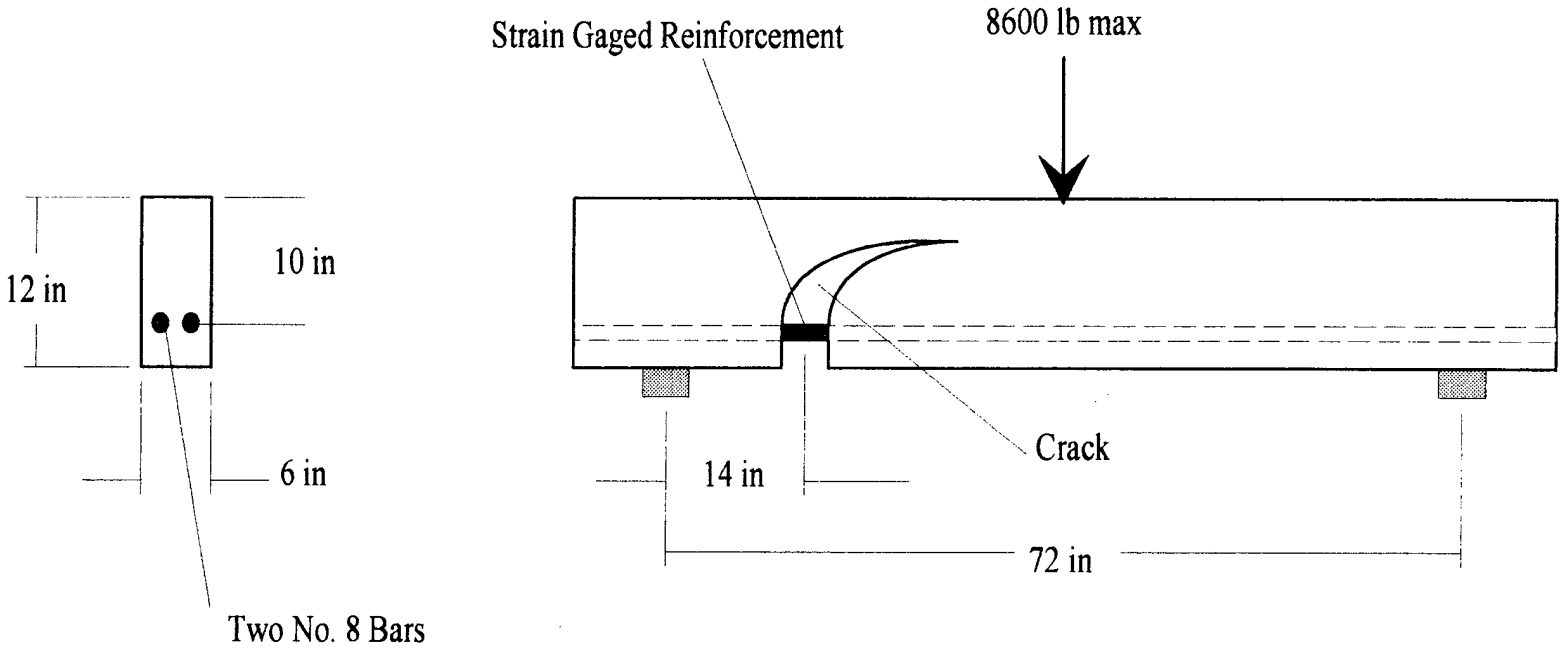

Model Data:
f 'c = 14.82 N/mm2
ρ =.066 for bottom 4 in of beam
Econcrete = 27,500 N/mm2

Figure 29. - Krefeld and Thurston Dowel Test DA10

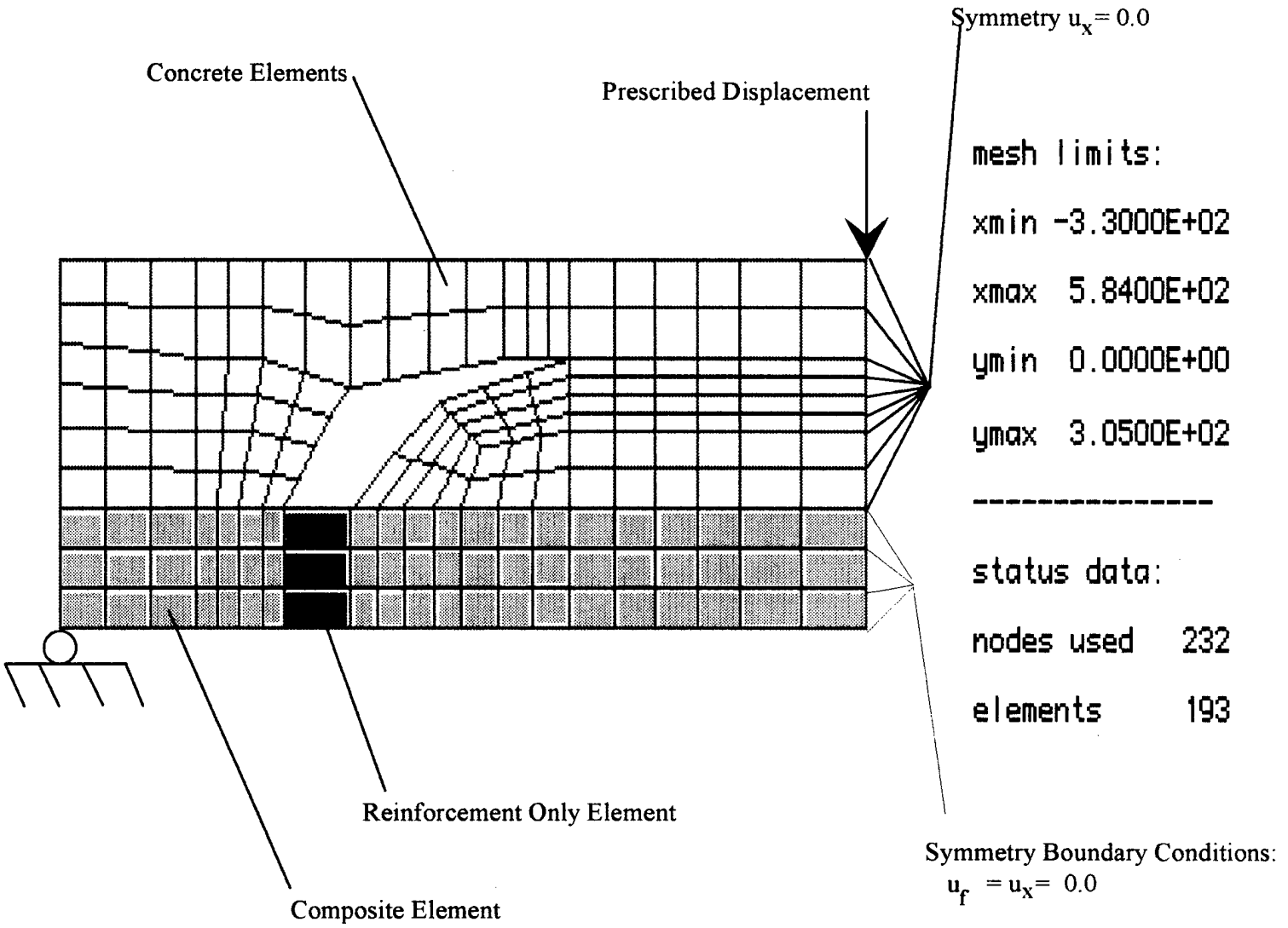

Figure 30. - Krefeld and Thurston Beam - Finite Element Plane Strain Model

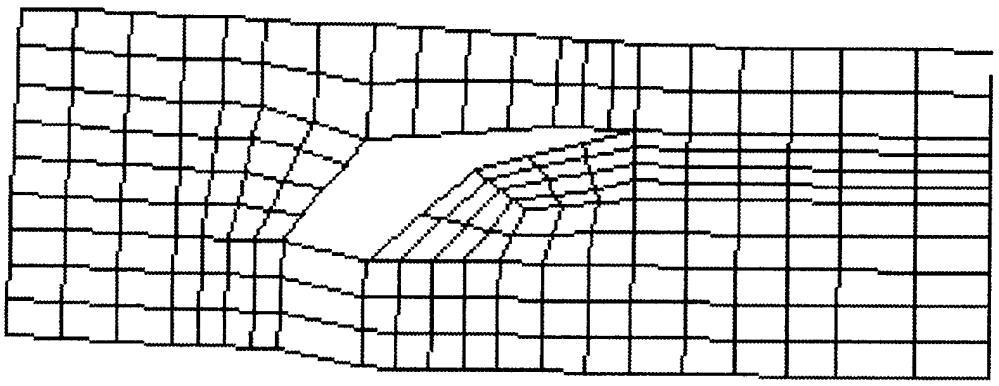

mesh limits:

xmin -3.3700E+02

xmax 5.8523E+02

ymin -3.6436E+01

ymax 3.0430E+02

---

status data:

nodes used 232

elements 193

Figure 31. - Krefeld and Thurston Model, Deformed Mesh Results

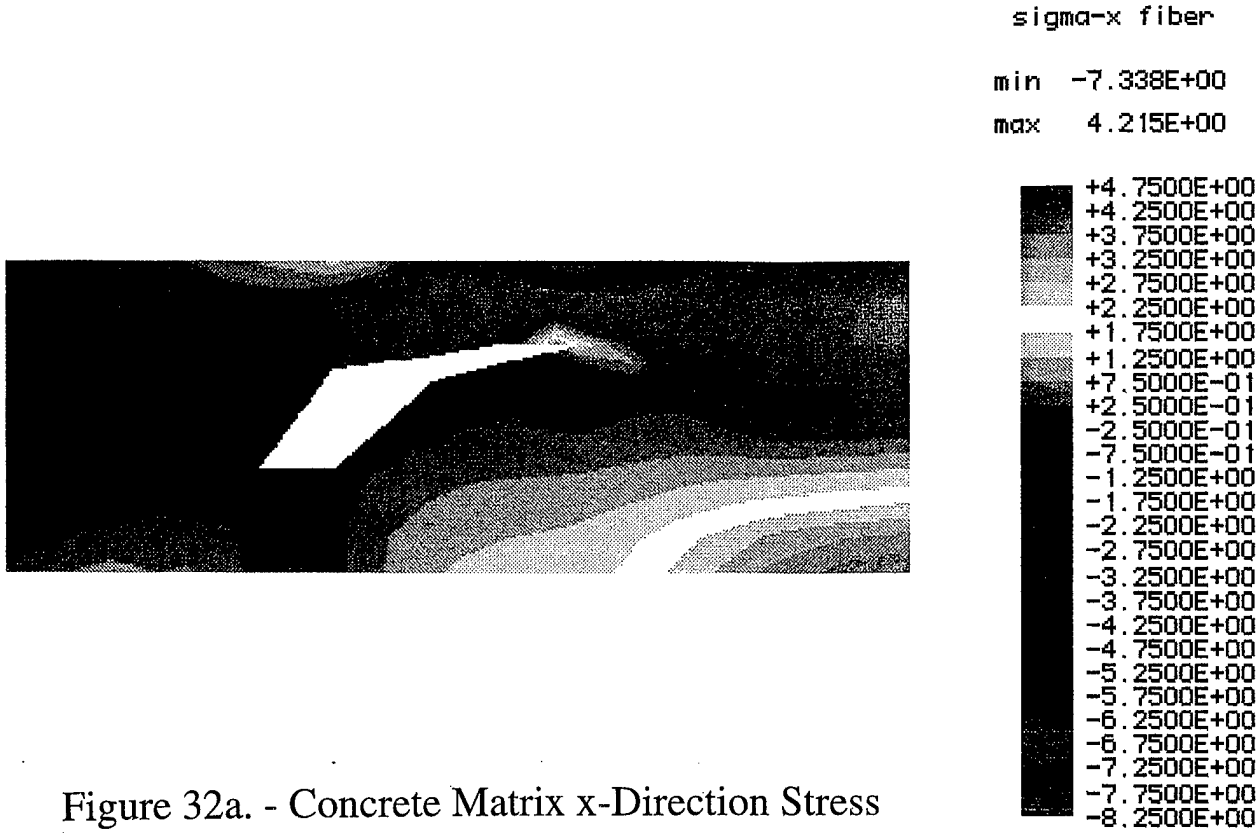

Figure 32a. - Concrete Matrix x-Direction Stress

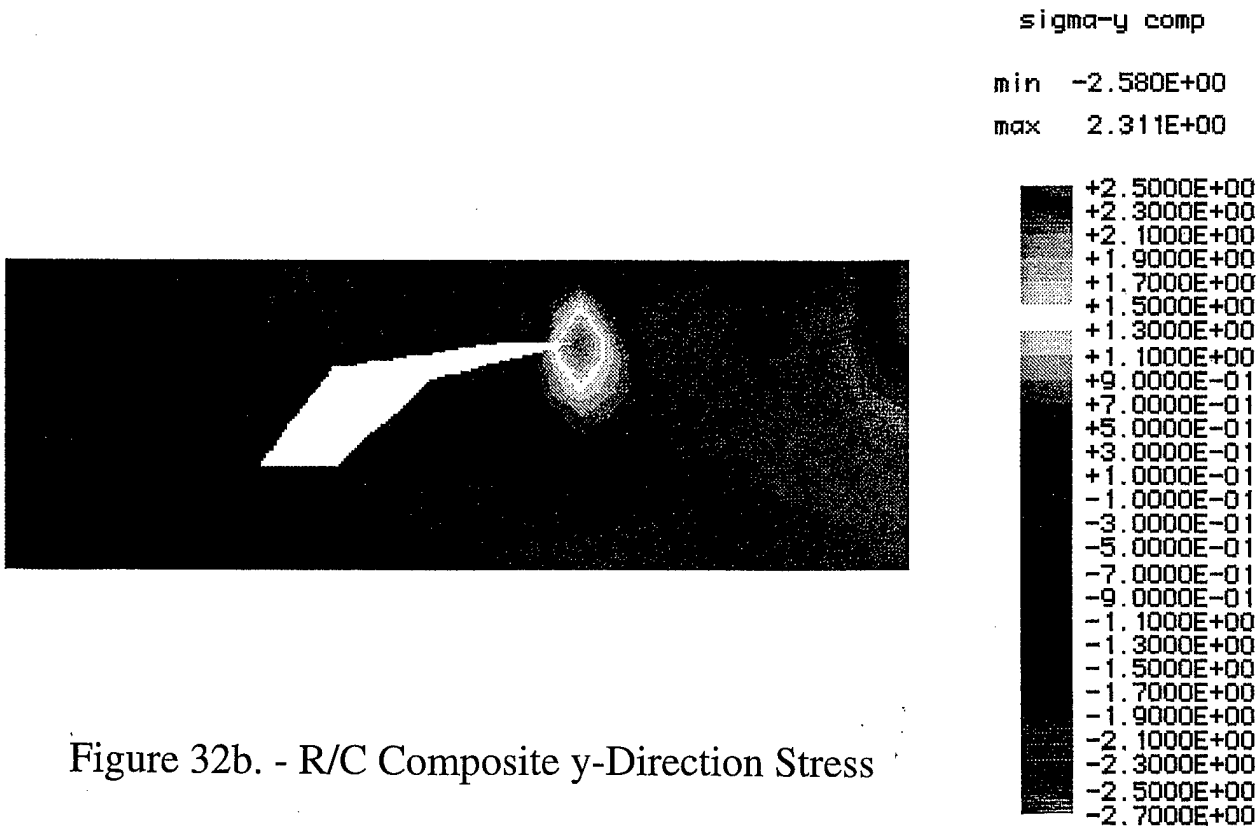

Figure 32b. - R/C Composite y-Direction Stress

Figure 32. - Krefeld and Thurston Beam Simulation

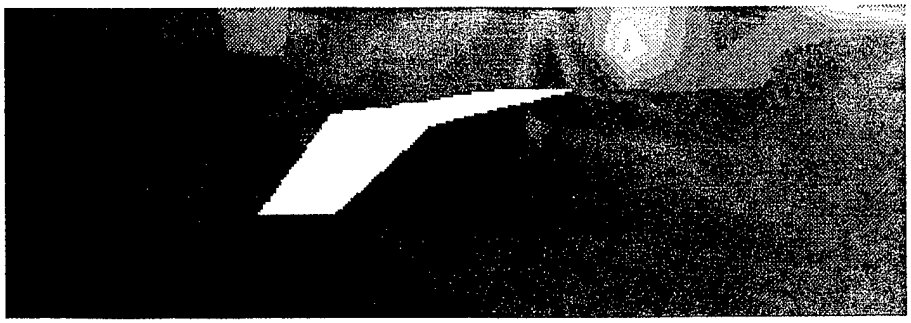

Figure 32c. - R/C Composite xy-Shear Stress

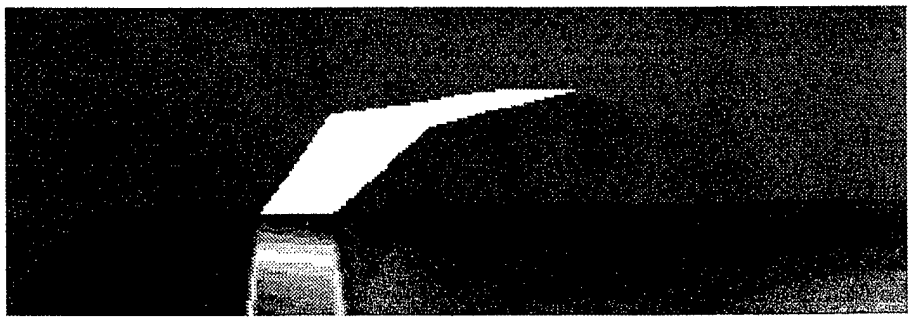

Figure 32d. - Bar x-Direction Stress

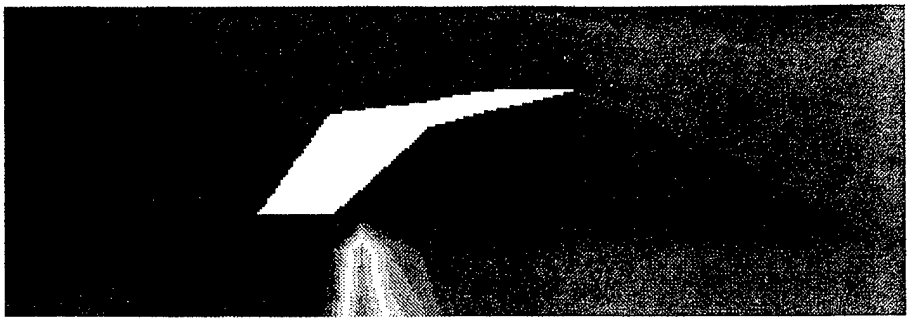

Figure 32e. - Bond Shear Stress

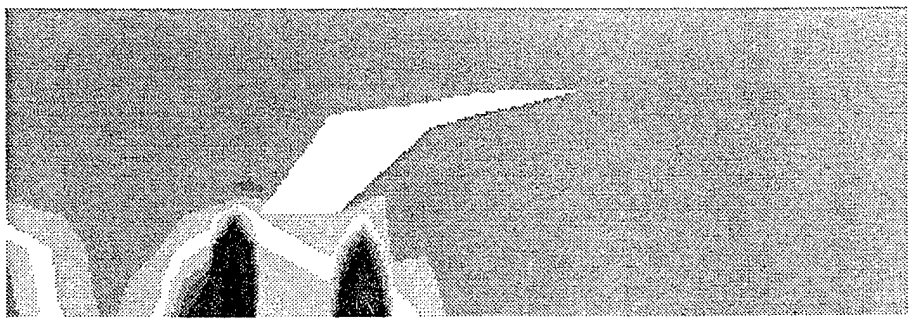

Figure 32f. - Bond Normal Stress

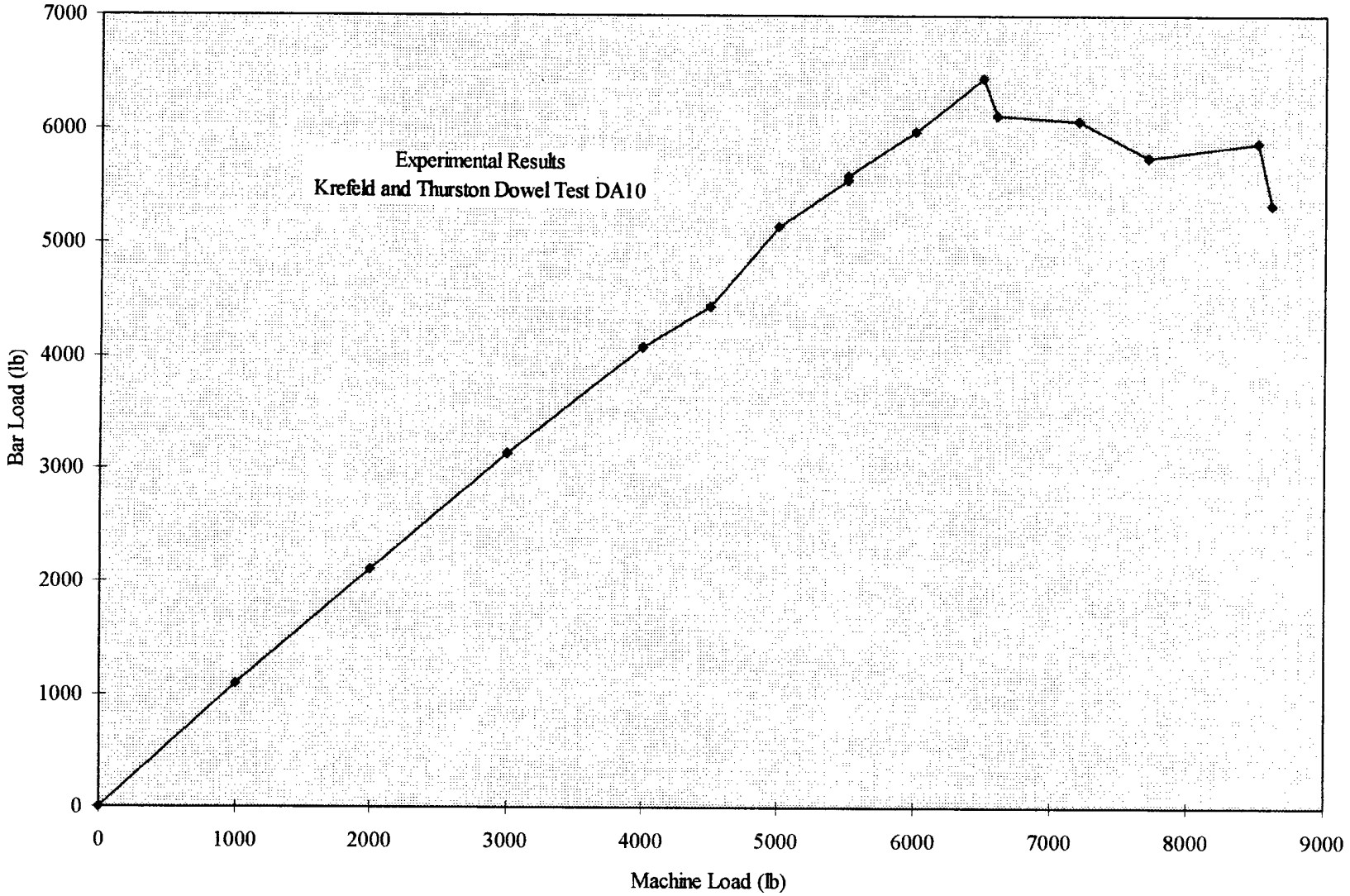

Figure 33. - Krefeld and Thurston Data; Bar vs. Machine Load Experimental Results

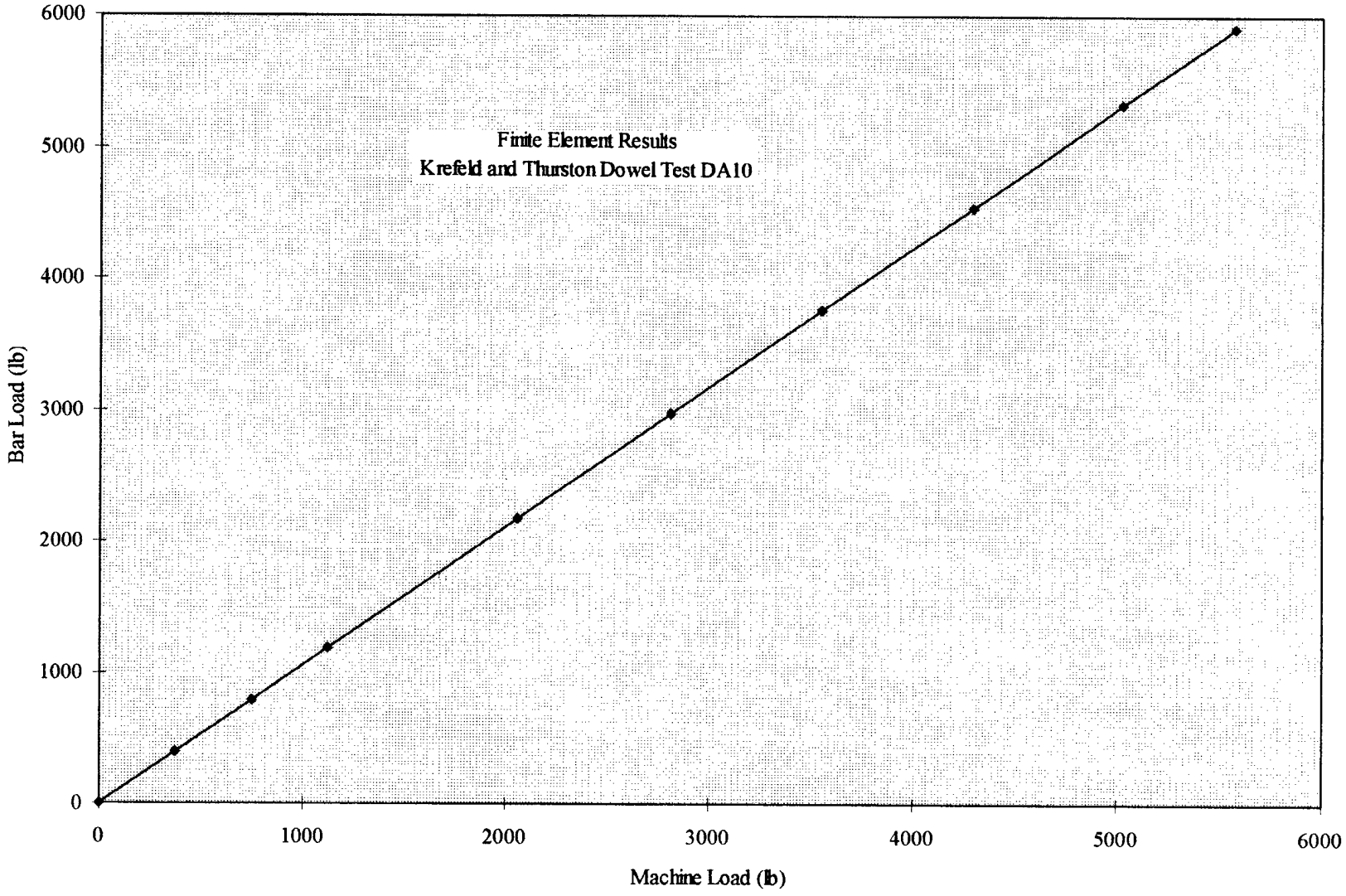

Figure 34. - Krefeld and Thurston Simulation; Bar vs. Machine Load Finite Element Results

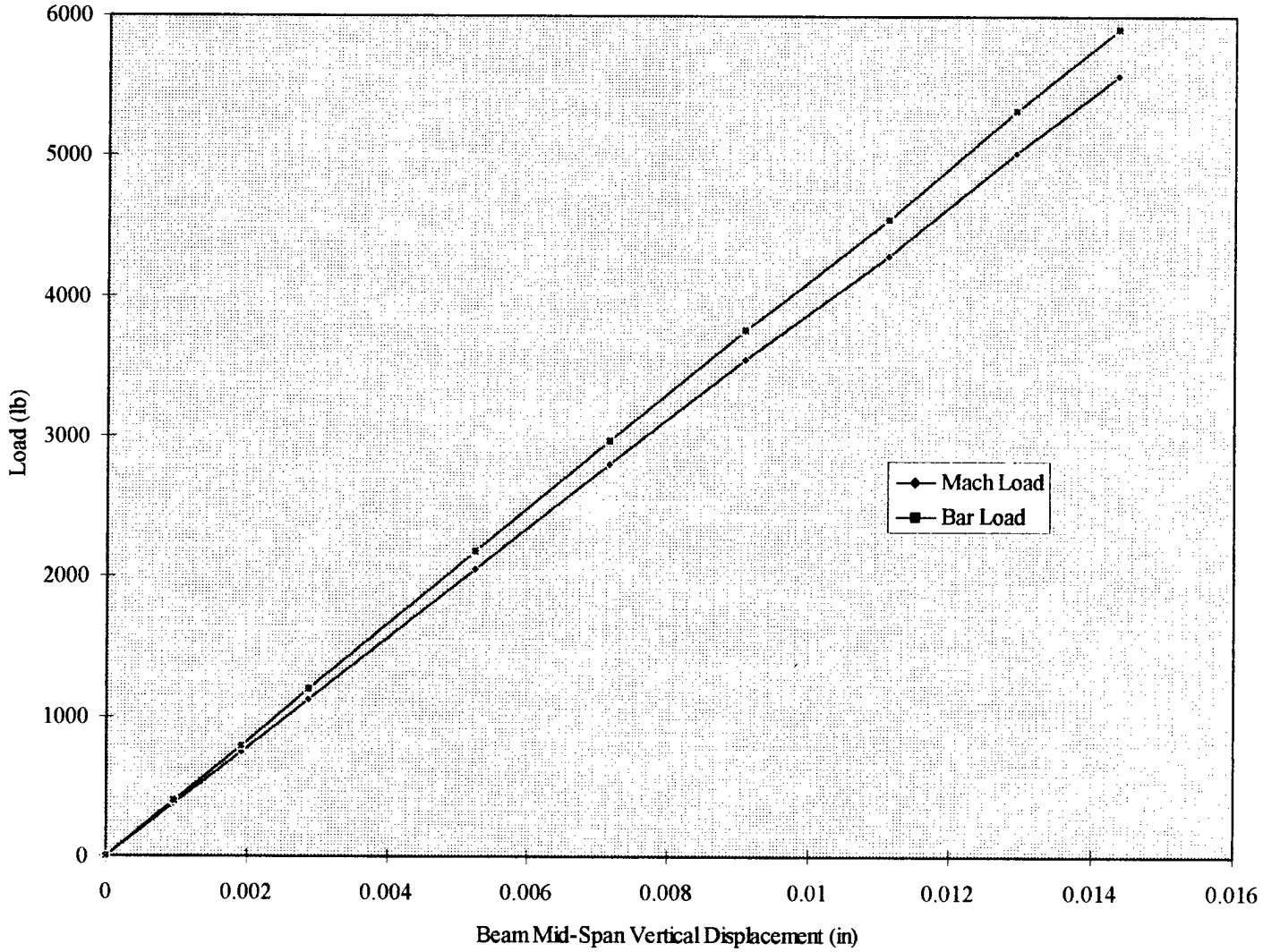

Figure 35. - Krefeld and Thurston Simulation; Load vs. Displacement Finite Element Results

This model also served as a rigorous test of the bond material algorithm. The initial results of this analysis motivated important needed changes and yielded lessons on implementation and usage. It was stated previously that the study was limited to monotonic loading. In initial attempts to analyze this test, it was observed that monotonic structural loading can still result in cyclic loading at the element level. As slip evolves, a region may go from slip in one direction to that of the other as the concrete flexural crack edge effects reach further into the structure. The bond model was modified to handle this simple one-cycle behavior. A very simple implementation, which assumed that slip in either direction results in damage and evolution of the yield surface, was conceived. While this is known to be incorrect (see the cyclic model of Herrmann and Cox, 1992), it was deemed adequate for this case where the amount of slip in the initial direction is very small and does not contribute significantly to the damage.

Another important observation made in the initial attempts to analyze this test was that the evaluation of the bond material algorithm for some elements is difficult for a real structure where there are regions of low confinement or near zero bond normal stress. The load had to be applied very slowly in the incremental scheme for the entire loading sequence to prevent numerical instabilities. However, there are also limits as to how small the load steps could be made because of numerical instability, possibly as a result of loss of precision. The distinction between too big or too small a load step was subtle in some cases, making it difficult to know how much load or displacement to apply in a given increment. The complete resolution of this problem will require additional study in future work.

8.3.3 Simulation of Bressler and Scordelis Reinforced-Concrete Beam. A second reinforced beam structure was analyzed. A series of beam tests were performed by Bressler and Scordelis (1963) to study the shear strength of reinforced-concrete beams. The series OA-1 was selected to model. The beam structure and test setup are shown in Figure 36. The beam was initially uncracked but the experimenters tracked and recorded flexural and diagonal tension cracks as they incrementally loaded the beam. Once again, the present composite element cannot be expected to model this complicated evolution and behavior. To do this would require as a minimum an inelastic concrete material model coupled with the ability to spawn concrete cracks in both composite and concrete elements.

However, it is still possible to test the present element's performance by assuming initial flexural cracks derived from Bressler and Scordelis' reported crack patterns. This model is shown in Figure 37. The model is plane strain which again is a limitation. It employs two rows of composite elements to represent the bottom portion of the beam where the four reinforcing bars were located. There are thin, bar-only quad elements between the composite elements at the

assumed crack locations. The 13 cracks, for the full beam, extend through the bottom three rows of elements. Additionally, preliminary one-crack and seven-crack models were also analyzed.

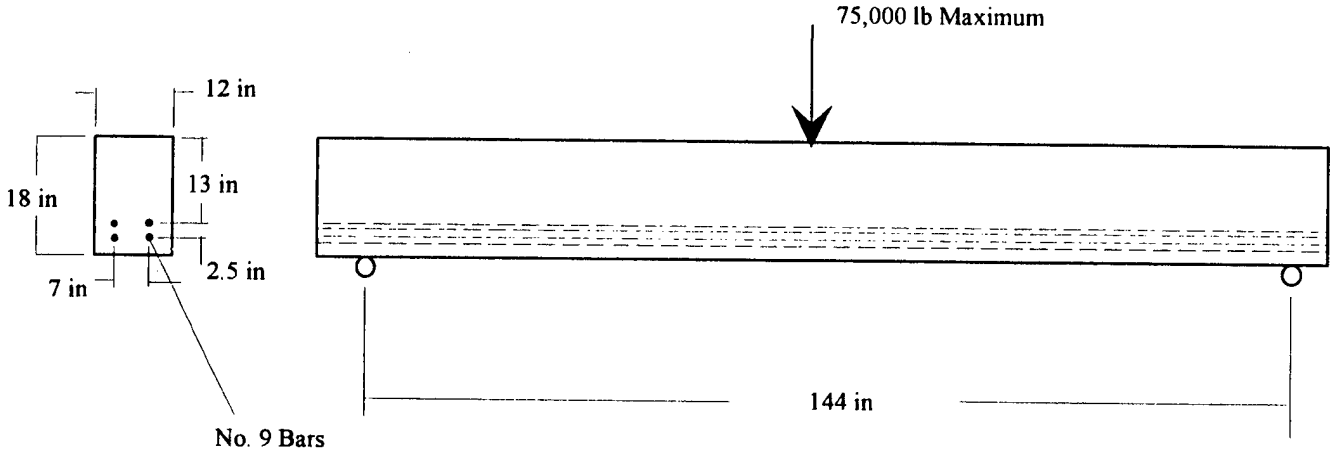

Model Data:
f 'c = 22.6 N/mm2
ρ = .044 for bottom 7.5 in of beam
Econcrete=37.5 N/mm2

Figure 36. - Bressler and Scordelis Beam Test OA-1

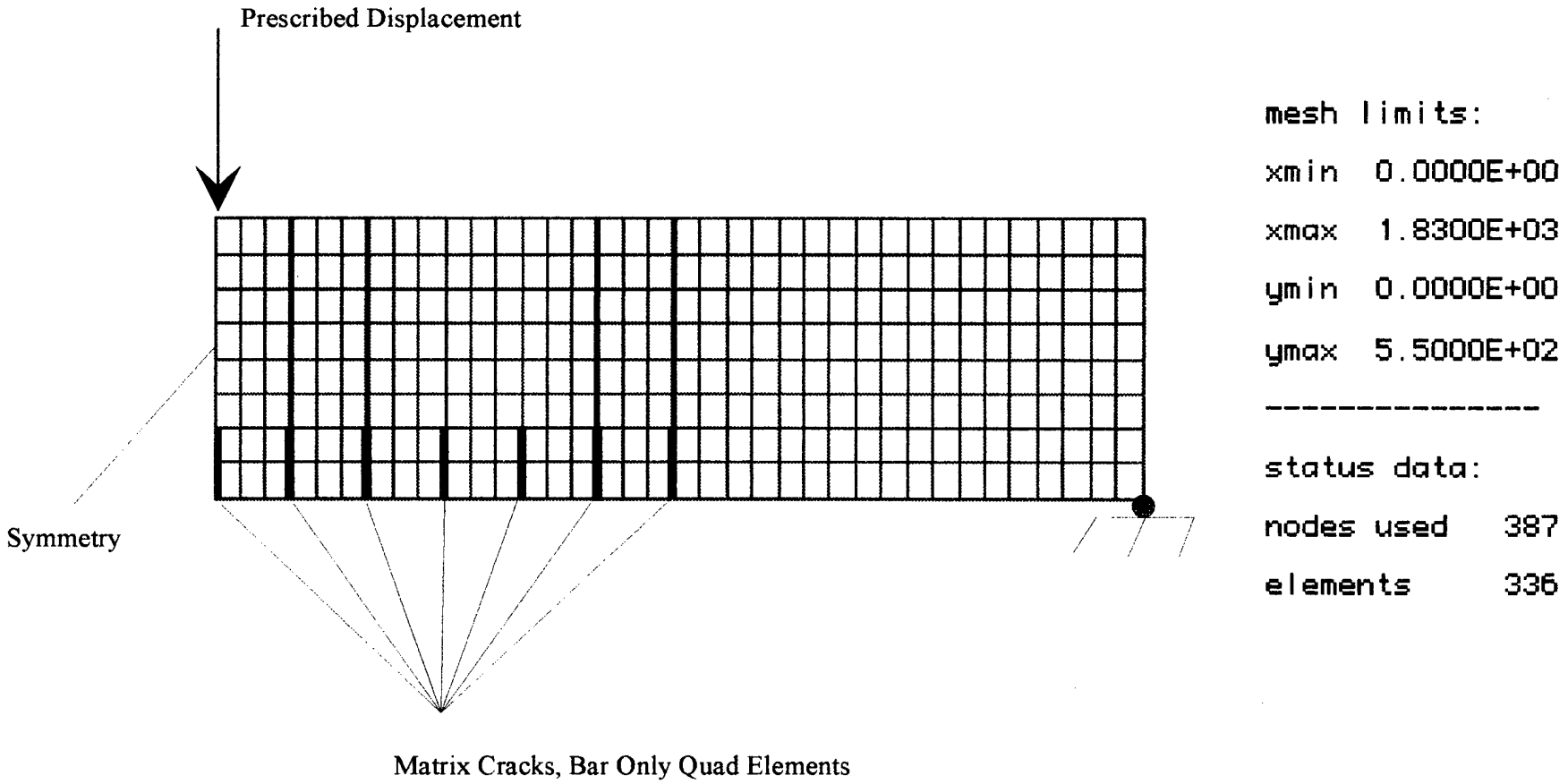

Figure 37. - Bressler and Scordelis Beam - Finite Element Model

The model was analyzed. The resulting deformed mesh plot is shown in Figure 38. The matrix cracks open as slip occurs. Stress contour plots are given in Figure 39. Again axial tensile stress cannot develop in the concrete because of the cracks and, thus, flows around them as can be seen in Figure 39a. Figure 39c shows the reversal in shear stress across the crack in the reinforced concrete. Figure 39d shows the gradient in bar tensile stress due to bond along the bar length. Figure 39e emphasizes the bond shear stress behavior between cracks. The contours show perfectly the locations of the cracks. Across a crack, the sign of the shear stress switches as it should. Approximately halfway between cracks the bond shear stress goes to zero. This can also be observed by reviewing the bond normal stress plotted in Figure 39f. In this case, the confinement pressure peaks at the crack and drops off to zero. The composite element was able to capture this detailed bond behavior provided the specified load or displacement was applied slowly enough.

Figure 40 compares experimental and analytical load-deflection behavior. Once again, one cannot expect close quantitative agreement in light of all the restrictions mentioned previously and the fact that the model is plane strain and starts with 13 cracks. The results are judged to be quite good considering all the limitations and approximations.

9. CONCLUSIONS

The results of this research clearly demonstrate the feasibility of incorporating a bond model, that includes both bond slippage and dilation, into a composite representation and accompanying finite element analysis for unidirectional reinforced materials.

A three-dimensional micro-mechanics model of an approximate representative volume for a unidirectional composite was formulated. The model assumes linear-elastic properties for the reinforcing and matrix materials and a plasticity model for the bond between them, including bond dilation. The resulting composite model was successfully incorporated into a two-dimensional composite finite element analysis.

Several sample analyses were successfully performed for simple reinforced-concrete tests. The analysis of the bond tension test served to demonstrate best the current capability of the composite element. The mesh was a simple row of quad elements. The results that were obtained were quite detailed. For example, the fiber or bar stress was determined and the bond stresses were predicted. Such results are normally only associated with a detailed, discrete finite element model of the reinforcement with an interface element and provision for bond-slip behavior. The composite element approach has been shown to be a powerful, efficient and capable method of modeling bond behavior in reinforced materials.

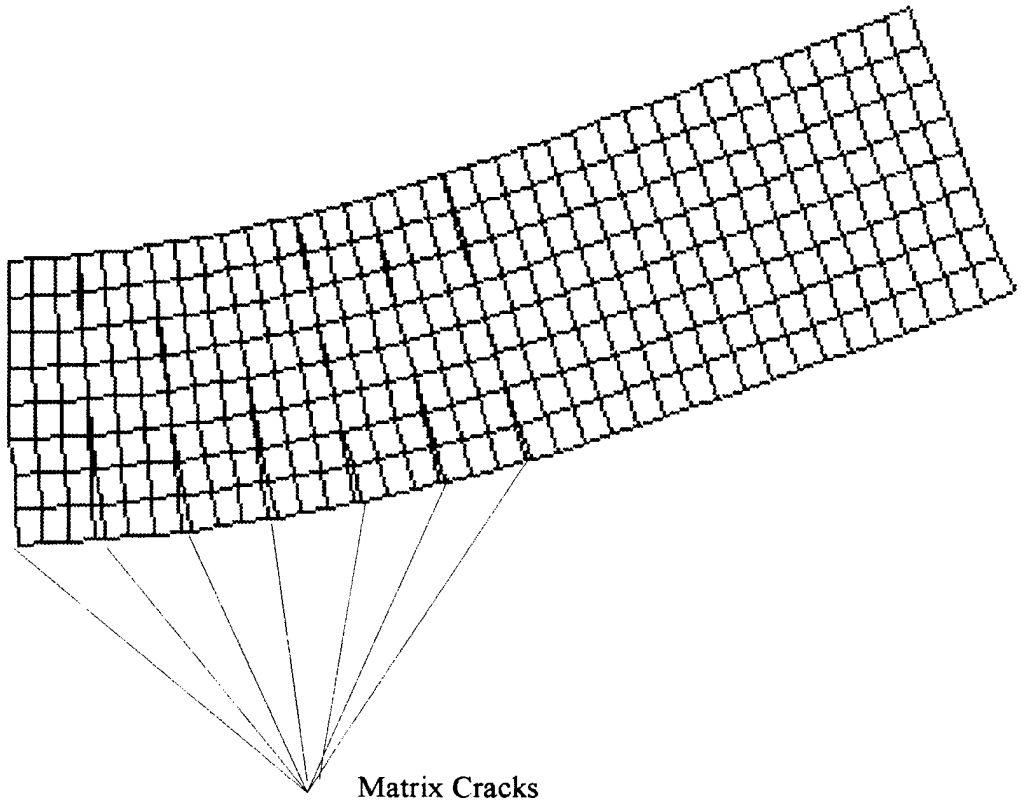

mesh limits:

xmin 0.0000E+00

xmax 1.9491E+03

ymin -4.9672E+02

ymax 5.4089E+02

---

status data:

nodes used 387

elements 336

Figure 38. - Bressler and Scordelis Beam - Finite Element Deformed Mesh

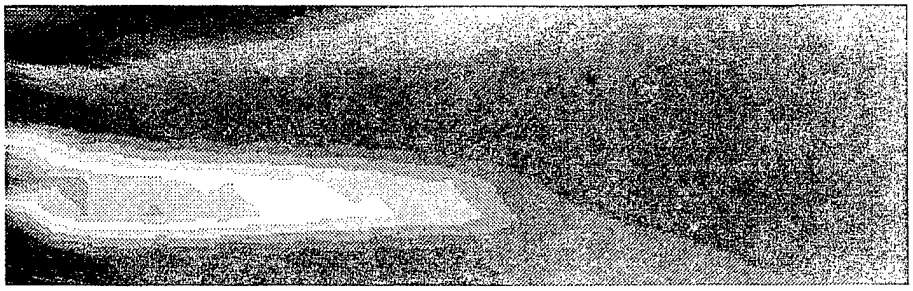

Figure 39a. - Concrete Matrix x-Direction Stress

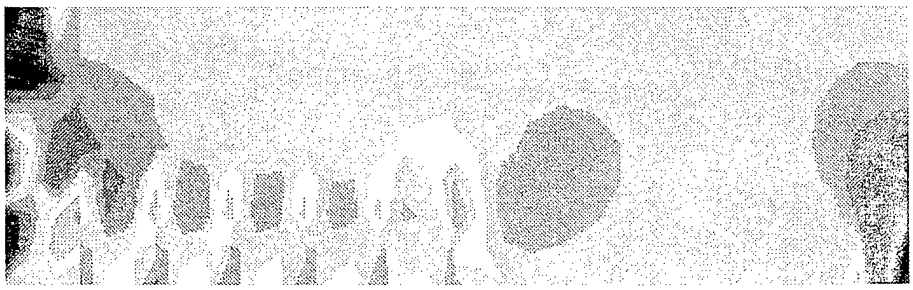

Figure 39b. - R/C Composite y-Direction Stress

Figure 39. - Bressler and Scordelis Beam Simulation

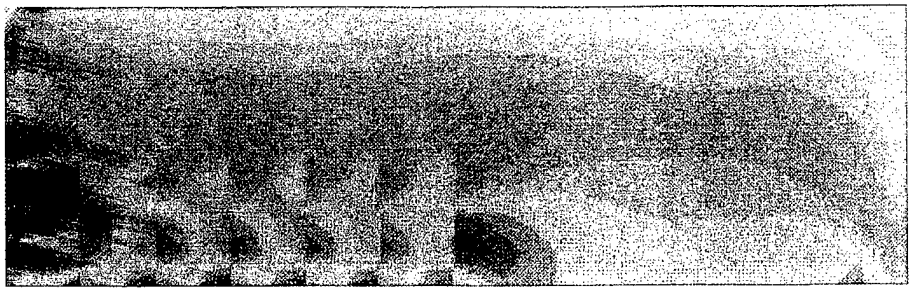

Figure 39c. - R/C Composite xy-Shear Stress

Figure 39d. - Bar x-Direction Stress

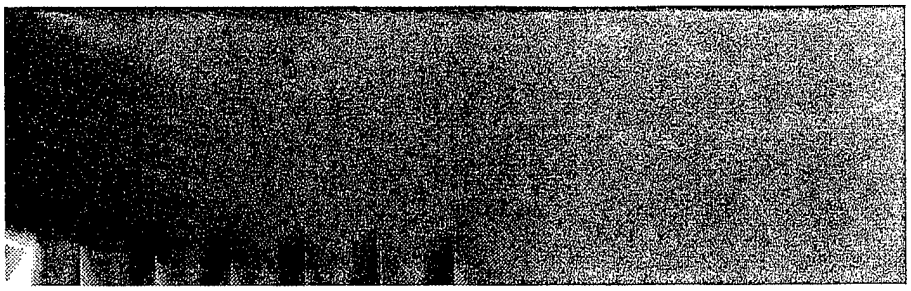

Figure 39e. - Bond Shear Stress

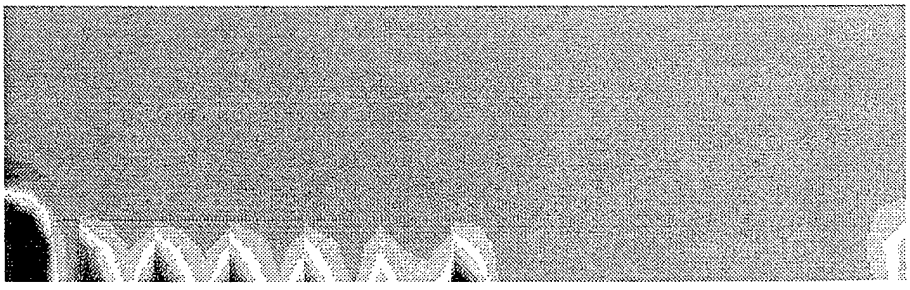

Figure 39f. - Bond Normal Stress

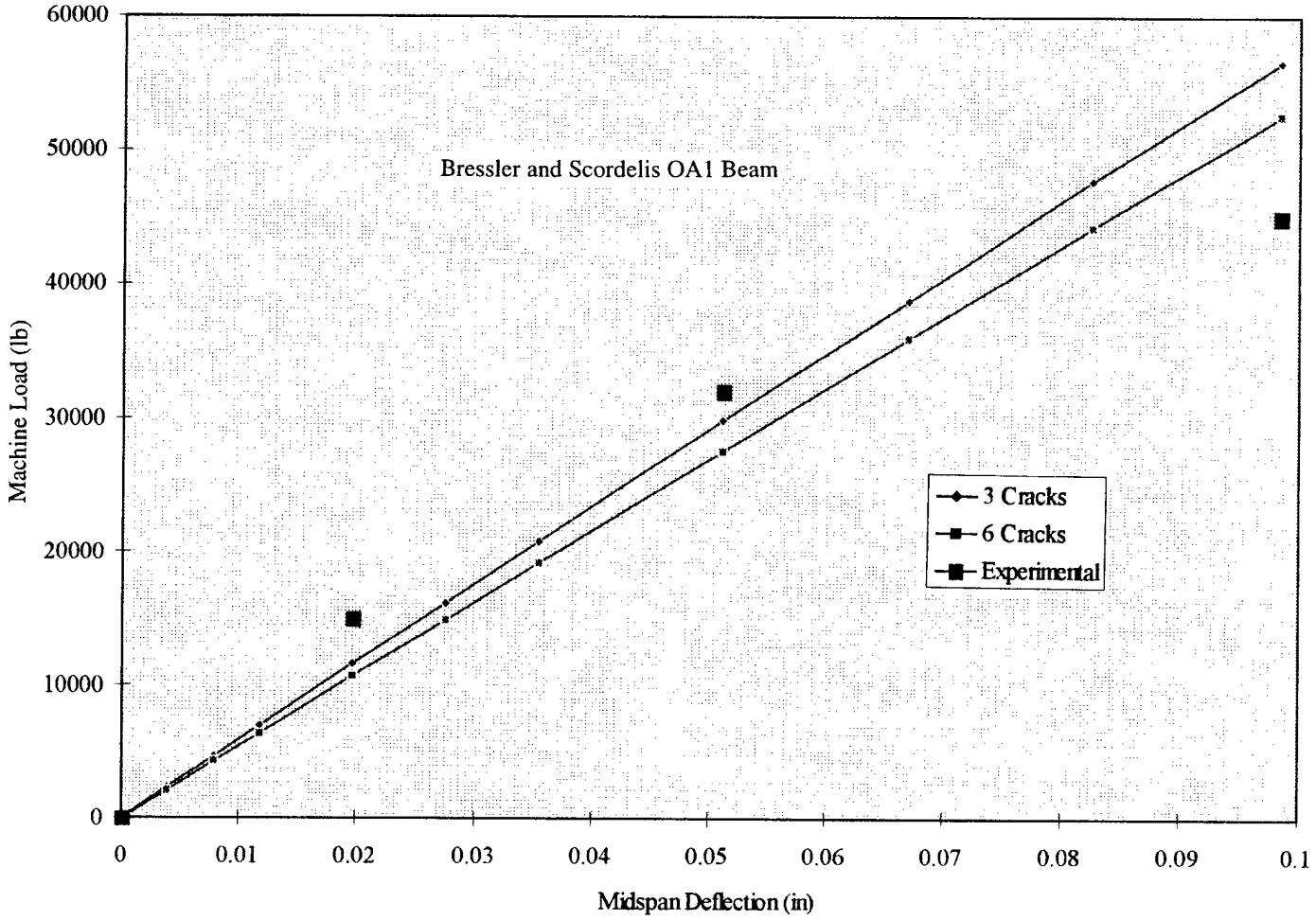

Figure 40. - Load vs. Deflection Results for Bressler and Scordelis Beam

The element employs two additional nodal degrees of freedom to capture slippage of the reinforcement relative to the matrix and the dilation of the bond zone. The use of the four degrees of freedom (two-dimensional) quad element is simple compared to a discrete model which would require finely meshed patches of elements for each constituent type, making it impractical to model bond-slip behavior at the structure level. The composite element results in savings in both the construction of the finite element model and the subsequent bond-slip analysis.

The virtual work micro-mechanics approach proved to be an effective means for deriving the specialized composite material relations used in the finite element scheme. The Reduced-Newton material algorithm, developed to evaluate the interface bond model, is quite efficient and reasonably robust.

10. RECOMMENDATIONS

While much was accomplished in this study, additional work is needed before the finite element analysis can be applied to significant reinforced-concrete problems. The model must be extended to include inelastic properties for the concrete and possibly for the reinforcing bars, and some means must be included for modeling the concrete cracking. For the latter extension, the introduction of smeared cracking (possibly by using a generalized plasticity model for the concrete) would seem the most appropriate. The extension of the finite element analysis to generalized plane stress and three-dimensional conditions would greatly increase the range of reinforced-concrete problems that could be addressed.

A second major thrust would involve the application of the bond-slip model and finite element analysis to fiber-reinforced composites. The key step would be to use whatever experimental data are available to calibrate (and modify as necessary) the bond model for one or more composite systems of this type. The finite element analysis could then be used to analyze any available structural tests of fiber-reinforced components and a judgment could be made as to the importance of including bond slippage and dilation in the modeling of such systems.

Finally, three components of the current composite model deserve further study: (1) the inclusion of the σ^* variable, the average bond equilibrium stress, in the stress vector is cumbersome - initial attempts to find an alternative scheme for specifying interface equilibrium were not successful but with additional investigation one might be found; (2) both the theoretical and practical advantages and disadvantages of using element condensation to eliminate the bond dilation from the global degrees of freedom need to be addressed in future work; and (3) an

automated global loading algorithm to eliminate time-consuming trial-and-error selection of load increment sizes is required for robust applications.

11. REFERENCES

Aboudi, J. (1991). Mechanics of composite materials -- A unified micromechanical approach. New York, NY, Elsevier, 1991.

Bathe, K. (1982). Finite element procedures in engineering analysis. Englewood, NJ, Prentice-Hall Inc., 1982.

Benveniste, Y. (1985). "The effective mechanical behavior of composite materials with imperfect contact between constituents," Mechanics of Materials, vol 4, 1985, pp 197-208.

Bresler, B. and A.C. Scordelis (1963). "Shear strength of reinforced concrete beams," American Concrete Institute (ACI) Journal, Title No. 60-4, Detroit, MI, 1963.

Cook, R.D. (1981). Concepts and applications of finite element analysis. Toronto, Canada, John Wiley and Sons, 1981.

Gambarova, P.G., G.P. Rosati, and R. Zasso (1989). "Steel-to-concrete bond after concrete splitting test tesults," Materials and Structures, vol 22, no. 127, Jan 1989, pp 35-47.

Hashin, Z. and W. Rosen (1964). "The elastic moduli of fiber-reinforced materials," Journal of Applied Mechanics, Jun 1964, pp 223-232.

Herrmann, L.R. and Z. Al-Yassin (1978). "Numerical analysis of reinforced soil systems," ASCE Spring Convention, Pittsburgh, PA, 1978.

Herrmann, L.R. and J.V. Cox (1992). Development of a plasticity bond model for reinforced concrete - Preliminary calibration and cyclic applications. U.C. Davis Report to Naval Civil Engineering Laboratory, Contract NCBC N47408-84-C-1056, Port Hueneme, CA, 1992 (or CR94.001-SHR, NFESC, Port Hueneme, CA, Mar 1994).

Herrmann, L. (1996). Finite element analysis of a sampling tube device for soils. Department of Civil and Environmental Engineering, University of California, Davis. Davis, CA, 1996

Herrmann, L.R. and V.N. Kaliakin (1987). Numerical implementation of the elastoplastic-viscoplastic bonding surface model for isotropic cohesive soils. The EVALP Computer program, University of California, Davis. Davis, California, 1987.

Houde, J. and M.S. Mirza (1974). "A finite element analysis of shear strength of reinforced concrete beams," Shear in Reinforced Concrete, vol 1, Special Publication, SP.42, American Concrete Institute Journal, Detroit, MI, 1974.

Hughes, T.J.R. (1987). Algorithms for the integration of inelastic constitutive equations, including rate and damage. Naval Civil Engineering Laboratory, Contract Report CR 87.004. Port Hueneme, CA, 1987.

Jones, R.M. (1975). Mechanics of composite material. New York, NY, McGraw-Hill, 1975.

Krefeld, W.J. and C.W. Thurston (1966). "Contribution of longitudinal steel to shear resistance of reinforced concrete beams," ACI Journal, Title No. 63-14, Detroit, MI, 1966.

Kreyszig, E. (1983). Advanced engineering mathematics. New York, NY, John Wiley and Sons, 1983.

Makin, T.J., P.D. Warren, and A.G. Evans (1992). "Effects of fiber roughness on interface sliding in composites," Acta Metall., vol 40, no. 6, 1992, pp 1251-57.

Malvar, L.J. (1991). Bond of reinforcement under controlled confinement. Naval Civil Engineering Laboratory, Technical Note N-1833. Port Hueneme, CA, Jun 1991.

Mathematica (1995). Enhanced Version 202. Wolfram Research, Inc., Champaign, IL, 1995.

Mish, K. (1992). Heat2D finite element code. Department of Civil Engineering, Chico State University. Chico, CA, 1992.

Mello, J. (1996). Finite element implementation of bond model, including dilation, for reinforced materials. Ph.D. Dissertation, University of California , Davis. Davis, CA, 1996

Owen, J.E. and E. Hinton (1980). Finite elements in plasticity. Swanson, United Kingdom, Pineridge Press Limited, 1980.

Pecknold, D.A. and R. Hajali (1993). "Integrated micromechanical/structural analysis of laminated composites," AMD - vol 159, Mechanics of Composite Materials: Nonlinear Effects, ASME, 1993, pp 197-221.

Schulz, J.C. (1965). Determination of the elastic moduli of square or hexagonally packed filament-wound composites by the finite element method. Aerojet General Corporation, Technical Paper No. 8 SRO. Sacramento, CA, 1965.

Theocaris, P.S. (1987). The mesophase concept in composites. Berlin, Germany, Springer-Verlag, 1987,

Tsai, S.W. (1992). Theory of composites design. Think Composites, Dayton, OH, 1992.

Valente, T. (1994). "Measurement of interfacial properties for aluminum and titanium matrix alloy composites manufactured by plasma spray," Journal of Composite Technology and Research, vol 16, no. 3, 1994, pp 256-261.

Zienkiewicz, O.C. and R.L. Taylor (1989). The finite element method, Volume 1. London, England, McGraw-Hill, 1989.

Zienkiewicz, O.C. and R.L. Taylor (1991). The finite element method, Volume 2. London, England, McGraw-Hill, 1991.

DISTRIBUTION LIST

AC ENGRG INC / BERRY, WEST LAFAYETTE IN
ADINA ENGRG, INC / WALCZAK, WATERTOWN MA
ADVENT ENGRG SVCS / DYRNESS, SAN RAMON CA
AEWES / LIB, VICKSBURG MS
AEWES / PETERS, VICKSBURG MS
AFOSR / NA (WU), WASHINGTON DC
AFWL/NTE / BALADI, KIRTLAND AFB NM
ALLIED BAR COATERS / HARTLEY, CARDIFF WALES
ANATECH APPLICATIONS / CASTRO, SAN DIEGO CA
ANATECH RESEARCH CORP / RASHID, SAN DIEGO CA
APPLIED PHYSICS TECH / SWANSON, MCLEAN VA
APPLIED RSCH ASSOC, INC / HIGGINS, ALBUQUERQUE NM
ARMY / R&D LAB, STRNC-UE, NATICK MA
ARMY CORPS OF ENGRS / HQ, DAEN-ECE-D, WASHINGTON DC
ARMY EWES / WES (NORMAN), VICKSBURG MS
ARMY EWES / WESIM-C (N. RADHAKRISHNAN), VICKSBURG MS
ASSOCIATED SCIENTISTS/ MCCOY, WOODS HOLE MA
BRITISH EMBASSY / ELLIS, WASHINGTON DC
BUREAU OF RECLAMATION / MCLEAN, DENVER CO
CALTRANS / ZELINSKI, SACRAMENTO CA
CALTRANS OFFICE OF RESEARCH / HOLLAND, SACRAMENTO CA
CATHOLIC UNIV / CE DEPT (KIM) WASHINGTON DC
CENTRIC ENGINEERING SYSTEMS INC / TAYLOR, PALO ALTO CA
CHALMERS UNIVERSITY OF TECHNOLOGY / TEPFERS, 412 74 GOTEBORG
CHEUNG AND ASSOCIATES / CHEUNG, COSTA MESA CA
CHILDS ENGRG CORP / K.M. CHILDS, JR., MEDFIELD MA
COLORADO SCHOOL OF MINES / GOLDEN CO
COLORADO ST UNIV / FORT COLLINS CO
COMPUTATIONAL MECHANICS / BREBBIA SOUTHAMPTON
CONSEJO SUPERIOR DE INVESTIGACIONES CIENTIFICAS / TORROJA, 28080 MADRI
CORNELL UNIV / ITHACA NY
COUNTY OF VENTURA / TAKAHASHI, VENTURA CA
CRREL / KOVACS, HANOVER NH
CSU CHICO / ARTHUR, CHICO CA
CSU CHICO / MISH, CHICO CA
CSU FULLERTON / RAMSAMOOJ, FULLERTON CA
DAMES & MOORE / LOS ANGELES CA
DET NORSKE VERITAS RESEARCH AS / BERGAN, VERITASVEIEN 1 N-1322 HOVIK
DOT / TRANSP SYS CEN (TONG), CAMBRIDGE MA
DTIC / ALEXANDRIA VA
DTRCEN / (CODE 1720), BETHESDA MD
FAU / REDDY, BOCA RATON FL
FHWA / LANE, MCLEAN VA
FORT F / VRETBLAD,
GEOCISA / RODRIGUEZ, 28820 COSLADA MADRID
GEORGE WASHINGTON UNIV / ENGRG & APP SCI SCHL (FOX), WASHINGTON DC
GERWICK INC / SAN FRANCISCO CA
HERIOT-WATT UNIV / CAIRNS,
HKS INC / PAWTUCKET RI

SRI INTL / ENGRG MECH DEPT (SIMONS), MENLO PARK CA
STANFORD UNIV / APP MECH DIV (HUGHES), STANFORD CA
STANFORD UNIV / CE DEPT (PENSKY), STANFORD CA
STANFORD UNIV / LAW, STANFORD CA
STRUCTURAL ANALYSIS PROGRAMS INC / WILSON, EL CERRITO CA
TEXAS A&M UNIV / ROSCHKE, COLLEGE STATION TX
TU DELFT / DE BORST, 2600 GA DELFT
TU DELFT / VAN MIER, 2600 GA DELFT
TUFTS UNIV / SANAYEI, MEDFORD MA
UCLA / HART, LOS ANGELES CA
UCLA / JU, LOS ANGELES CA
UCLA / MAL, LOS ANGELES CA
UCSB / MECH ENGRG DEPT (JANSSON), SANTA BARBARA CA
UCSB / MECH ENGRG DEPT (KEYWARD), SANTA BARBARA CA
UCSB / MECH ENGRG DEPT (LECKIE), SANTA BARBARA CA
UCSB / MECH ENGRG DEPT (MCMEEKING), SANTA BARBARA CA
UCSB / MECH ENGRG DEPT (TULIN), SANTA BARBARA CA
UCSD / SEIBLE, LA JOLLA CA
UNIV OF ARIZONA / EHSANI, TUCSON AZ
UNIV OF CAL BERKELEY / AMERO, BERKELEY CA
UNIV OF CAL BERKELEY / FILIPPOU, BERKELEY CA
UNIV OF CAL BERKELEY / GOVINDJEE, BERKELEY CA
UNIV OF CAL DAVIS / REHFIELD, DAVIS CA
UNIV OF CALIFORNIA DAVIS / CE DEPT (HERRMANN), DAVIS CA
UNIV OF CALIFORNIA DAVIS / CE DEPT (KUTTER), DAVIS CA
UNIV OF CALIFORNIA DAVIS / CE DEPT (RAMEY), DAVIS CA
UNIV OF COLORADO / MECH ENGRG DEPT (PARK), BOULDER CO
UNIV OF CONN / LEONARD, STORRS CT
UNIV OF DELAWARE / NEWARK DC
UNIV OF HAWAII / HONOLULU HI
UNIV OF HAWAII / HONOLULU HI
UNIV OF ILLINOIS / CE LAB (PECKNOLD), URBANA IL
UNIV OF KANSAS / DARWIN, LAWRENCE KS
UNIV OF MICH / ANN ARBOR ME
UNIV OF N CAROLINA / CE DEPT (GUPTA), RALEIGH NC
UNIV OF N CAROLINA / CE DEPT (TUNG), RALEIGH NC
UNIV OF NY / BUFFALO NY
UNIV OF RHODE ISLAND / KOVACS, KINGSTON RI
UNIV OF STUTTGART / ELIGEHAUSE,
UNIV OF TENNESSEE / KNOXVILLE TN
UNIV OF WYOMING / CIVIL ENGRG DEPT, LARAMIE WY
UNIVERSIDAD POLITECNICA DE MADRID / ELICES, 28040 MADRIC
UNIVERSIDAD POLITECNICA DE MADRID / PLANAS, 28040 MADRID
UNIVERSITAT POLITECNICA DE CATALUNYA / GETTU, 08034 BARCELONA
WEIDLINGER ASSOCIATES / LEVINE, LOS ALTOS CA
WEST VIRGINIA UNIV / BARBERO, MORGANTOWN WV
WEST VIRGINIA UNIV / KIGER, MORGANTOWN WV
WEST VIRGINIA UNIV / PRUCZ, MORGANTOWN WV
WILSON COMPOSITE GROUP INC / WILSON, FOLSOM CA